

AN INVESTIGATION OF TRANSITION PROBABILITIES  
IN THE SPECTRUM OF THE HYDROXYL RADICAL

by

Jeyarajan Anketell, B.Sc., A.R.C.S.

A Thesis submitted for the Degree of  
Doctor of Philosophy

in

the University of London

Department of Physics,  
Imperial College of Science & Technology,  
London.

June 1967.

| <u>CONTENTS</u>  |   | <u>Page No.</u> |
|------------------|---|-----------------|
| ACKNOWLEDGEMENTS |   | 4               |
| ABSTRACT         |   | 5               |
| CHAPTER I        | <u>INTRODUCTION</u>   |                 |
|                  | 1.1. General Introduction                                     | 7               |
|                  | 1.2. Survey of Past Work                                      | 9               |
|                  | 1.3. Choice of Method   | 19              |
|                  | 1.4. Outline of the Hook Method                               | 20              |
| CHAPTER II       | <u>THEORETICAL (A) - TRANSITION PROBABILITIES IN OH</u>       |                 |
|                  | 2.1. The Einstein Transition Probabilities and Wave Mechanics | 23              |
|                  | 2.2. The Born-Oppenheimer Approximation                       | 26              |
|                  | 2.3. The Ultra-Violet Band Spectrum of OH                     | 32              |
|                  | 2.4. The Morse-Pekeris Rotating Oscillator                    | 39              |
|                  | 2.5. The Electronic Transition Moment in OH                   | 41              |
|                  | 2.6. The Band Oscillator Strength                             | 45              |
| CHAPTER III      | <u>THEORETICAL (B) - THE HOOK METHOD</u>                      |                 |
|                  | 3.1. Dispersion Theory  | 47              |
|                  | 3.2. The Puccianti Method                                     | 51              |
|                  | 3.3. The Roschdestwensky Modification                         | 53              |
|                  | 3.4. Application to a Number of Close Lines                   | 57              |
| CHAPTER IV       | <u>EXPERIMENTAL (A) - THE MACH-ZEHNDER INTERFEROMETER</u>     |                 |
|                  | 4.1. Introduction   | 60              |
|                  | 4.2. Theory of the Interferometer                             | 63              |
|                  | 4.3. Modifications to the Interferometer                      | 67              |
|                  | 4.4. Adjustment of the Interferometer                         | 69              |
|                  | 4.5. Experimental Precautions                                 | 74              |

|             |   |     |
|-------------|---|-----|
| CHAPTER V   | <u>EXPERIMENTAL (B) - THE REMAINDER OF THE SYSTEM</u>             |     |
|             | 5.1. The Background Source  | 78  |
|             | 5.2. The Optical System   | 79  |
|             | 5.3. The Spectrograph   | 82  |
|             | 5.4. The Gas System   | 87  |
|             | 5.5. The Furnace  | 92  |
|             | 5.6. Temperature Control  | 97  |
|             | 5.7. Temperature Calibration                                      | 100 |
| CHAPTER VI  | <u>OSCILLATOR STRENGTH RESULTS</u>                                |     |
|             | 6.1. Introduction   | 104 |
|             | 6.2. Population Density of the Absorbing Levels                   | 109 |
|             | 6.3. Vibration-Rotation Interaction in the (0,0) Band             | 114 |
|             | 6.4. Absolute Oscillator Strength of the (0,0) Band               | 117 |
|             | 6.5. Absolute Oscillator Strength of the (1,0) Band               | 119 |
| CHAPTER VII | <u>DISCUSSION OF RESULTS</u>                                      |     |
|             | 7.1. Comparison of $f_{00}$ with Previous Measurements            | 120 |
|             | 7.2. Comparison of $f_{10}$ with Previous Results                 | 124 |
|             | 7.3. The Electronic Transition Moment for Vibrational Interaction | 125 |
|             | 7.4. The Electronic Transition Moment and Rotational Coupling     | 131 |
|             | 7.5. Thermometric Molecules                                       | 139 |
| REFERENCES  |   | 140 |

ACKNOWLEDGEMENTS

The author would like to thank Dr. A. Pery-Thorne for her supervision and encouragement throughout the work comprising this thesis.

The author would also like to thank Dr. R.C.M. Learner, for many helpful discussions throughout this work.

Thanks are also due to the Science Research Council (then D.S.I.R.) for providing, through the Aerodynamics Division of the National Physical Laboratory, funds which enabled this work to be carried out; to Mr. C.A.R. Anketell for financial support during part of the project; and to Professor W.R.S. Garton and the Department of Physics, Imperial College of Science & Technology, for providing a Temporary Research Assistantship.

The author would also like to thank Mr. T.W. Shand and the Physics Departmental Workshop for constructing the spectrograph and modifying the interferometer; Mr. E. Menage and Mr. C.V. Cooper for working the optical components; Dr. P.S. Rogers and the Nuffield Research Group, in the Department of Metallurgy, for advice and assistance in constructing the furnace; Dr. K.E. Seal, lately of the Department of Chemical Engineering, for use of a computer programme; the Imperial College Computer Unit for their advice and for the use of their facilities; Mr. M.J. Wallace for taking the photographs; Mr. O.R. Milbank for making the glassware used in the work; Mrs. C.A.R. Anketell for her assistance during the preparation of this thesis; and the many other people with whom the author has had very helpful discussions.

ABSTRACT

The hook method has been used to obtain oscillator strengths for twenty lines in three branches of the (0,0) band of the  $A^2\Sigma^+ - X^2\Pi$  system of OH. It is found that vibration-rotation interaction decreases the effective f-value for this band by about 7% over the first ten lines of each branch. The absolute f-value obtained for the rotationless molecule is  $f_{00} = (14.8 \pm 1.3) \times 10^{-4}$ . Although this falls within the range of previous measurements, it is nearly twice as large as the value hitherto considered most probable. For the (1,0) band, in which vibration-rotation interaction could not be measured, the absolute oscillator strength is found to be  $(8.9 \pm 1.7) \times 10^{-4}$ , giving for the relative oscillator strengths the ratio  $f_{10}/f_{00} = 0.60 \pm 0.10$ .

The value for the ratio  $f_{10}/f_{00}$  obtained here leads to a re-examination of the distribution of band strengths in the  $A^2\Sigma^+ - X^2\Pi$  band system of OH, resulting in an electronic-vibrational transition moment  $R_{ov}(r) = e^{-(5.97 \pm 0.12)r}$ , where  $r$  is the internuclear distance in Angstrom units. It is shown that this value for the electronic transition moment will not explain the variation of effective band strength with rotational quantum number. The interaction of rotational and electronic motion leads to a second, electronic-rotational, transition moment. This term is related to the centrifugal distortion of the molecule and, for the (0,0) band, is given by  $R_{oJ}(r) = e^{+(3.60 \pm 1.0) \times 10^{-4}J(J+1)}$ . Within the (0,0) band the combination of these two moments is equivalent to a single function  $R_{ovJ}(r) =$

$e^{-(2.67 \pm 0.9)r}$ . In consequence, (0,0) band vibration-rotation interaction and temperature corrections remain as given by Learner, 1962.<sup>18</sup> The relative J-dependent vibrational transition probabilities for the rest of the system are corrected. The effect of the total electronic transition moment on the measurement of rotational temperature is discussed for both OH and other diatoms.

CHAPTER I.INTRODUCTION.1.1. General Introduction

Both absolute and relative values of transition probabilities of radiative transitions, and the corresponding oscillator strengths or f-values, are of great interest. They are important as atomic and molecular constants, not only in their application to laboratory and celestial problems, but also for the light they throw on questions of atomic and molecular structure.

Transition probabilities are chiefly required for the determination of atomic and molecular abundances in flames, discharges, stellar atmospheres, etc. A question of astrophysical interest is whether the abundance of molecules in stellar atmospheres can be accounted for on the assumption of thermal equilibrium, given the abundance of their constituent atoms - Herzberg, 1965.<sup>1</sup> For the latter problem, it is additionally necessary to know the dissociation energy of the molecule.

Important among the applications of transition probabilities is its use in temperature determinations. If the relative intensities of absorption or emission lines in the spectrum of an absorbing or emitting medium are measured, and if the transition probabilities are already known, then the relative populations of the energy levels involved may be easily obtained, and the appropriate temperature determined. In the case of molecules, comparison of the temperatures

~~obtained by consideration of the relative populations of different~~ types of energy levels (electronic, vibrational, and rotational) may throw light on the physical processes involved - Shuler, 1950.<sup>2</sup>

Any treatment of the emissivity and general radiative transfer properties of hot gases requires a knowledge of the transition probabilities.

In cases where there is competition between spontaneous radiation and one or more nonradiative processes such as collisional quenching, predissociation, or chemical reaction, the rate of the non-radiative process can be found if the probability of the radiative process is known - Carrington, 1959.<sup>3</sup>

The OH radical is widely used in many of these applications, particularly as a thermometric molecule in the measurement of rotational temperatures. It is a constituent or an easily introduced impurity in many spectroscopic sources, e.g. flames, low temperature shock waves, and gas discharges - Pearse and Gaydon, 1963,<sup>4</sup> p.246. The OH ultra-violet spectrum has been observed in the emission spectrum of the heads of comets, and in the absorption spectrum of the solar atmosphere. A line in the radio-frequency spectrum has been observed in the absorption spectrum of the interstellar medium - Weinreb et al, 1963.<sup>5</sup>

The  $f$ -value of the (0,0) band of the  $A^2\Sigma^+ - X^2\Pi$  transition of OH has been measured by more workers (references 6 to 16), using a variety of techniques, than that of any other electronic transition in a diatomic molecule. However the results cover a fairly wide range



of values, and some of them require significant corrections to account for instrument effects - Kostkowsky and Bass, 1956<sup>17</sup> - and vibration-rotation interaction - Learner, 1962.<sup>18</sup> Moreover all these values are based either on measurements on a few lines in the band, or on the band as a whole, individual lines being unresolved, so that the vibration-rotation interaction effect cannot be evaluated experimentally. The effect of vibration-rotation interaction is to alter the relative f-values of the rotational lines in a vibrational band, and hence the relative intensities of the lines in absorption or emission. A knowledge of the magnitude of the interaction is necessary for accurate rotational temperature determinations, since it is from the relative intensities of the lines that the relative populations of the rotational energy levels are calculated and the temperature obtained.

The aim of this investigation was to investigate the vibration-rotation interaction effect experimentally, and to measure the absolute f-values of both the (0,0) and (1,0) bands.

## 1.2. Survey of Past Work

The experimental determinations of the absolute f-values of the (0,0) band ( $f_{00}$ ), theoretical calculations of  $f_{00}$ , experimental determinations of the relative band strengths ( $p_{v^0v''}/p_{00}$ ), theoretical calculations of  $p_{v^0v''}/p_{00}$ , and vibration-rotation interaction investigations, will be presented separately for the sake of clarity. The relationships between the f-value ( $f_{J^0J''}$ ) of a given spectrum line in the ( $v^0v''$ ) band, the f-value ( $f_{v^0v''}$ ) of the band, and the band strength ( $p_{v^0v''}$ ) is given by

$$f_{J^0 J''} = f_{\nu^0 \nu''} S_{J^0 J''} / (2J'' + 1)$$

$$= \nu P_{\nu^0 \nu''} S_{J^0 J''} / (2J'' + 1) \quad \dots\dots(1.1)$$

where  $\nu$  is the frequency of the line, and  $S_{J^0 J''}$  is the rotational line strength, depending only on the total angular momenta  $J^0$ ,  $J''$  and the coupling between their various components.  $f_{\nu^0 \nu''}$  may be taken as a constant for a given band if one neglects both, the variation of frequency, and vibration-rotation interaction over the band.

#### Experimental Determinations of $f_{00}$

Oldenberg and Rieke, 1938,<sup>6</sup> used the method of integrated absorption coefficients. The background was the continuum from a hydrogen discharge tube, and the OH was produced by dissociation of  $H_2O$  in a mixture of gases ( $\frac{2}{3}H_2O + \frac{1}{3}O_2$ ) at 1473°K. They obtained f-values for lines in the (0,0) band corresponding to  $f_{00} = (2.9 \pm 0.4) \times 10^{-4}$ . This value was subsequently corrected by Dwyer and Oldenberg, 1944,<sup>7</sup> with regard to a later and more accurate determination of the OH dissociation energy  $D_{OH}$ , to  $f_{00} = (12.3 \pm 1.8) \times 10^{-4}$ ; and once more to  $f_{00} = (9.5 \pm 1.4) \times 10^{-4}$  by Golden, Del Greco and Kaufman, 1963,<sup>8</sup> for thermochemistry, again chiefly on account of the availability of a more accurate value for  $D_{OH}$ .

Oldenberg and Rieke, 1938<sup>9,10</sup> refer to an investigation by Avramenko and Kondratjew using a line absorption technique, the background source emitting the OH spectrum, the emission lines being narrower than the absorption lines. The dominant line broadening process was pressure broadening, and the pressures of the gas in the emitting and absorbing

media were 1.5 mm and 760 mm respectively. The  $f$ -values obtained by Avramenko and Kondratjew were about  $10^3$  times larger than those of Oldenberg and Rieke, 1938.<sup>6</sup> However Oldenberg and Rieke, 1938,<sup>9,10</sup> re-interpreted the results of Avramenko and Kondratjew, and corrected them with regard to the pressure broadening of the OH lines, so that both sets of results were ultimately in agreement to about 25%.

Dyne, 1958,<sup>11</sup> essentially repeated Oldenberg and Rieke's 1938<sup>6</sup> experiment, obtaining  $f$ -values of lines both by resolved absorption and by the curve of growth method. His values for  $f_{00}$  were about half as large as theirs.

Carrington, 1959,<sup>12</sup> studied the line shape and  $f$ -value of lines in the (0,0) band by the curve of growth method using a variety of flames as sources of the OH spectrum. He obtained an  $f$ -value of  $(11.7 \pm 4) \times 10^{-4}$  for the  $Q_1(6)$  line, corresponding to  $f_{00} = (13.0 \pm 5.2) \times 10^{-4}$ . This was later corrected to give  $f_{00} = (11.1 \pm 5.0) \times 10^{-4}$ , by Learner, 1962,<sup>18</sup> with regard to vibration-rotation interaction and thermochemistry.

Lapp, 1960,<sup>13</sup> made photoelectric measurements of the emissivity of the unresolved (0,0) band of OH produced at 3300 - 3900°K in a shock tube, and related this to  $f_{00}$  by an absolute intensity calibration. He obtained  $f_{00} = (9.0 \pm 5.0) \times 10^{-4}$ .

Golden, Del Greco and Kaufman, 1963,<sup>8</sup> used the line absorption technique of Avramenko and Kondratjew. The OH in the absorbing medium was produced by means of the fast atom-molecule reaction  $H + NO_2 \rightarrow OH + NO$ . They obtained  $f_{00} = (7.1 \pm 1.1) \times 10^{-4}$ . They also corrected

the results of previous workers with regard to thermochemistry and vibration-rotation interaction, and presented a table of the corrected values.

Watson's, 1964,<sup>14</sup> work superseded that of Lapp, 1960,<sup>13</sup> essentially repeating it and eliminating light scattering in the absolute intensity calibration, to give the revised value  $f_{00} = (39 \pm 9) \times 10^{-4}$ .

Bennet and Dalby, 1964,<sup>15</sup> measured the radiative lifetime of the  $2\Sigma^+ - 2\Pi$  transition, and presented the value  $f_{00} = (8.0 \pm 0.8) \times 10^{-4}$ , independent of thermochemical data. The OH population was produced by electron bombardment of methanol ( $\text{CH}_3\text{OH}$ ), and also water vapour.

Bird and Schott, 1965,<sup>16</sup> computed expressions for the population density of OH in shocked gases in terms of the absorption from a pulsed discharge source of OH line radiation, and the optical density, temperature, f-value, and a pressure broadening parameter. These were reconciled with calibration experiments with reflected shock waves in  $\text{H}_2 - \text{O}_2 - \text{Ar}$  mixtures, giving  $f_{00} = (12.8 \pm 0.3) \times 10^{-4}$ .

All the experimental determinations of  $f_{00}$  are presented in Table (1.1). They cover the wide range from  $4.9 \times 10^{-4}$  to  $39 \times 10^{-4}$ , and depend on a correction for vibration-rotation interaction. The scatter will be discussed in chapter VII.

#### Theoretical Calculations of $f_{00}$

Mulliken, 1940,<sup>19</sup> made theoretical calculations of the absolute dipole strength (proportional to the f-value) of the transition  $A^2\Sigma^+ - X^2\Pi$ , using both Linear Combinations of Atomic Orbitals (LCAO) and Molecular Orbital (MO) approximations, and related these to the

Table 1.1. Summary of Experimental f-values for the (0,0) band.

| Investigator                                  | $f_{00} \times 10^4$ |  |                  |
|---|----------------------|--|------------------|
|   | Uncorrected          | Corrected for<br>Thermo- & Vibration-<br>chemistry      rotation<br>interaction <sup>a</sup> |                  |
| Oldenberg and Rieke <sup>6,7</sup>            | $12.3 \pm 1.8$       | $9.2 \pm 1.4$  | $9.5 \pm 1.4^b$  |
| Dyno <sup>11</sup>                            | $6.4 \pm 1.3$        | $5.2 \pm 1.0$  | $5.4 \pm 1.0^b$  |
|   | $5.8 \pm 1.2$        | $4.8 \pm 1.0$  | $4.9 \pm 1.0^b$  |
| Carrington <sup>12</sup>                      | $13.0 \pm 5.2$       |  | $11.1 \pm 5.0^c$ |
| Goldon, Del Greco and<br>Kaufman <sup>8</sup> |                      |  | $7.1 \pm 1.1$    |
| Watson <sup>14</sup>                          |                      |  | $39 \pm 9$       |
| Bennett and Dalby <sup>15</sup>               |                      |  | $8.0 \pm 0.8$    |
| Bird and Schott <sup>16</sup>                 |                      |  | $12.8 \pm 0.3$   |

<sup>a</sup> The vibration-rotation interaction correction follows Learner's<sup>18</sup> treatment.

<sup>b</sup> Tabulated by Goldon, Del Greco and Kaufman.<sup>8</sup>

<sup>c</sup> Estimated by Learner.<sup>18</sup>

f-values of Oldenberg and Rieke, 1938.<sup>6</sup> His results give  $f_{00} = 6 \times 10^{-4}$  and  $42 \times 10^{-4}$ , for the LCAO and MO approximations respectively.

Hurley, 1959,<sup>20</sup> obtained semi-theoretical f-values for the transition, using Self-Consistent Field Molecular Orbital theory (SCFMO), LCAO, and also intra-atomic correlation correction methods (i.c.c.), applying both dipole length and equivalent dipole velocity formulae. The values obtained using the dipole length formula were  $f_{00} = 18 \times 10^{-4}$ ,  $35 \times 10^{-4}$ , and  $43 \times 10^{-4}$  respectively, while for the dipole velocity formula he obtained  $f_{00} = 950 \times 10^{-4}$ ,  $1500 \times 10^{-4}$ , and  $1500 \times 10^{-4}$  respectively.

The theoretical values of  $f_{00}$  are presented in Table 1.2. They cover an even wider range than the experimental values, from  $6 \times 10^{-4}$  to  $1500 \times 10^{-4}$ . The chief cause of the scatter is the great difficulty of obtaining the molecular electronic wave functions, and hence precise values for the electronic transition moment.

#### Experimental Determinations of $p_{v^1v^0}/p_{CO}$ .

Dieke and Crosswhite, 1948,<sup>21</sup> made a detailed survey of the OH ultra-violet band system. They presented relative values of the band strengths ( $p_{v^1v^0}/p_{00}$ ), obtained by photographic photometry, for nine bands in the system. Dieke and Crosswhite, 1949, (22, unpublished) obtained more accurate values of  $p_{v^1v^0}/p_{00}$  for these bands from photoelectric measurements of the intensities.

Bass and Broida, 1953,<sup>23</sup> published a Spectrophotometric Atlas giving the wavelength and relative intensities (obtained photoelectrically) of individual lines in the whole  $A^2\Sigma^+ - X^2\Pi$  band system, from 2600 Å to

Table 1.2. Summary of Theoretical f-values for the (0,0) Band.

| <u>Investigator</u>    | <u>Method</u>            | <u><math>f_{00} \times 10^4</math></u> |
|------------------------|--------------------------|--|
| Mulliken <sup>19</sup> | Dipole length (LCAO)     | 6                                      |
|                        | Dipole length (MO)       | 42                                     |
| Hurley <sup>20</sup>   | Dipole length (SCFMO)    | 18                                     |
|                        | Dipole length (LCAO)     | 35                                     |
|                        | Dipole length (i.c.c.)   | 43                                     |
|                        | Dipole velocity (SCFMO)  | 950                                    |
|                        | Dipole velocity (LCAO)   | 1500                                   |
|                        | Dipole velocity (i.c.c.) | 1500                                   |

3500 Å, obtained from the hot gases above a hydrogen-oxygen flame. The values of  $p_{v',v''}/p_{00}$  obtained from these measurements require a correction for the spectral response of the grating spectroradiometer used.

#### Theoretical Calculations of $p_{v',v''}/p_{00}$ .

Shuler, 1950,<sup>2</sup> calculated the relative band strengths (or vibrational transition probabilities) of bands arising from the first four vibrational levels of the  $A^2\Sigma - X^2\Pi$  system, using anharmonic wave functions derived from the Morse potential, 1929,<sup>24</sup> and assuming an electronic transition moment of the form  $R_e(r) = \text{const.}(1 + ar)$ , where  $r$  is the internuclear distance in Å. He fitted his theoretical values to the improved photoelectric values of Dieke and Crosswhite, 1949,<sup>22</sup> obtaining a numerical value for the constant  $a$ , giving  $R_e(r) = \text{const.}(1 - 0.75r)$ , and presented a table of relative band strengths obtained for this value of  $a$ .

Nicholls, 1956,<sup>25</sup> examined the distribution of band strengths given by Dieke and Crosswhite's, 1949,<sup>22</sup> values and studied the dependence of the electronic transition moment  $R_e(r)$  on the internuclear separation  $r$  (in Å) by means of the "r-centroid" approach. (Nicholls and Jarman, 1956.<sup>26</sup>) Nicholls obtained  $R_e(r) = \text{const.}(1 - 0.756r)$ , and used this to produce a "smoothed" array of relative band strengths within the system.

Learner, 1962,<sup>18</sup> used an exponential form for the electronic transition moment,  $R_e(r) = e^{-ar}$ , and obtained a value for  $a$  by fitting his theoretical band strengths to the smoothed values of Nicholls, 1956.<sup>25</sup>



He obtained  $R_0(r) = e^{-2.5r}$  and presented the corresponding array of relative band strengths.

In all these calculations of  $p_{v',v''}/p_{00}$ , the results are significantly lower than the experimental values from which they are derived.

#### Vibration-Rotation Interaction.

Bass and Broida, 1953,<sup>27</sup> found that the rotational temperatures, obtained from the relative intensities of rotational lines within a given vibrational band, varied significantly from band to band (in the emission spectrum of a hydrogen-oxygen flame), even for those bands with the same initial vibrational state. They suggested that the most probable explanation of the discrepancy was the neglect of vibration-rotation interaction in the theory of transition probabilities.

Learner and Gaydon, 1959,<sup>28</sup> and Learner, 1962,<sup>18</sup> discussed the effect of vibration-rotation interaction in electronic transitions, showing that it is not always negligible. Learner included the correction term  $T_{J',J''}$  into equation (1.1), giving

$$f_{J',J''} = f_{v',v''} S_{J',J''} T_{J',J''} / (2J'' + 1)$$

$$= \sqrt{p_{v',v''}} S_{J',J''} T_{J',J''} / (2J'' + 1) \quad \dots (1.2)$$

to account for vibration-rotation interaction. Now  $f_{v',v''}$  and  $p_{v',v''}$  are for the rotationless molecule, for which  $T_{J',J''} = 1$ .  $T_{J',J''}$  depends both on the angular momenta  $J'$  and  $J''$ , as well as the band ( $v',v''$ ) concerned. Learner calculated the effect of the interaction in the  $A^2\Sigma^+ - X^2\Pi$  system of OH using Morse-Pekeris (Pekeris, 1934<sup>29</sup>) wave functions and the value  $R_0(r) = e^{-2.5r}$ , obtained by fitting his

theoretical band strengths to the "smoothed" values of Nicholls, 1956.<sup>25</sup> He presented a table of  $T_{J',J''}$  values for all bands with  $v', v'' \leq 5$ , and  $J''$  up to 25. He also calculated the corrections  $\Delta T$  required to be added to rotational temperatures  $T$  determined without taking vibration-rotation interaction into account, and plotted  $\Delta T$  as a function of  $T$ .

James, 1959,<sup>30</sup> also discussed the effect of vibration-rotation interaction on the relative intensities of rotational lines within a given band, and hence on rotational temperature determinations. He used Nicholls', 1956,<sup>25</sup> form for the electronic transition moment  $R_0(r) = \text{const.}(1 - 0.756r)$ , and a comparatively crude form for the potential function for different rotational states of each electronic state. The potential functions were parabolas, effectively shifted towards increasing values of internuclear distance, to account for centrifugal distortion, with increasing rotational quantum number,  $J$ . The parabola for each  $J$ -value was chosen to fit the true potential curve near the equilibrium position.

Zirnan and Bogdan, 1964,<sup>31</sup> used the  $R_2(0,0)$  and  $R_2(1,0)$  branches in the OH ultra-violet system to determine rotational temperatures in various hydrogen flames, from both emission and absorption spectra. The temperatures obtained using the Learner<sup>18</sup> correction were self-consistent, while those obtained using the James<sup>30</sup> correction were not. The Learner correction also gave temperatures in good agreement with the sodium-line reversal temperature, but for a hydrogen-oxygen flame at 1 atmosphere, the emission temperature was significantly higher than the absorption temperature.

### 1.3. Choice of Method

In order to evaluate the magnitude of the vibration-rotation interaction effect in the (0,0) band, it is necessary to determine the relative oscillator strengths of several lines in one or more branches of the band. According to Learner's calculations,<sup>18</sup> the interaction results in a drop of about 10% in the effective transition probability of the band over the first 15 lines in each branch. In order to establish the presence of an effect of this magnitude, it would be necessary for the final experimental error in the measurements on each line to be significantly smaller.

Apart from the anomalous dispersion or "hook" method, almost all investigations require absolute or relative intensity measurements. Not only are such methods tedious on account of the various calibration experiments involved, but they are also of limited accuracy, on account of trouble with resolving power or the need to know the line profile.

It is also desirable to obtain measurements of the absolute  $f$ -values by means of a previously untried method based on assumptions different from those made by previous investigators.

The hook method has been frequently used to measure  $f$ -values of atomic transitions to a high degree of accuracy, but has not been applied before to molecular spectra, so far as the author is aware. Apart from yielding independent values of the  $f$ -values of the (0,0) and (1,0) bands, it is a particularly suitable way of obtaining relative transition probabilities for a number of lines having a common lower state. Its advantages over the various methods involving absorption coefficients are that it is independent of the line shape, and there is no need to

correct for the finite instrumental width of the spectrograph.

The hook method shares with most of the other techniques the disadvantage that a calculation of OH concentration is required before absolute  $f$ -values are obtained. This is the chief source of error in the determinations of the absolute values, even when the absorbing medium is in thermal equilibrium, on account of the uncertainties in the OH population ( $\sim 8\%$ ) produced by even a small ( $\sim 3\%$ ) uncertainty in the dissociation energy. However, this disadvantage does not apply to the determinations of the relative  $f$ -values when thermal equilibrium is assured.

Having regard to the above considerations, this investigation was designed to measure absolute  $f$ -values by the hook method.

#### 1.4. Outline of the Hook Method

The technique adopted is based on the hook method initially used by Roschdestwensky for anomalous dispersion measurements on the sodium D lines, 1912,<sup>32</sup> 1921.<sup>33</sup>

In an earlier version of this method devised by Puccianti, 1901,<sup>34</sup> 1904,<sup>35</sup> horizontal zero order fringes from a Jamin interferometer are focussed on the slit of a stigmatic spectrograph. A set of horizontal fringes traverses the continuous spectrum of the background source viewed through the spectrograph. One of the beams in the interferometer passes through a tube containing the gas or vapour to be investigated, and the other beam passes through an evacuated compensating tube of equal length. Near an absorption line of the medium investigated, the

refractive index changes rapidly with wavelength, resulting in a displacement of the fringes near the line so that they trace out the hyperbolic variation of the refractive index on either side of it. The hyperbolic curves near each line are related to  $N$ ,  $f$  and  $l$ , which are the number density of absorbing atoms (or molecules) in the lower state of the transition, its  $f$ -value, and the path length of the medium, respectively.

Roschdestwensky showed that when a plane parallel glass plate is introduced into the beam traversing the compensating tube, the interference fringes observed through the spectrograph were inclined fringes of high order. The gradient of the fringes is such that their slope is in the opposite direction to that of the rapid change near the absorption lines, so that the two effects combine to produce symmetrically placed maxima and minima on either side of each absorption line. The relation between anomalous dispersion and  $f$ -value is simplified to the extent that the product  $Nf^2l$  is now proportional to the square of the separation of the maxima and minima along the wavelength direction. By measuring these separations for lines arising from the same lower state, their relative  $f$ -values are easily obtained. In order to obtain the absolute  $f$ -values of the lines, it is usually necessary to obtain the population density of absorbing centres in the lower state of the transitions. It is interesting to see that recently Ostrovskii and Penkin, 1961,<sup>36,37</sup> have eliminated this requirement, obtaining absolute  $f$ -values in Na, Ca, Br, and Sr spectra by combining anomalous dispersion measurements with photoelectric measurements of the equivalent widths of the absorption

lines. This technique must fulfil two conditions, if it is not to give erroneously high f-values. First, the medium investigated must be sufficiently optically thick for the equivalent width ( $A_\lambda$ ) to be large compared with the Doppler width ( $\Delta\lambda_D$ ) -  $A_\lambda/\Delta\lambda_D > 10$ . Secondly, the density and pressure of the medium must be sufficiently low for the time interval between collisions to be large compared to the radiative lifetime of the upper state of the transition investigated.

CHAPTER II

THEORETICAL (A) - TRANSITION PROBABILITIES IN OH

2.1. The Einstein Transition Probabilities and Wave Mechanics

Einstein laid the basis for the theoretical work on the interaction between radiation and matter in terms of transition probabilities. He defined three probability coefficients,  $A_{mn}$ ,  $B_{mn}$  and  $B_{nm}$ , relating two atomic or molecular states  $m$  and  $n$ , such that absorption of radiation of frequency between  $\nu$  and  $\nu + d\nu$  by the atom or molecule when in state  $n$  would raise it to the state  $m$ .

- (1)  $B_{nm}I_\nu$  is the probability per second that the molecule, say, in state  $n$  would absorb a quantum  $h\nu$  when exposed to isotropic radiation of frequency between  $\nu$  and  $d\nu$  and intensity  $I_\nu$  and so pass to state  $m$ .
- (2)  $A_{mn}$  is the probability per second that the molecule in state  $m$  will spontaneously emit, in a random direction, a quantum  $h\nu$  and pass to state  $n$ .
- (3)  $B_{mn}I_\nu$  is the probability per second that the molecule in state  $m$  will undergo the transition to state  $n$  when it is exposed to isotropic radiation of frequency between  $\nu$  and  $\nu + d\nu$  and intensity  $I_\nu$ , thereby emitting a quantum  $h\nu$  in the same direction as the stimulating radiation.

From a consideration of the thermodynamic equilibrium between radiation and matter in a Hohlraum, Einstein obtained the following relations between these quantities:

$$\left. \begin{aligned} \frac{A_{mn}}{B_{mn}} &= \frac{2h\nu^3}{c^2} \\ \text{and } \frac{B_{mn}}{B_{nm}} &= \frac{g_n}{g_m} \end{aligned} \right\} \dots(2.1),$$

where  $g_m$  and  $g_n$  are the degeneracies of the states  $m$  and  $n$  respectively,  $c$  is the velocity of light, and  $h$  is Planck's constant. The relation between the classical oscillator strength, or  $f$ -value, and the Einstein transition probability for spontaneous emission is well known and given by

$$f_{mn} = \frac{mc^3}{8\pi^2e^2} \frac{g_m}{g_n} \frac{A_{mn}}{\nu^2} \dots(2.2),$$

where  $e$  and  $m$  are the electronic charge and mass respectively - see, for example, Mitchel and Zemansky, 1934, p.97.<sup>38</sup>  $f$  may be defined as the number of classical oscillators which give the same absorption for a given transition as a real atom.

The interaction of an electromagnetic wave with an atomic or molecular system is, in a first approximation, the interaction with the (variable) electric dipole moment of the system. There are also interactions with the magnetic dipole moment and the electric quadrupole moment, but their magnitudes are usually, respectively, about  $10^{-5}$  and  $10^{-8}$  times the magnitude of the electric dipole interaction. By introducing this electric dipole interaction into the wave equation, Dirac showed that the probability of a transition between two states  $m$  and  $n$  on account of this interaction is proportional to the square of the magnitude of the vector  $R^{mn}$ , the time-averaged matrix element of the electric moment. The relation between the Einstein transition



probability and the electric dipole moment matrix element is well known - see, for example, Herzberg, 1950, p.21<sup>39</sup> - and is given by

$$A_{mn} = \frac{64\pi^4}{3hc^3} \frac{\nu^3}{E_{mn}} |R^{mn}|^2 \quad \dots(2.3).$$

The components of  $R^{mn}$  along three co-ordinate axes, taking the z-axis as the internuclear axis in a diatomic molecule for convenience in later discussions, are given by

$$R_x^{mn} = \int \psi_m^* M_x \psi_n d\tau, \text{ etc.} \quad \dots(2.4),$$

where  $M_x = \sum_k e_k x_k$ , etc.

Here  $e_k$  are the charges of each of the particles whose co-ordinates are  $x_k, y_k, z_k$ , and  $\psi_m$  and  $\psi_n$  are the eigenfunctions of the two states.  $M_x$ , etc. are the instantaneous dipole moment components, and the integration is taken over the whole of space.

$R^{mn}$ , the dipole length matrix element, is equivalent to  $V^{mn}$ , the dipole velocity matrix element, where

$$V_x^{mn} = \frac{1}{E_{mn}} \int \psi_m^* \nabla_x \psi_n d\tau, \text{ etc.},$$

and  $\nabla_x = \sum_k \frac{e_k}{m_k} \frac{\partial}{\partial x_k}$ , etc.,

$m_k$  is the mass of the  $k^{\text{th}}$  particle, and  $E_{mn}$  is the energy difference between the two states.

$R^{mn}$  is zero if the transition under consideration is forbidden as a dipole transition. If  $R^{mn}$  is non-zero, then the two states combine

with each other with emission or absorption of radiation, with a definite probability. The selection rules for dipole radiation limit the number of components  $R_x^{mn}$ ,  $R_y^{mn}$ ,  $R_z^{mn}$ , to one component for each type of transition, "parallel" or "perpendicular". A parallel transition is one where the two states  $m$  and  $n$  have the same quanta of electronic angular momentum, and a perpendicular transition is one where those electronic angular momenta differ by one quantum. For parallel transitions only  $R_z^{mn}$  is non-zero, while for perpendicular transitions, only  $R_x^{mn}$  or  $R_y^{mn}$  is non-zero, as given by Mulliken, 1939.<sup>40</sup> Evaluation of the integral (2.4) to give the dipole matrix element, or transition moment as it is sometimes called, requires a knowledge of the wave functions.

## 2.2. The Born-Oppenheimer Approximation

In a diatomic molecule having  $n$  electrons, there are  $3n + 6$  independent variables and the generation of accurate forms for the wave functions of the molecule is thus very difficult. The way round this exceedingly difficult problem is to use perturbation theory. Born and Oppenheimer showed how this could be handled by successive approximations amounting to an expansion in powers of  $(m/M)^{1/2}$ , where  $m$  is the electronic mass and  $M$  is of the order of the nuclear mass. Their work justifies the postulate that the co-ordinates of the nuclei remain approximately separable from those of the electrons in the Schrödinger equation - see Herzberg, 1950, p.148;<sup>39</sup> Condon, 1928.<sup>41</sup> This can be explained semi-classically by saying that the nuclear motion is so much slower

than the electronic motion, on account of the much larger mass, that the electrons can adapt themselves continuously to the changing electronic levels. The quantum mechanical criterion for the validity of this adiabatic approximation is that the energy spacing of the states of nuclear motion should be very much smaller than the spacing of the electronic levels. The basis for the approximation is that there is negligible interaction between the nuclear and electronic motions of the molecules.

The total eigenfunction of the molecule can therefore be written in this approximation as

$$\Psi = \Psi_e(r_e, r) \Psi_n(r) \quad \dots(2.5).$$

$\Psi_e(r_e, r)$  is the solution of the Schrödinger equation for the electrons moving in the field of the fixed nuclei and having a potential energy  $V_e$  which is a function both of the internuclear distance  $r$ , and the electronic co-ordinates symbolised by  $r_e$ . The eigenvalues obtained for the electronic motion are thus functions of  $r$ , and are given by  $E_e(r)$ .  $\Psi_n(r)$  is the solution of the Schrödinger equation for the nuclei moving in the potential  $E_e(r) + V_n(r)$ , where  $V_n(r)$  is the potential of the nuclei in the field of the repulsive Coulomb force between them. It is often also assumed that the nuclear eigenfunction  $\Psi_n(r)$  can be split into two parts, giving

$$\Psi_n(r) = \Psi_v(r) \frac{1}{r} \Psi_{J\Lambda}(\theta, \varphi) \quad \dots(2.6).$$

$\Psi_v(r)$  is the radial eigenfunction for the motion of the nuclei in the vibrational mode, described by the quantum number  $v$ .  $\Psi_{J\Lambda}(\theta, \varphi)$  is

the angular part of the nuclear eigenfunction associated with the rotation of the nuclei about an axis perpendicular to the internuclear axis, where  $J$  is the quantum number of the total angular momentum of the molecule and  $\Lambda$  is the quantum number of the orbital angular momentum of the electrons in the direction of the internuclear axis.

Further, the total dipole moment  $M$  of the molecule may be represented as the sum of contributions due to the electrons ( $M_e$ ) and nuclei ( $M_n$ ) alone. Let us suppose, in the following discussion, that we are dealing with a parallel-type transition, so that we now require only the z-component of the molecular dipole moment,  $M_z = M \cos \theta$  in order to calculate the dipole matrix element  $R$ . Denoting the upper state by one prime, and the lower state by two, and denoting the nuclear and electronic co-ordinates by  $\tau_n$  and  $\tau_e$  respectively, we have

$$R_z = \int \psi'_0(r_e, r) \psi'_{v'}(r) \frac{1}{r} \psi'_{J'\Lambda'}(\theta, \varphi) (M_e + M_n) \cos \theta \\ \times \psi''_0(r_e, r) \psi''_{v''}(r) \frac{1}{r} \psi''_{J''\Lambda''}(\theta, \varphi) d\tau_e d\tau_n \dots (2.7).$$

Since  $d\tau_n = r^2 \sin \theta dr d\theta d\varphi$ , we now have

$$R_z = \int \psi'_0(r_e, r) \psi'_{v'}(r) (M_e + M_n) \psi''_0(r_e, r) \psi''_{v''}(r) d\tau_e dr \\ \times \int \psi'_{J'\Lambda'}(\theta, \varphi) \psi''_{J''\Lambda''}(\theta, \varphi) \sin \theta \cos \theta d\theta d\varphi \dots (2.8).$$

The second half of the integral (2.8) depends only on the statistical weight and the coupling in the states concerned, and may be represented by  $S_{J''\Lambda''}^{J'\Lambda'}$ .  $S_{J''\Lambda''}^{J'\Lambda'}$  is often referred to as the rotational line strength,

and was first given by Hönl and London, 1925,<sup>42</sup> on the basis of the old quantum theory, and later justified on a wave mechanical basis by Dennison, 1926,<sup>43</sup> Rademacher and Reiche, 1927,<sup>44</sup> and others.

We thus have, dividing (2.8) into its electronic and nuclear components, that

$$R_z = S_{J_e \Lambda_e}^{J_e \Lambda_e} \left[ \int \psi_e^v(r_e, r) \psi_{v'}^v(r) M_e \psi_e^{v''}(r_e, r) \psi_{v''}^{v''}(r) d\tau_e dr \right. \\ \left. + \int \psi_e^v(r_e, r) \psi_{v'}^v(r) M_n \psi_e^{v''}(r_e, r) \psi_{v''}^{v''}(r) d\tau_e dr \right] \\ \dots(2.9).$$

In the second integral of (2.9), we have  $M_n$ , which is independent of  $\tau_e$ , so that

$$\int \psi_e^v(r_e, r) \psi_{v'}^v(r) M_n \psi_e^{v''}(r_e, r) \psi_{v''}^{v''}(r) d\tau_e dr \\ = \int \psi_{v'}^v(r) M_n \psi_{v''}^{v''}(r) dr \int \psi_e^v(r_e, r) \psi_e^{v''}(r_e, r) d\tau_e \\ \dots(2.10).$$

Now the electronic eigenfunctions of a molecule form an orthogonal set, and so  $\int \psi_e^v(r_e, r) \psi_e^{v''}(r_e, r) = 0$ , reducing (2.9) to the one term. Integrating this separately over the nuclear and electronic co-ordinates, we have

$$R_z = S_{J_e \Lambda_e}^{J_e \Lambda_e} \int \psi_{v'}^v(r) \psi_{v''}^{v''}(r) dr \int \psi_e^v(r_e, r) M_e \psi_e^{v''}(r_e, r) d\tau_e \\ \dots(2.11).$$

The integral with regard to the electronic components,

$$R_e(r) = \int \psi_e^v(r_e, r) M_e \psi_e^{v''}(r_e, r) d\tau_e \\ \dots(2.12),$$

is called the electronic transition moment, as in Herzberg, 1950, p.200.<sup>39</sup>

The intensity in emission of the transition from one electronic-vibrational-rotational state to the corresponding lower state is thus given by

$$I_{em} = \frac{64\pi^4}{3c^3} N^u \nu^4 S_{J^u \Lambda^u}^{J^l \Lambda^l} \left| \int \psi_{v^u}^e(r) R_e(r) \psi_{v^l}^e(r) dr \right|^2 \dots(2.13).$$

where  $N^u$  is the population density of the upper state.

Not much can be said about  $R_e(r)$  in general, on account of the great difficulty in obtaining accurate expressions for the electronic wave functions. However, its most important property is its variation with internuclear distance. It is often assumed to be a constant, or a slowly varying function of  $r$ , so that its mean value  $\bar{R}_e$  may be removed from inside the integral (2.11), giving

$$R_z = S_{J^u \Lambda^u}^{J^l \Lambda^l} \bar{R}_e \int \psi_{v^u}^e(r) \psi_{v^l}^e(r) dr \dots(2.14).$$

and this is the basis of the wave mechanical formulation of the Franck-Condon principle - Franck, 1925;<sup>45</sup> Condon, 1926,<sup>46</sup> 1928,<sup>41</sup> 1947.<sup>47</sup> When (2.14) holds, (2.13) becomes

$$I_{em} = \frac{64\pi^4}{3c^3} N^u \nu^4 S_{J^u \Lambda^u}^{J^l \Lambda^l} \bar{R}_e^2 \left| \int \psi_{v^u}^e(r) \psi_{v^l}^e(r) dr \right|^2 \dots(2.15).$$

The integral  $\int \psi_{v^u}^e(r) \psi_{v^l}^e(r) dr$  is called the overlap integral, and its square is the Franck-Condon factor  $q_{v^u, v^l}$  for the electronic-vibrational states concerned. For a constant, or slowly varying electronic transition moment, we see that the intensity of a transition is proportional to the Franck-Condon factor. If the eigenfunctions are

properly normalised, then it follows from the properties of systems of orthogonal functions that

$$\sum_{v''} q_{v',v''} = \sum_{v''} q_{v',v''} = 1.$$

The vibrational eigenfunctions  $\Psi_v$  are oscillatory functions of  $r$  - see Fig. (2.1), section 2.4 - with particularly large amplitudes near the extremes of the vibrational motion. Consequently the Franck-Condon factor in (2.15) is large when the eigenfunctions are in phase, as it were, particularly when the terminal maxima cover the same range of  $r$ . The potential functions for a harmonic oscillator (which are fair approximations for small  $v', v''$ ) are parabolic, and consequently the locus of the strong bands on a Deslandres' array is also approximately parabolic. When the equilibrium values  $r_{eq}^o, r_{eq}''$  of the two electronic states are approximately equal, this locus is a narrow parabola, and if  $r_{eq}^o$  and  $r_{eq}''$  differ widely, then the locus is a wide parabola.

Mulliken, 1939,<sup>40</sup> and Condon, 1947,<sup>47</sup> state that the value of the electronic transition moment is a characteristic of the pair of electronic levels concerned, and is independent of the vibrational and rotational levels involved. Hence Mulliken, 1939,<sup>40</sup> states that

$$\left. \begin{aligned} \sum_{v''} p_{v',v''} &= \text{constant} \\ \text{and } \sum_{v''} p_{v',v''} &= \text{constant} \end{aligned} \right\} \dots(2.16),$$

where

$$p_{v',v''} = \left| \int \Psi_{v'}^o(r) R_e(r) \Psi_{v''}''(r) dr \right|^2 \dots(2.17).$$

$P_{v^0 v^0}$  is called the "Vibrational transition probability", or "Band Strength".

The rotational line strengths  $S_{J^0 \Lambda^0}^{J^0 \Lambda^0}$  obey the sum rules,

$$\left. \begin{aligned} \sum_{J^0} S_{J^0 \Lambda^0}^{J^0 \Lambda^0} &= \text{const.} \times (2J^0 + 1) \\ \text{and } \sum_{J^0} S_{J^0 \Lambda^0}^{J^0 \Lambda^0} &= \text{const.} \times (2J^0 + 1) \end{aligned} \right\} \dots(2.18).$$

The rotational line strengths are usually normalised so that the constant in equation (2.18) is equal to 1, although Dieke and Crosswhite, 1948,<sup>21</sup> normalise their  $S_{J^0 \Lambda^0}^{J^0 \Lambda^0}$  to make the constant equal to 4.

### 2.3. The Ultra-Violet Band Spectrum of OH

Dieke and Crosswhite, 1948,<sup>21</sup> give an account of the discovery, analysis, and identification of the transition that gives rise to the ultra-violet band system  $A^2\Sigma^+ - X^2\Pi$  in OH. They also present comprehensive tables of wavelength, identification, line strength, etc. relating to the transition. About sixteen bands of the system have been observed in the wavelength region 2400 to 3500 Å, each band consisting of six strong and six weak branches. The vibrational intensity distribution corresponds to a fairly narrow Franck-Condon parabola, as a consequence of the nearly equal values,  $r_0^0 = 1.0121$  and  $r_0^0 = 0.9706$  Å, of the equilibrium internuclear distances of the two electronic states. The observed vibrational quantum numbers go up to  $v^0$  and  $v^0 = 3$ .

There are five different ways, Hund's cases (a) to (e), of



relating the interactions between the various types of angular momenta of the molecule, so as to account for the structure of the spectra of diatomic molecules. For OH, the coupling between the momenta is intermediate between case (a) and case (b).

In case (a), the total orbital angular momentum  $L$  and the total spin  $S$  of the electrons are strongly coupled both to each other, and to the internuclear axis of the molecule. Their resultants along this axis  $\Lambda$  and  $\Sigma$  are both quantised,  $\Lambda$  being integral, and  $\Sigma$  taking integral or half-integral values, depending on whether the number of electrons in the molecule is even or odd respectively. The total electronic angular momentum along the internuclear axis is given by  $\Omega = \Lambda + \Sigma$ .  $\Omega$  can take values from  $(L + S)$  down to  $|(L - S)|$  in integral steps. The total angular momentum, including rotation of the molecule, is also quantised and is given by  $J = \Omega, \Omega + 1, \Omega + 2 \dots$ . (all values of angular momenta are in terms of units  $\frac{h}{2\pi}$ ). The rotational energy of the molecule can be represented, to a good approximation, by  $E_J = B[J(J + 1) - \Omega^2]$ , where  $B$  is a constant, depending on the molecule and its vibrational state. We see that in case (a) the coupling between the nuclear (rotational) and electronic motions is negligible, and hence the Born-Oppenheimer approximation should be fairly accurate.

In case (b), only the orbital angular momentum is strongly coupled to the internuclear axis. Here the rotational motion is described in terms of  $K$ , the angular momentum quantum number for the resultant of electron orbital and molecular rotational motion.  $K$  is an integer

given by  $K \geq \Lambda$ . The rotational energy is now given by  $E_K = B[K(K+1) - \Lambda^2]$ . Now the electron spin  $S$  is coupled to the resultant  $K$  of the orbital and rotational motions, to give the total angular momentum  $J$  of the molecule. Here we have some interaction between the nuclear and electronic motions, and there is obviously a breakdown of the Born-Oppenheimer approximation with regard to the rotational and electronic motions.

For electronic states with  $\Lambda = 0$ , case (b) affords the best description, while the states with  $\Lambda \neq 0$  are usually intermediate between case (a) and case (b), and the nomenclature of either is appropriate. As the molecule rotates faster and faster, and  $K$  increases, the state of the molecule moves closer to that of case (b).

In the OH radical, the electron spin has the value  $\frac{1}{2}$ , producing doublet electronic levels. The two components will be characterised by the subscripts 1 and 2, so that for  $F_1(K)$ ,  $f_1(K)$ ,  $J = K + \frac{1}{2}$ ; and for  $F_2(K)$ ,  $f_2(K)$ ,  $J = K - \frac{1}{2}$ .  $F_1(K)$  and  $F_2(K)$  are used for the rotational levels of the  ${}^2\Sigma^+$  state ( $\Lambda = 0$ ), while  $f_1(K)$  and  $f_2(K)$  correspond to those of the  ${}^2\Pi$  state ( $\Lambda = 1$ ).

### The ${}^2\Sigma^+$ state

Here there is no orbital electronic motion, and the electron spin is loosely coupled to the nuclear rotation - case (b). The two doublet components  $F_1(K)$ ,  $F_2(K)$  nearly coincide for  $K = 0$ , but there is a  $\rho$ -type doubling for  $K \neq 0$ , due to the magnetic coupling between the electron spin and the rotation of the nuclei - Van Vleck, 1929.<sup>48</sup> The

rotational energies are given by

$$\left. \begin{aligned} F_1(K) &= BK(K+1) - DK^2(K+1)^2 + R(K + \frac{1}{2}) \\ \text{and } F_2(K) &= BK(K+1) - DK^2(K+1)^2 - R(K + \frac{1}{2}) \end{aligned} \right\} \dots(2.19),$$

where the term  $-DK^2(K+1)^2$  allows for the effect of centrifugal distortion of the molecule by rotation. (All the constants are functions of the vibrational quantum number  $v^0$ .)

### The $2\Pi$ State

For OH, the  $2\Pi$  state is close to case (a) for slow rotation and close to case (b) for fast rotations, so that the intermediate case must be considered. Hill and Van Vleck, 1928,<sup>49</sup> found that the rotational energy of a  $2\Pi$  state may be given by

$$f_{1,2} = B \left[ (J + \frac{1}{2})^2 - 1 \pm \frac{1}{2} \sqrt{\{(2J+1)^2 + a(a-4)\}} \right] - DJ^2(J+1)^2 \dots(2.20),$$

where  $a$  is the so-called coupling constant. Expressed in terms of  $K$ , the levels are

$$\begin{aligned} f_1(K) &= B \left[ (K + \frac{1}{2})^2 - 1 - \frac{1}{2} \sqrt{\{4(K+1)^2 + a(a-4)\}} \right] - DK^2(K+1)^2 \\ f_2(K) &= B \left[ K^2 - 1 + \frac{1}{2} \sqrt{\{4K^2 + a(a-4)\}} \right] - DK^2(K+1)^2 \end{aligned} \dots(2.21).$$

The coupling constant  $a$  has a value related to the degree of intermingling of the two coupling cases. When  $a$  is small, the state is near case (b), and when  $a$  is large, it is near case (a).

Both  $f_1$  and  $f_2$  are double. This splitting is called

" $\Lambda$ -doubling", and may be explained by a slight interaction between the electron orbital angular momentum and the rotation of the nuclei - Van Vleck, 1929.<sup>48</sup> In the first approximation, the difference between the split energy levels is proportional to  $K(K + 1)$ . The two components are called  $f_i$  and  $f_i'$ . They have opposite symmetry ( $\Pi_i^+$  and  $\Pi_i^-$ ) with respect to inversion at the origin of co-ordinates. ( $\Lambda$ -doubling may also be explained as a perturbation between levels, in different electronic states, having equal  $J$  and the same symmetry.)

### The $2\Sigma^+ - 2\Pi$ Transitions

For dipole transitions in the free molecule the selection rule for  $J$ ,  $\Delta J = 0, \pm 1 (J = 0 \nrightarrow J = 0)$ , must be strictly satisfied. For case (b), the selection rule for  $K$ ,  $\Delta K = 0, \pm 1$  also applies. In intermediate coupling, transitions that satisfy both selection rules, and for which  $\Delta K = \Delta J$ , are strong, while those that violate the  $K$  rule or for which  $\Delta K \neq \Delta J$  are weak, except for small values of  $K$  and  $J$ . In addition, the symmetry rule even  $\leftrightarrow$  odd is also strict for the free molecule. With these selection rules there are twelve possible branches; six strong "main" branches, and six "satellite" branches whose intensity falls off rapidly after the first few lines, as the coupling gets closer to case (b).

The branches are named below for case (b), which is more convenient in this case.

O branch for  $K - 2 \rightarrow K$

P branch for  $K - 1 \rightarrow K$

Q branch for  $K \rightarrow K$

R branch for  $K + 1 \rightarrow K$

S branch for  $K + 2 \rightarrow K$

|             |                |              |                       |
|-------------|----------------|--------------|-----------------------|
| $O_{12}(K)$ | $= F_1(K - 2)$ | $- f_2^0(K)$ | $J - 1 \rightarrow J$ |
| $P_1(K)$    | $= F_1(K - 1)$ | $- f_1(K)$   | $J - 1 \rightarrow J$ |
| $P_2(K)$    | $= F_2(K - 1)$ | $- f_2(K)$   | $J - 1 \rightarrow J$ |
| $P_{12}(K)$ | $= F_1(K - 1)$ | $- f_2(K)$   | $J \rightarrow J$     |
| $Q_1(K)$    | $= F_1(K)$     | $- f_1^0(K)$ | $J \rightarrow J$     |
| $Q_{21}(K)$ | $= F_2(K)$     | $- f_1^0(K)$ | $J - 1 \rightarrow J$ |
| $Q_2(K)$    | $= F_2(K)$     | $- f_2^0(K)$ | $J \rightarrow J$     |
| $Q_{12}(K)$ | $= F_1(K)$     | $- f_2^0(K)$ | $J + 1 \rightarrow J$ |
| $R_1(K)$    | $= F_1(K + 1)$ | $- f_1(K)$   | $J + 1 \rightarrow J$ |
| $R_{21}(K)$ | $= F_2(K + 1)$ | $- f_1(K)$   | $J \rightarrow J$     |
| $R_2(K)$    | $= F_2(K + 1)$ | $- f_2(K)$   | $J + 1 \rightarrow J$ |
| $S_{21}(K)$ | $= F_2(K + 2)$ | $- f_1^0(K)$ | $J + 1 \rightarrow J$ |

Diöke and Crosswhite, 1948,<sup>21</sup> tabulated the relative rotational transition probabilities (or rotational line strengths)  $S_{J''A''}^{J'A'}$  from Earls, 1935,<sup>50</sup> Hill and Van Vleck, 1928.<sup>49</sup> These expressions replace the Hönl-London factors which are only valid for case (a), where the Born-Oppenheimer approximation holds fairly well. Diöke and Crosswhite, 1948,<sup>21</sup> 1949,<sup>22</sup> also published experimental values for the relative transition probabilities  $p_{v''v''}/p_{CO}$  for nine of the vibrational bands

in the system. These values are given in a Deslandres array in Table (2.1). The photoelectrically determined and thus more reliable values<sup>22</sup> are tabulated and the sums  $\sum_{v''} P_{v^0 v''} / p_{00}$  are given on the right hand side of the array, in order to evaluate the validity of the Born-Oppenheimer approximation for OH with regard to electronic-vibrational interaction. The values given in brackets are estimated values for intensities of transitions from the upper and less populated vibrational levels, for which the intensities in emission were too low to be determined. The estimations were made with regard to the intensity distribution in the experimental array. The sums  $\sum_{v''} P_{v^0 v''} / p_{00}$  including these values are likewise given in brackets.

It can be seen from Table (2.1) that the sum  $\sum_{v''} P_{v^0 v''} / p_{00}$  cannot be regarded as a constant. Even considering only the experimental values, there is a difference of 27% between the extreme values of the sum. When the reasonably estimated numbers are included, this difference increases to about 50% between  $v^0 = 0$  and  $v^0 = 3$ . It is thus obvious that requirement (2.16) for negligible interaction between the vibrational and electronic motions does not hold for OH.

Table 2.1. Relative Experimental Transition Probabilities  $P_{v^0 v''} / p_{00}$ .

| $v^0 \downarrow$<br>$v'' \rightarrow$ | 0     | 1     | 2   | 3    | 4    | $\sum_{v''} P_{v^0 v''} / p_{00}$ |
|---------------------------------------|-------|-------|-----|------|------|-----------------------------------|
| 0                                     | 1000  | 5     |     |      |      | 1005                              |
| 1                                     | 480   | 780   | 13  |      |      | 1273                              |
| 2                                     | (150) | 680   | 520 | (25) |      | 1200 (1375)                       |
| 3                                     | (40)  | (340) | 810 | 300  | (25) | 1110 (1515)                       |

#### 2.4. The Morse-Pekeris Rotating Oscillator

In determinations of the solution of the Schrödinger equation for the nuclear motions for intensity work, it has usually been assumed that the solution  $\Psi_n(r)$  is separable into mutually independent vibrational and rotational parts, as given by (2.6). The interaction between rotation and vibration has however been recognised for many years in terms of the energy levels in the variation of the rotational constant  $B$  with vibrational quantum number. Dunham, 1932,<sup>51</sup> showed that the energy levels of an anharmonic oscillator could be represented by the double infinite sum

$$E_{vJ} = \sum_v \sum_J Y_{vj} (v + \frac{1}{2})^j J(J+1)^j \quad \dots(2.22),$$

which includes terms which are combinations of powers of both variables  $(v + \frac{1}{2})$  and  $J(J+1)$ , as well as terms in powers of each variable independently. Learner, 1961,<sup>52</sup> 1962,<sup>18</sup> has discussed the effects of the separability approximation (2.6) on the intensities of electronic transitions of diatomic molecules in detail.

The potential function most commonly used to obtain the vibrational eigenfunctions and eigenvalues has been that for the rotationless molecule. However this is only the founder member of a set of potential functions, one for each value of the rotational quantum number. The set may be represented by

$$U(r)_J = U(r) + \frac{h^2}{8\pi^2} \frac{J(J+1)}{\mu r^2} \quad \dots(2.23),$$

where  $U(r)$  is the potential function for the rotationless molecule.

The added term represents the kinetic energy of rotation, the moment of

inertia being  $\mu r$ , where  $\mu$  is the reduced mass of the diatom. The importance of the added term to intensity calculations is that the resulting shift of the potential curves to increasing values of  $r$  is not always negligible, particularly for hydrides with low dissociation energy (e.g.  $\text{HgH}$ , as shown by Herzberg, 1950, p.427<sup>39</sup>). If the relative shift of the potential energy curves, and hence the wave-functions, of two combining electronic states, is large enough with increasing values of  $J$ , then the overlap integral and the vibrational transition probabilities for the bands may be expected to vary significantly with  $J$ .

Methods of performing relative intensity calculations for the rotating oscillator are few in number. Herman and Rubin, 1955,<sup>53</sup> treated analytically the infra-red spectrum of a Morse-Pekeris oscillator, where the eigenfunctions are for different vibrational states of the same electronic potential function. This analytical approach cannot be extended to include electronic transitions in molecules, since the eigenfunctions now belong to different electronic potential curves and have different constants. Nicholls and Fraser, 1958,<sup>54</sup> have shown that their analytical approach for the rotationless case can be extended to include rotation. Learner and Gaydon, 1959,<sup>28</sup> and Learner, 1961,<sup>52</sup> 1962,<sup>18</sup> performed numerical integrations of Morse-Pekeris wave functions. James, 1959,<sup>30</sup> developed an approximate method in which the rotational energy term serves to displace a parabolic potential function to higher values of internuclear distance with increasing  $J$ .

The potential function for the Morse-Pekeris rotating oscillator is given by



$$U(r) = D_e \left[ 1 - e^{-\beta(r-r_e)} \right]^2 + \frac{h^2}{8\pi^2} \frac{J(J+1)}{\mu r^2} \quad \dots (2.24),$$

where  $\beta = \left( \frac{8\pi^2 D_e}{B r_e^2} \right)^{\frac{1}{2}}$ , and  $D_e = \frac{\omega^2}{4\pi^2 \nu}$ , the dissociation energy.

The following functions are defined:

$A$  = the rotational energy,

$W$  = the total nuclear energy, measured from the potential minimum.

The eigenfunctions are given by

$$\Psi_{vJA} = N_0 e^{-dy} (2dy)^{b/2} {}_1F_1(-v, b+1; 2dy) \quad \dots (2.25),$$

in which

$$N_0 = \beta^{\frac{1}{2}} \left( \frac{v+b}{v} \right)^{\frac{1}{2}} \left[ \Gamma(b) \right]^{-\frac{1}{2}}, \quad b^2 = - \left[ \frac{32\pi^2 \mu}{\beta^2 h^2} \right] \left[ W - A(3\varepsilon^2 - \varepsilon + 1) \right],$$

$$dy = \left[ \left\{ \frac{8\pi^2 \mu}{\beta^2 h^2} \right\} \left\{ D_e + A(3\varepsilon^2 - \varepsilon) \right\} \right] e^{-\beta(r-r_e)}, \quad \varepsilon = \frac{1}{\beta r_e},$$

and  ${}_1F_1(a, b; x) = \sum_k \frac{a(a+1)\dots(a+k-1)x^k}{b(b+1)\dots(b+k-1)k!}$  is the confluent

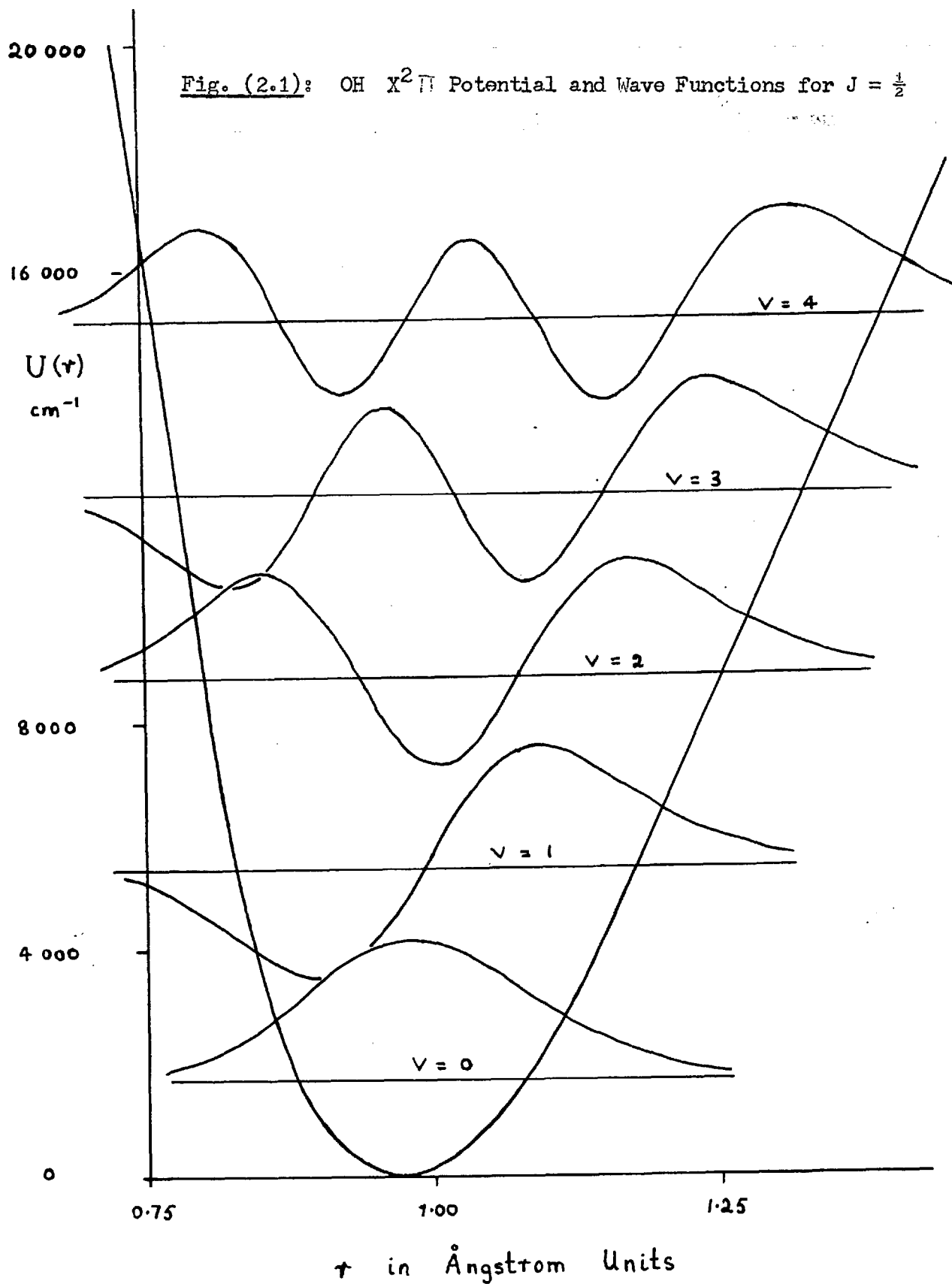
hypergeometric function.

Learner, 1961,<sup>52</sup> has shown that the Morse-Pekeris model is a very good representation of the rotating oscillator for low values of the vibrational quantum number -  $v \ll 5$ , in the case of OH.

The oscillatory vibrational wave functions given by Learner, 1961, p.25,<sup>52</sup> are reproduced in Fig. (2.1).

## 2.5. The Electronic Transition Moment in OH

Theoretical determinations of the electronic transition moment  $R_0(r)$  in OH based on a more or less ab initio method are not adequate



at present, Mulliken's 1940<sup>19</sup> calculations being only an order of magnitude assessment. Moreover Hurley's 1959<sup>20</sup> calculations gave a difference of nearly two orders of magnitude between the results for the dipole length and the equivalent dipole velocity approach.

Various expressions for the variation of  $R_e(r)$  with internuclear distance  $r$  have been obtained empirically. Shuler, 1950,<sup>2</sup> assumed a linear function of  $r$  (he only considered the first two terms in a polynomial expansion on account of the scanty data available). The parameter of the function was adjusted to give the best fit between the resulting calculated vibrational transition probabilities and Dieke and Crosswhite, 1949,<sup>22</sup> observed relative intensities of the vibrational bands in the system. He obtained  $R_e(r) = \text{const.}(1 - 0.75r)$ .

Nicholls, 1956,<sup>25</sup> assumed a slowly varying function  $R_e(r)$  and adopted the  $r$ -centroid approach which is valid for this condition. With this approximation he determined the variation of  $R_e(\bar{r})$  with  $\bar{r}$ , again by comparison with the experimental results of Dieke and Crosswhite, 1949.<sup>22</sup>

Both Shuler and Nicholls used their calculated values of  $R_e(r)$ , based on the experimental data for all the vibrational bands, to recalculate theoretical values for the relative intensities of the bands. This process results in a "smoothing" of the experimental data, assuming that the expressions used for the electronic transition moment are fair approximations.

Learner, 1961,<sup>52</sup> 1962,<sup>18</sup> chose an exponential form  $R_e(r) = \text{const.}e^{-ar}$ . The value of the parameter  $a$  was obtained by fitting the calculated values for the relative vibrational transition probabilities

at  $J = 10\frac{1}{2}$  (for which the experimental line intensities would have been strongest) with Nicholls', 1956,<sup>25</sup> smoothed values obtained from Dieke and Crosswhite's, 1949,<sup>22</sup> original results. He obtained  $R_e(r) = \text{const.} \cdot e^{-2.5r}$ .

In each of the empirical calculations above,  $R_e(r)$  was obtained from the variation of vibrational transition probability within the band system. This procedure implicitly includes a correction for the breakdown of the Born-Oppenheimer approximation, with regard to electronic and vibrational motions, in the expression for the electronic transition moment. There is no reason to suppose that  $R_e(r)$  should not also include factors allowing for the breakdown in terms of the interaction between electronic and rotational energy discussed in section 2.3, and even for the 3-cornered electronic-vibrational-rotational interaction. This interaction manifests itself in the variation of the coupling constant  $a$  (for electronic-rotational interaction) with vibrational quantum number. Although the effect of this interaction on the energy levels is small, the effect on the  $f$ -values is not necessarily small too. It is well known in the atomic case that different wave functions which give energy levels that are very close to the experimental values still give  $f$ -values that differ widely from each other as well as the experimental values. However the scarcity of experimental data does not yet allow determinations of the effect of these other interactions.

Using his derived value for the electronic transition moment, Learner predicted the variation of vibrational transition probability with the change of rotational quantum number for lines within each band with  $v', v'' \leq 4$ , for values of  $J$  up to 25.

## 2.6. The Band Oscillator Strength

The relation between oscillator strength  $f_{J^{\circ}, J^{\circ}}$  and vibrational transition probability  $p_{\nu^{\circ}, \nu^{\circ}}$  is easily obtained by combining (2.2), (2.3), (2.11) and (2.17) to give the well-known relation

$$f_{J^{\circ}, J^{\circ}} = \frac{8\pi^2 m}{3he^2} \nu \frac{S_{J^{\circ}, J^{\circ}}^{J^{\circ}, \Lambda^{\circ}}}{g^{\circ}} p_{\nu^{\circ}, \nu^{\circ}} \quad \dots(2.26).$$

Putting  $F_{\nu^{\circ}, \nu^{\circ}} = \frac{8\pi^2 m}{3he^2} \nu p_{\nu^{\circ}, \nu^{\circ}}$ , and since  $g^{\circ} = 2J^{\circ} + 1$ , we have

$$f_{J^{\circ}, J^{\circ}} = F_{\nu^{\circ}, \nu^{\circ}} S_{J^{\circ}, J^{\circ}}^{J^{\circ}, \Lambda^{\circ}} / (2J^{\circ} + 1) \quad \dots(2.27).$$

where  $F_{\nu^{\circ}, \nu^{\circ}}$  may be considered a constant over a given band, neglecting vibration-rotation interaction and the variation of frequency over the band. The latter is reasonable since the frequency range is small compared to the mean frequency of the band. The band oscillator strength is then defined by

$$f_{\nu^{\circ}, \nu^{\circ}} = \sum_{J^{\circ}} f_{J^{\circ}, J^{\circ}} = \frac{F_{\nu^{\circ}, \nu^{\circ}}}{(2J^{\circ} + 1)} \sum_{J^{\circ}} S_{J^{\circ}, J^{\circ}}^{J^{\circ}, \Lambda^{\circ}} \quad \dots(2.28).$$

From (2.18) we see that

$$f_{\nu^{\circ}, \nu^{\circ}} = F_{\nu^{\circ}, \nu^{\circ}} \quad \text{or} \quad 4F_{\nu^{\circ}, \nu^{\circ}} \quad \text{respectively} \quad \dots(2.29),$$

depending on whether one follows the usual normalisation rule, or that of Dieke and Crosswhite, 1948.<sup>21</sup>

The effect of vibration-rotation interaction can be included by incorporating the correction factor  $T_{J^{\circ}, J^{\circ}}$  in (2.27), so that we have, following Dieke and Crosswhite, that

$$f_{J^{\circ}, J^{\circ}} = f_{\nu^{\circ}, \nu^{\circ}} \frac{\frac{1}{4} S_{J^{\circ}, J^{\circ}}^{J^{\circ}, \Lambda^{\circ}}}{2J^{\circ} + 1} T_{J^{\circ}, J^{\circ}} \quad \dots(2.30),$$

where  $f_{\nu, \nu''}$  now refers to the rotationless molecule, for which  $T_{J, J''}$  is defined as unity. This value  $f_{\nu, \nu''}$  is the most meaningful representation of the strength of the transition.

If the quantity  $(2J'' + 1) f_{J, J''} \frac{1}{4} S_{J'', J''}^J \frac{\Lambda''}{\Lambda''}$  is plotted against  $J''$ , one obtains a curve whose departure from a straight horizontal line gives  $T_{J, J''}$ . The band oscillator strength for the rotationless molecule is determined by extrapolating the curve back to zero rotation.

Learner, 1961,<sup>52</sup>, 1962,<sup>18</sup> calculated and tabulated values of  $T_{J, J''}$  for lines in all the main branches of the (0,0) band, up to  $J = 30$ , using his empirical value for the electronic transition moment.

CHAPTER IIITHEORETICAL (B) - THE HOOK METHOD.3.1. Dispersion Theory

The early investigators of the phenomenon of dispersion found that the refractive index  $F$  increases slowly as the wavelength  $\lambda$  of the incident light decreases. The refractive index and its rate of change varied not only with  $\lambda$ , but also with dispersing medium. Cauchy derived a relation between  $F$  and  $\lambda$  on the elastic solid theory of the ether. He obtained

$$F = a + b/\lambda^2 + d/\lambda^4 + f/\lambda^6 + \dots \dots \dots (3.1),$$

which gives  $F$  in terms of  $\lambda$ , and four or more constants  $a, b, d, f \dots$ , for  $F$  slowly increasing as  $\lambda$  decreases, and having no discontinuities, as in Fig. (3.1), which is typical of "normal dispersion".

Lo Roux, Christiansen, and others, found that in the neighbourhood of absorption lines the dispersion phenomenon was as shown in Fig. (3.2), different from that shown by a glass prism. The first striking demonstration of this "anomalous dispersion" was given by Wood, 1904,<sup>55</sup> who used a "prism" of sodium vapour to form an anomalous spectrum along the slit of a prism spectrograph. The spectrum formed in the spectrograph traced out the familiar anomalous dispersion curve for the sodium D lines.

The Cauchy formula (3.1) is obviously inadequate to describe the anomalous dispersion phenomenon, but is found to give satisfactory values for the case of normal dispersion, i.e. in the spectral region well away from any absorption lines.

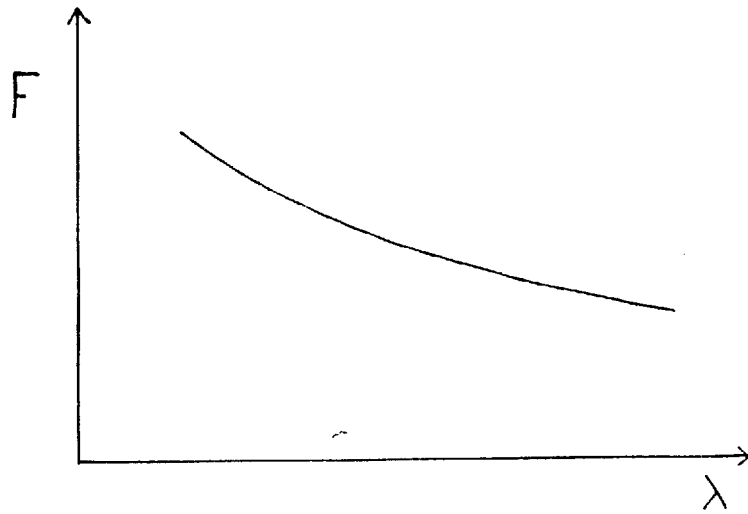
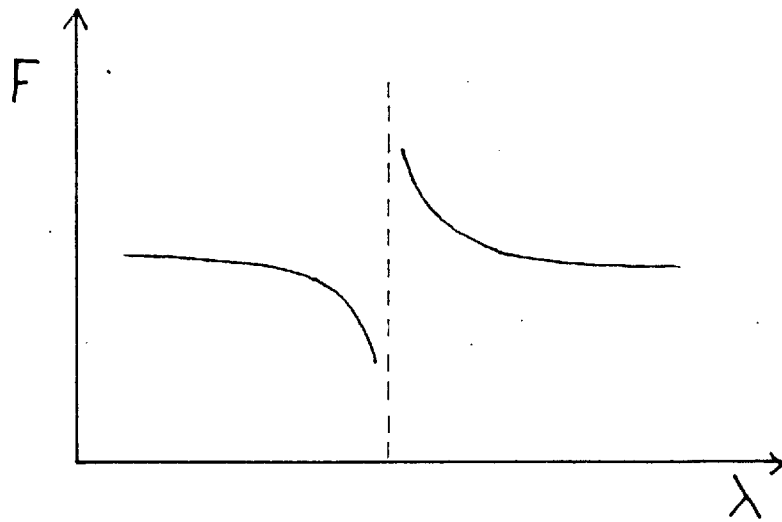


Fig. (3.1): Normal Dispersion





To account for the sudden change in  $F$  near an absorption line of wavelength  $\lambda_0$ , Sellmeier derived the equation

$$F^2 - 1 = a\lambda^2/(\lambda^2 - \lambda_0^2) \quad \dots(3.2).$$

Since most spectra consist of many absorption lines, this becomes

$$F^2 - 1 = \sum_j a\lambda^2/(\lambda^2 - \lambda_j^2) \quad \dots(3.3),$$

summing over all the absorption lines. At  $\lambda = \lambda_j$ , this gives infinite values for  $F$ , and in order to obtain a finite value of  $F$  for all  $\lambda$ , a frictional term was introduced, giving

$$F^2 - 1 = \sum_j a\lambda^2/(\lambda^2 - \lambda_j^2 + b^2\lambda^2) \quad \dots(3.4).$$

The derivation of this form is not rigorous in the light of the more developed electron theory of matter. Drude and Voigt led the way to a new deduction, and were followed by Lorentz, who derived an expression for  $F$  from Maxwell's equations, finally giving

$$F^2 - 1 = \frac{4\pi e^2}{m} \sum_j \frac{\mathcal{N}_j}{\omega_j^2 - \omega^2 + i\delta_j\omega} \quad \dots(3.5),$$

for low density media whose magnetic permeability is unity (the latter is true for nearly all transparent media), where

$\mathcal{N}_j$  = number of oscillators per unit volume with frequency  $\omega_j$ ,

$e$  = electronic charge,  $m$  = electronic mass,

$\omega$  = frequency for which  $F$  is calculated,

$\delta_j$  =  $g_j/m$ , where  $g_j$  = damping force.

This is equivalent to having a medium with  $N$  particles per unit volume, each with  $f_j$  oscillators of frequency  $\omega_j$ , so that  $\mathcal{N}_j = Nf_j$ .

Since the absorption is small at the edge of an absorption line,  $\gamma_j \omega \ll \omega_j^2 - \omega^2$ , and (3.5) can be written as

$$F^2 - 1 = \frac{4\pi N e^2}{m} \sum_j \frac{f_j}{\omega_j^2 - \omega^2} \quad \dots(3.6).$$

Substituting  $\omega = \frac{2\pi c}{\lambda}$  ( $c =$  velocity of light,  $\lambda =$  wavelength corresponding to frequency  $\omega$ ), and since for a gas  $F \approx 1$ , we have

$$F - 1 = \frac{N e^2}{2\pi m c^2} \sum_j \frac{f_j \lambda_j^2}{\lambda^2 - \lambda_j^2} \quad \dots(3.7).$$

All the absorption wavelengths of a given medium can be included by considering all transitions from level  $j$  to levels  $k$  ( $k > j$ ), for each  $j$ , giving, in regions of small absorption,

$$F - 1 = \frac{e^2}{2\pi m c^2} \sum_j \sum_{k>j} \frac{N_j f_{kj} \lambda_{kj}^2}{\lambda^2 - \lambda_{kj}^2} \quad \dots(3.8),$$

where  $N_j =$  number of particles per unit volume in state  $j$ .

In the region of an isolated absorption line, only the one transition under the summation has a significant effect, and  $\lambda \approx \lambda_{kj}$ , so that  $\lambda^2 - \lambda_{kj}^2 \approx 2\lambda_{kj}(\lambda - \lambda_{kj})$ , and

$$F - 1 = \frac{e^2}{4\pi m c^2} \frac{N_j f_{kj} \lambda_{kj}^3}{\lambda - \lambda_{kj}} \quad \dots(3.9),$$

which may be written as

$$F - 1 = C N_j f_{kj} \frac{\lambda_{kj}^3}{\lambda - \lambda_{kj}} \quad \dots(3.10).$$

where

$$C = \frac{e^2}{4\pi m c^2}$$

Classically, the oscillator strength  $f_{kj}$  is a whole number by

definition, but quantum mechanically and also in practice, this is not the case, and usually  $f < 1$ .

In the quantum mechanical treatment it is seen that expression (3.8) is only true in the case of weak excitation of the gas. Ladenburg, 1921,<sup>56</sup> and Kramers, 1924,<sup>57</sup> showed that when the upper levels are appreciably populated, a "negative dispersion" term has to be included, giving

$$F - 1 = \frac{e^2}{2\pi mc^2} \sum_j \sum_{k>j} \frac{N_j f_{kj} \lambda_{kj}^2 \lambda^2}{\lambda^2 - \lambda_{kj}^2} \left( 1 - \frac{g_j N_k}{g_k N_j} \right) \dots (3.11),$$

where  $g_j$  and  $g_k$  are the statistical weights of the levels  $j$  and  $k$  respectively, and  $N_k$  is the population of the upper level  $k$ .

Whereas before we had  $\mathcal{W}_j = N f_j$ , and more generally

$$\mathcal{W}_{kj} = N_j f_{kj} \dots (3.12),$$

we now have

$$\mathcal{W}_{kj} = N_j f_{kj} \left( 1 - \frac{g_j N_k}{g_k N_j} \right) = N_j f_{kj} Q_{kj} \dots (3.13),$$

where  $Q_{kj} = \left( 1 - \frac{g_j N_k}{g_k N_j} \right)$  is the negative dispersion term resulting from induced emission. For weak excitation, as in this experiment,  $N_k \ll N_j$ , and the effect of the negative dispersion term is negligible.

### 3.2. The Puccianti Method

Puccianti, 1901,<sup>34</sup> 1904,<sup>35</sup> made use of relation (3.9) in his method of focussing zero order horizontal fringes from a Jamin-type interferometer onto the slit of a stigmatic spectrograph. For any given wavelength, the distance between fringes is equal along the height

of the slit, and the path difference  $\Delta$  between the interfering beams is given by

$$\Delta = by \quad (b \simeq \text{constant}) \quad \dots(3.14),$$

where  $y$  is measured along the slit from a point such that  $y = 0$ , when  $\Delta = 0$ . (In fact  $b$  varies very slowly with  $\lambda$ , decreasing with decreasing  $\lambda$ .)

Considering only points of maximum intensity, we have

$$\Delta = n\lambda \quad (n = \text{an integer}) \quad \dots(3.15).$$

From (3.14) and (3.15), we have

$$by = n\lambda \quad \dots(3.16),$$

for a bright fringe.

If one of the interfering beams is passed through a thickness  $\ell$  of gas with refractive index  $F$ , a path difference  $(F - 1)\ell$  is created, so from (3.16) we have

$$\left. \begin{array}{l} by - (F - 1)\ell = n\lambda \\ \text{or } by - G(\lambda)\ell = n\lambda \\ \text{where } G(\lambda) = F - 1 \end{array} \right\} \quad \dots(3.17).$$

For the zero order fringe,  $n = 0$ , and  $by = G(\lambda)\ell$ , giving

$$y = \frac{\ell}{b} G(\lambda) \simeq \text{const. } G(\lambda) \quad \dots(3.18),$$

for this fringe.

Since  $b \simeq \text{const.}$ , we see that all the fringes trace out anomalous dispersion curves in the spectrograph, if  $G(\lambda)$  is given by (3.9). Away from an absorption line the fringes are nearly horizontal, but near one they trace out hyperbolic curves.

### 3.3. The Roschdestwensky Modification

Obtaining the  $f$ -value from the hyperbolic curve by a complete parameterisation or even using a small number of selected points is a long and involved process liable to errors and difficult to check. Roschdestwensky, 1912,<sup>32</sup> 1921,<sup>33</sup> simplified the relation between  $f$ -values and experimental observation by introducing a plane parallel glass plate into the path of the second beam in the interferometer.

Let the thickness of the glass plate be  $\ell^*$ , and its refractive index  $F^*$  ( $F^* > 1$ , and is a function of  $\lambda$ ;  $F^*-1 = r(\lambda)$ ). Replacing  $\Delta$  (= by) by the more general function  $\varphi(y, \lambda)$  for white light, equation (3.17) becomes

$$\varphi(y, \lambda) - G(\lambda)\ell = n\lambda,$$

giving for the case with the glass plate,

$$\varphi(y, \lambda) - G(\lambda)\ell + r(\lambda)\ell^* = n\lambda \quad \dots(3.19).$$

Near the absorption line, sharp maxima and minima are observed, as in Fig. (3.3), the hitherto nearly horizontal fringes now being high order inclined fringes, giving rise to symmetrically placed hooks close to the absorption line.

The position of the maxima and minima are given by  $\frac{dy}{d\lambda} = 0$ , so that  $\frac{d\varphi}{d\lambda} = \frac{\partial\varphi}{\partial y} \frac{dy}{d\lambda} + \frac{\partial\varphi}{\partial\lambda} = \frac{\partial\varphi}{\partial\lambda}$  at these points. Differentiating with respect to  $\lambda$ , we have

$$\varphi_y \cdot y' + \frac{\partial\varphi}{\partial\lambda} - G'\ell + r'\ell^* = n \quad \dots(3.20),$$

where  $\varphi_y = \frac{\partial\varphi}{\partial y}$ , and the dash denotes differentiation with respect to  $\lambda$ . Thus for  $\lambda = \Lambda$ , where  $\Lambda$  denotes the position of a hook and  $y' = 0$ ,

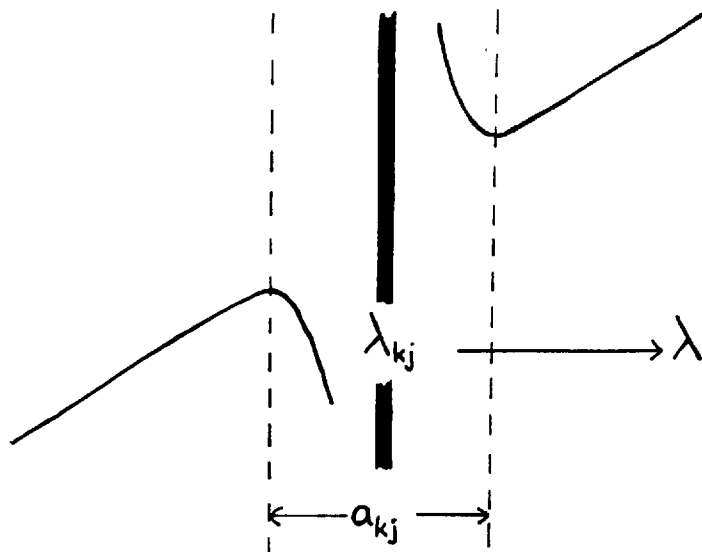


Fig.(3.3): "Hooks" near  $\lambda_{kj}$

we have

$$G^{\circ} = -\frac{K}{\ell} \quad \left. \vphantom{G^{\circ}} \right\} \dots(3.21),$$

$$\text{where } K = n - \ell^* r^{\circ} - \varphi^{\circ}$$

Comparing (3.21) with (3.9) differentiated with respect to  $\lambda$ ,

$$\text{i.e. } F^{\circ} = -\frac{cN_{jfkj}\lambda_{kj}^3}{(\Lambda - \lambda_{kj})^2} \quad \dots(3.22),$$

we see that

$$\Lambda = \lambda_{kj} \pm \sqrt{\frac{cN_{jfkj}\lambda_{kj}^3}{K}} \quad \dots(3.23).$$

Thus, for an isolated line, the hooks lie symmetrically about  $\lambda_{kj}$ .

Putting  $a_{kj} = 2(\Lambda - \lambda_{kj})$ , we have

$$N_{jfkj}\ell = \frac{1}{4c} \frac{K a_{kj}^2}{\lambda_{kj}^3} \quad \dots(3.24).$$

The hook separation is easily obtained by measurements on photographs of the fringe pattern, and it will be shown that  $K$  may be determined by measuring the slope of fringes at  $\lambda_0$ , near  $\lambda_{kj}$  but well outside the region of anomalous dispersion.

Suppose that in moving from  $\lambda_0$  to  $\lambda_0 + \Delta\lambda$ , one passes  $\Delta n$  fringes (observed at constant height  $y$ ), near the region of anomalous dispersion due to  $\lambda_{kj}$ . From (3.19) we have two equations corresponding to  $\lambda_0$  and  $\lambda_0 + \Delta\lambda$ , namely

$$\varphi(\lambda_0) - \ell G(\lambda_0) + \ell^* r(\lambda_0) = n\lambda_0 \quad \dots(3.25)$$

$$\begin{aligned} \text{and } \varphi(\lambda_0 + \Delta\lambda) - \ell G(\lambda_0 + \Delta\lambda) + \ell^* r(\lambda_0 + \Delta\lambda) \\ = (n + \Delta n) \cdot (\lambda_0 + \Delta\lambda) \quad \dots(3.26). \end{aligned}$$

Using the Taylor expansion, and neglecting terms higher than the first

order, we have, subtracting (3.25) from (3.26),

$$\varphi^0 \Delta \lambda - \ell G^0 \Delta \lambda + \ell^* r^0 \Delta \lambda = n \Delta \lambda + \lambda_0 \Delta n + \Delta n \Delta \lambda \quad \dots (3.27).$$

Now  $G$  is in a region where it is very nearly constant, so on the left hand side of (3.27), the second term is negligible compared to the sum of the other two. On the right hand side of (3.27),  $\Delta n \Delta \lambda$  may be neglected as the product of two small quantities. Thus we have  $\Delta \lambda (n - \ell^* r^0 - \varphi^0) = -\lambda_0 \Delta n$ , giving, since  $\lambda_0 \simeq \lambda_{kj}$ , and  $K = n - \ell^* r^0 - \varphi^0$ , that

$$K = \frac{\Delta n}{\Delta \lambda} \lambda_{kj} \quad \dots (3.28),$$

showing that  $K$  is obtained by measuring the slope of the undistorted fringes near each  $\lambda_{kj}$  in turn.

We have from (3.24), and expressing  $C$  in terms of its constituents, that

$$N_{jf_{kj}} \ell = \frac{\pi c^2 m}{e^2} \frac{K a_{kj}^2}{\lambda_{kj}^3} \quad \dots (3.29).$$

Putting  $\beta_{kj} = N_{jf_{kj}} \ell \left( \frac{e^2 \lambda_{kj}^3}{4 \pi c^2 m K} \right)$ , we have

$$\beta_{kj} = \left( \frac{a_{kj}}{2} \right)^2 = (\Lambda - \lambda_{kj})^2, \text{ and}$$

$$\frac{\beta_{kj}}{(\Lambda - \lambda_{kj})^2} = 1 \quad \dots (3.30).$$

From (3.29) we see that the product  $(N_{jf_{kj}} \ell)$ , which is the number of classical oscillators of frequency  $\omega_{kj}$  per unit cross-section, is given in terms of the constants  $\pi$ ,  $c$ ,  $m$ ,  $e$ , the wavelength



$\lambda_{kj}$ , and the quantities  $K$  and  $a_{kj}$  which are easily obtained from measurements on the spectrogram.

### 3.4. Application to a Number of Close Lines

In the application of the hook method to atomic spectra, it has rarely been necessary to consider more than two or three close lines. In the general case, as required for molecular spectra, the effect of an absorption line on the hook separations of other lines close to it may not be negligible, and has been treated briefly by Roschdestwensky and Penkin, 1941.<sup>58</sup> For an arbitrary number  $r$  of close lines, (3.30) may be extended to show that a hook occurs at each of the  $2r$  roots of the equation

$$\sum_{j=1}^r \frac{\beta_j}{(\lambda - \lambda_j)^2} = 1 \quad \dots(3.31),$$

where, as before

$$\beta_j = (Nf\ell)_j \left( \frac{e^2 \lambda_j^3}{4\pi m c^2 K} \right).$$

If  $\delta_{1j}$  and  $\delta_{2j}$  represent the distances from the centre of the  $j^{\text{th}}$  line to the two hooks belonging to it (so that  $\delta_{1j} + \delta_{2j} = \Delta_j$ ), substitution of each measured  $\delta$  combined with the known line separations  $\mathcal{E}$  into equation (3.31) gives  $2r$  equations for the determinations of the  $\beta_j$ 's if all the hooks are measurable. For this particular experiment, the formulae can be simplified to deal with two extreme cases, as follows.

If the lines are more than about  $\frac{1}{2}\overset{\nu}{\text{Å}}$  apart, far enough for hooks

to appear between them in this experiment (where  $Nf\ell \sim 10^{13}$ ,  $\lambda \sim 3000 \text{ \AA}$ ),  $\delta_{1j} = \delta_{2j}$  within the errors of measurement (about 10%). Equation (3.31) can then be approximated by

$$\frac{\beta_j}{\delta_j} = 1 - \sum_{k \neq j} \frac{\beta_k}{\epsilon_{jk}^2} \quad \dots (3.32),$$

where  $\epsilon_{jk} = |\lambda_j - \lambda_k|$ . Using as a first approximation for  $\beta_k$ , the "isolated line" value  $\beta_k = \delta_k^2 = \left(\frac{\Delta_k}{2}\right)^2$ , and substituting in equation (3.32), a second approximation  $\beta_j$  may be obtained for each  $\beta_j$  in turn. This procedure is repeated until the necessary accuracy ( $|n_\beta - n_{\beta}^{-1}|/n_\beta < 1\%$ ) is obtained. The calculation is tedious, since in this experiment the hook separation of each line is influenced by more than 1% by all other lines within about  $2 \text{ \AA}$  of it, and was therefore programmed for the IBM 7090 computer at Imperial College.

The other extreme case is that of a pair of lines too close to have hooks between them. This pair is first treated separately from all other lines. If the lines are designated a and b, and are distant  $\delta_a$  and  $\delta_b$  respectively from the nearest hook, equation (3.31) leads to the simultaneous equations

$$\left. \begin{aligned} \frac{\beta_a}{\delta_a^2} + \frac{\beta_b}{(\epsilon_{ab} + \delta_a)^2} &= 1 \\ \frac{\beta_a}{(\epsilon_{ab} + \delta_b)^2} + \frac{\beta_b}{\delta_b^2} &= 1 \end{aligned} \right\}$$

from which  $\beta_a$  and  $\beta_b$  are obtained to the necessary accuracy, again using the computer, programmed now for this particular case. In nearly all the pairs of lines falling into this category, one of the lines

was a satellite, whose  $f$ -value was  $\sim \frac{1}{5}$  that of the main line investigated, and the correction to the  $\beta$ -value of the main line was only  $\sim 5\%$ .

Thus in practice, the final  ${}^n\beta_a$  value of only one of these lines, say  $a$ , was nearly always required, and the "isolated line"  $\delta_a$  value ( $= {}^n\beta_a^{\frac{1}{2}}$ ) is then fed into the computer programme for the previous case, so that  $\beta_a$  can be corrected for the influence of all other (relatively distant) lines.

## CHAPTER IV

### EXPERIMENTAL (A) - THE MACH-ZEHNDER INTERFEROMETER

#### 4.1. Introduction

Fig. (4.1) gives an outline of the experimental system, and a general view of the apparatus is shown in Plate 1.

The OH to be investigated was produced in adequate concentrations by dissociating water vapour in an alumina reaction tube, heated up to nearly 2000°K in a molybdenum wound, tubular alumina furnace. The water vapour was introduced in the form of saturated oxygen, by bubbling oxygen slowly through about 8 cm of water, before passing it through the reaction tube.

The anomalous dispersion adjacent to a number of absorption lines in the (0,0) and (1,0) bands in the  $A^2\Sigma^+ - X^2\Pi$  band system of OH was observed by means of interference fringes produced by a Mach-Zehnder interferometer. A parallel beam of light from a source of continuous radiation was passed through the interferometer, and the horizontal interference fringes produced were focussed on the slit of a stigmatic spectrograph, where they were photographed, having undergone dispersion. The reaction tube and a similar compensating tube were placed one in each arm of the interferometer.

Each item of the experimental system will be described in detail - the Mach-Zehnder interferometer in this chapter, and the rest of the system in the next.

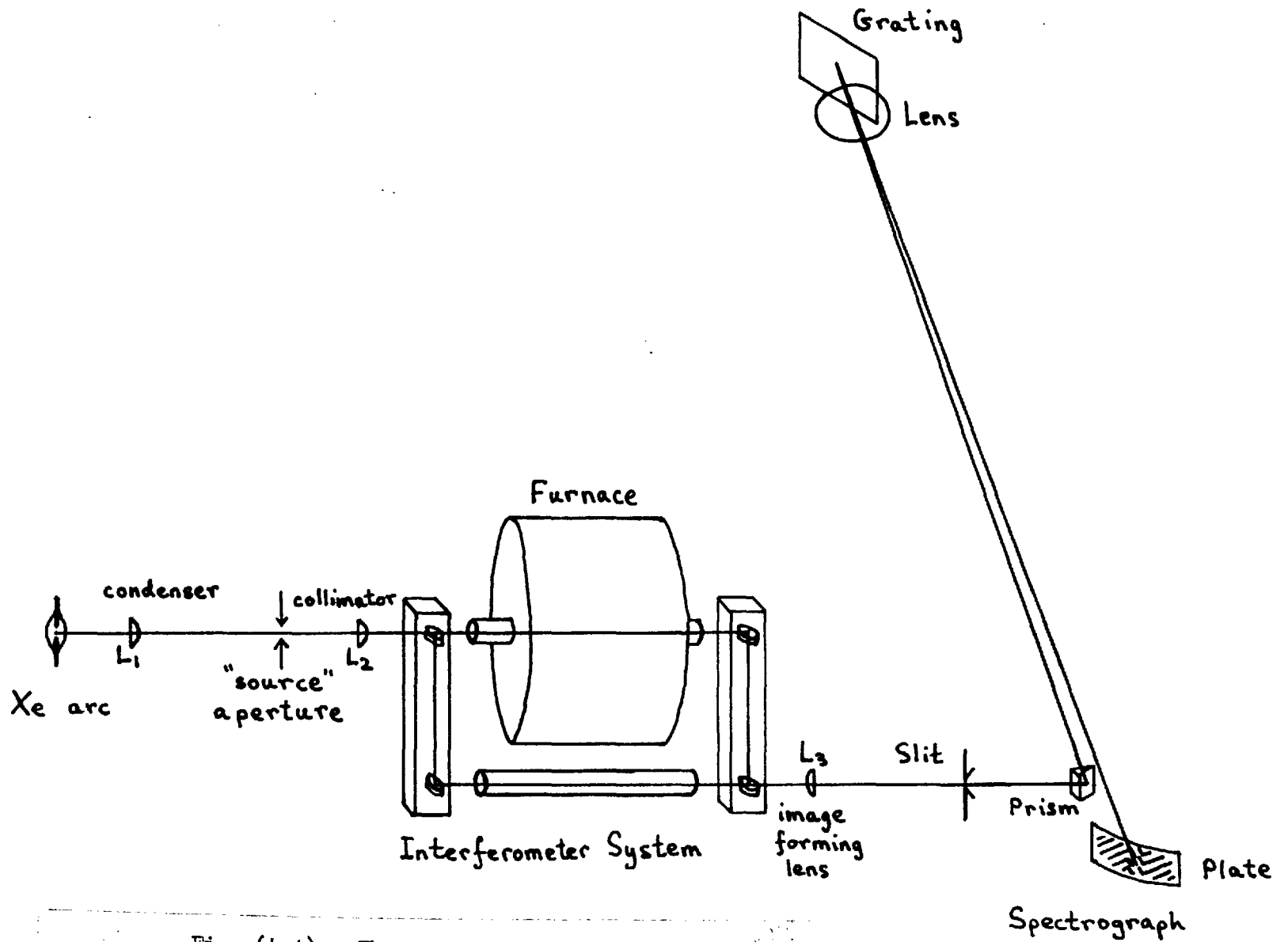


Fig. (4.1): The Experimental System



Plate 1: A General View of the Apparatus

#### 4.2. Theory of the Interferometer

The original determinations of  $f$ -values using the hook method were made with a Jamin interferometer. Later workers, for example Ostrovskii and Penkin, 1961,<sup>36,37</sup> and Pery-Thorne and Chamberlain, 1963<sup>59</sup> have made use of a Mach-Zehnder interferometer - Mach, 1892;<sup>60</sup> Zehnder, 1891,<sup>61</sup> - which is related to the Jamin and Michelson instruments. Whereas with the Jamin, the separation of the two beams is limited by the thickness of the interferometer plates, with the Mach-Zehnder, the interfering beams can be widely separated; also much thinner (and consequently cheaper) plates may be used. A disadvantage of the Mach-Zehnder is that there are many more degrees of freedom in the movement of the plates, making adjustment more difficult. In this experiment a Mach-Zehnder interferometer was used in a Jamin-type arrangement, with horizontal fringes located at infinity.

The instrument consists of two beam splitters  $P_1$ ,  $P_4$  and two plane mirrors  $P_2$ ,  $P_3$ .  $P_1$  and  $P_4$  are ideally two identical plates made of a homogeneous transmitting material, polished optically flat both for transmission as well as reflection at the surfaces, and partially aluminised on one surface to give equal transmission and reflection at  $45^\circ$  incidence.  $P_2$  and  $P_3$  are two plates polished optically flat and completely aluminised on one side. The plates are placed at the corners of a rectangle, as shown in Fig. (4.2), and at  $45^\circ$  to the sides.  $P_4$  may be moved along the direction of the line joining  $P_2$  and  $P_4$ . Rays of light from a small source  $S$  are amplitude divided at  $P_1$  into two beams of approximately equal intensity,  $B_{12}$  and  $B_{13}$ .  $B_{12}$  is totally

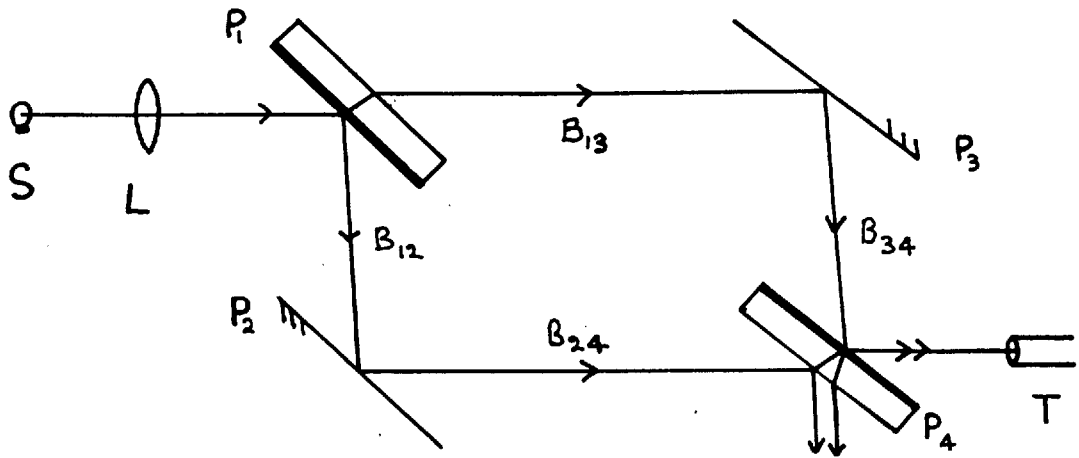


Fig.(4.2): The Mach-Zehnder Interferometer



reflected at  $P_2$  along  $B_{24}$ , and recombines at  $P_4$  with  $B_{34}$ , totally reflected from  $P_3$ , in two "double" beams emerging from  $P_4$ . The two beams  $B_{24}$ ,  $B_{34}$  which recombine at  $P_4$  are coherent, and hence interference fringes may be formed. The interference is usually observed in the recombined beam travelling towards T, while the light in the other beam is lost. Since the mirrors are arranged at the corners of a rectangle, the geometrical path lengths of the two interfering beams between the plates are equal.

In the Jamin-type arrangement, the light from S is rendered parallel by the optical system L, and may be viewed through the telescope T, focussed at infinity. If all the plates are exactly parallel to each other, then the corresponding rays in each beam are parallel and make equal angles with the (identical) beam splitters, and hence have equal path lengths inside them, as well as in the space between them. Then the optical path lengths of the two recombining components of all the rays from S are equal and the components interfere constructively at  $P_4$ , giving emergent rays of equal intensity, so that the field of view of the telescope is one of uniform brightness.

If  $P_4$  is now rotated through a small angle about a horizontal axis parallel to its surfaces, and  $P_3$  is similarly rotated to keep it parallel to  $P_4$ , then the recombining beams emerging from  $P_4$  are still parallel to each other. Now the optical path lengths of each pair of corresponding rays are no longer equal. This is so because each component passes through only one of the beam splitters, and now does so at a different angle from the other, making the path lengths inside  $P_1$  and  $P_4$

different, although the path lengths in the space between them are still equal.  $P_4$  may be traversed slightly in the horizontal direction towards or away from  $P_2$ , to equalise the optical path lengths covered by each pair of corresponding rays that lie in a horizontal plane in the space between  $P_1P_2$  and  $P_3P_4$  (and thus make particular angles with  $P_1$  and  $P_4$ ).

The rays of light from a given point in  $S$  are made parallel by  $L$ , and make particular angles with the beam splitters. Parallel rays in a given direction are focussed at a particular point in the primary image plane of  $T$ , so that each point in this plane corresponds to a point in the plane of the source  $S$ . Rays travelling in different directions in a horizontal plane between  $P_1P_2$  and  $P_3P_4$  come from points along a particular horizontal line in  $S$ , and are focussed at points along a particular horizontal line in the image plane of  $T$ . From the discussion in the previous paragraph, we see that each point along this line corresponds to a zero path difference between the two interfering beams, and the line is therefore a zero order bright fringe. Rays that are focussed at points along another horizontal line in the image plane of  $T$  make different angles with the beam splitters, and so the interfering components have unequal optical path lengths, the difference increasing for lines farther and farther away from the zero order fringe. Thus a pattern of dark and bright horizontal fringes is set up in the image of  $S$  in  $T$ .

### 4.3. Modifications to the Interferometer

The interferometer used in this experiment was basically that designed and described in detail by Chamberlain, 1962<sup>62</sup> subject to two primary and one secondary modification. The primary modifications were:

- (1) that the glass beam splitters be replaced by spectrosil ones,
- and (2) that the separation of the two beams be increased from about 8 cm to about 27 cm so as to accommodate the furnace described in 5.5.

The spectrosil beam splitters were, like the glass ones, 2" in diameter,  $5/8$ " thick, and flat to within a tenth of a wavelength (now at  $3000 \text{ \AA}$ ). They were aluminised on one surface so as to give equal intensities for the transmitted and reflected components at  $3000 \text{ \AA}$  and at  $45^\circ$  incidence.

The increased height, and thus weight, necessitated by the second of these primary modifications carries with it an increased susceptibility to vibrations. To counteract this, a secondary modification was made in the design. The  $\frac{1}{2}$ " brass stalks by means of which the interferometer carriages were previously mounted on the optical bench saddles were dispensed with, and the carriages were bolted directly on to the saddles. Plate 2 shows a detail of one of the modified carriages.

As before, two long horizontal lengths of "Handy Angle" connected the two interferometer carriages to ensure complete rigidity of the interferometer as a whole. In this case, they were clamped half way up

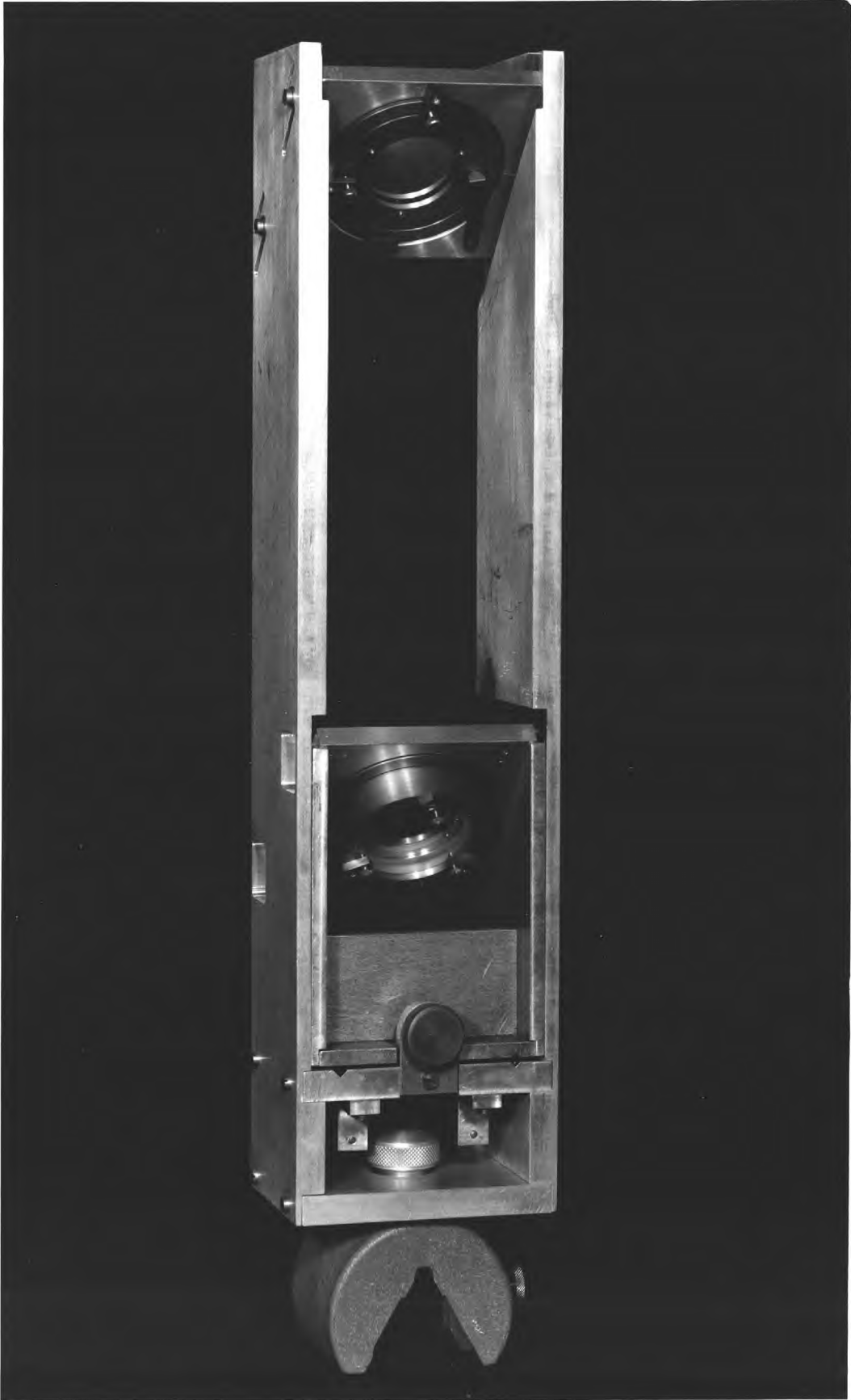


Plate 2: Detail of One Interferometer Carriage

the interferometer carriages, since the bulk of the furnace was an obstruction in the upper half of the interferometer.

#### 4.4. Adjustment of the Interferometer

In this interferometer the adjustment is made as easy as possible, in that all degrees of freedom are independent, i.e. the two axes of rotation of each plate are perpendicular to each other, and also lie in the reflecting surfaces of the plates.

The height of the table carrying the interferometer was altered so that, with the interferometer carriages mounted on the optical bench, the lower plates  $P_1$  and  $P_3$  were at the same height as the spectrograph slit S - see Fig. (4.3a).

The pointolite P was first placed at the plateholder end of the spectrograph, and its height adjusted until it could be seen centrally in the grating when viewed through S, shortened to about 2 mm in height and opened as wide as it would go ( $1\frac{1}{2}$  mm). The table was now moved sideways, and the height of  $P_1$  altered slightly, in order that the patch of light emerging from the slit be seen centrally through  $P_1$ .

P was now placed directly in front of S, and aligned so as to be seen centrally in the grating when viewed through the spectrograph. P was now on the spectrograph axis. A small circular aperture A was placed between P and  $P_1$ , so that the patch of light passing through A fell centrally on  $P_1$ . Now A was also on the spectrograph axis. The alignment of the table and the height of  $P_3$  were now altered slightly, so that the patch of light from A fell centrally on  $P_3$  as well as on  $P_1$ . The

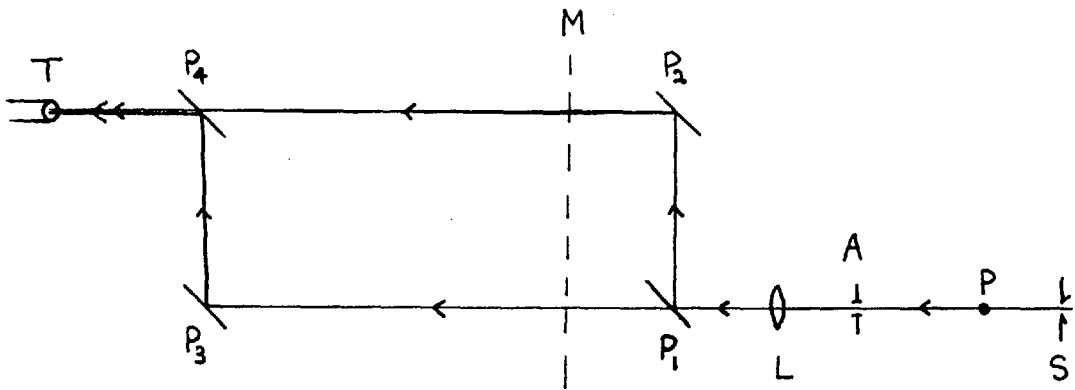


Fig. (4.3a)

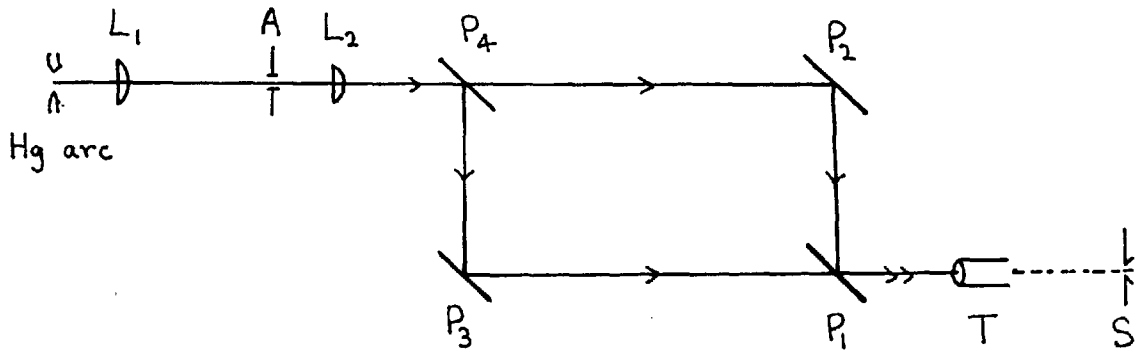


Fig. (4.3b)

Fig. (4.3): Adjustment of the Interferometer

position of the table was then marked out on the floor, as had been that of the spectrograph.

The positions of  $P_2$  and  $P_4$  were adjusted so that they were vertically above, and at the same distance from,  $P_1$  and  $P_3$  respectively. A lens  $L$  was introduced between  $P_1$  and  $A$ , at its focal distance from  $A$ , so that the resulting parallel beam of light fell centrally on  $P_1$  and  $P_3$ .  $P_1$  was rotated about its two axes until the patch of light reflected from it fell centrally on  $P_2$ . A long  $\frac{1}{4}$ " thick plane mirror strip  $M$  was clamped vertically behind  $P_1$  and  $P_2$ , and tilted so that the light reaching it from  $P_1$  was reflected back and imaged exactly on  $A$ . Now  $P_2$  was rotated so that the reflected image due to the light reflected in it fulfilled the same condition.  $P_1$  and  $P_2$  were now parallel and  $M$  was removed.

Only a very small adjustment was now required in the height of  $P_4$  for the patch of light from  $P_2$  to pass centrally through it.  $P_3$  was then rotated so that the patch of light from  $P_1$ , reflected on to  $P_4$  fell centrally on it, the patches of light from both beams now overlapping exactly in the reflecting surface of  $P_4$ . The light from  $P_4$  was then viewed through a telescope  $T$  focussed at infinity, and the two images of  $A$  formed in it were made to coincide by rotating  $P_4$ . The interferometer is now in approximate adjustment with  $P_1$  and  $P_2$  accurately parallel, and  $P_3$  and  $P_4$  accurately parallel and approximately parallel to  $P_1$  and  $P_2$ .

If  $P$  is replaced by an approximately monochromatic source, such as a low pressure mercury arc, interference fringes may be seen across the image of  $A$  seen in the telescope.

The interferometer is now lined up on the axis of the spectrograph, and the rest of the optical system was then aligned as described in 5.2.

The fine adjustments to the interferometer were carried out by replacing P with a high pressure mercury arc ME/D, once the whole optical system had been aligned, and viewing the fringes formed by the interferometer through T now placed behind  $P_1$ , as in Fig. (4.3b). The fringes were sharpened and made horizontal by rotations of  $P_1$  and  $P_2$  about their horizontal and inclined axes. The fringe spacing was altered by rotations about the horizontal axes to give initially about 5 fringes in the field of view, which is the magnified image of the aperture A.

At first fringes of high contrast were visible, but these became less clear as the arc heated up, owing to the pressure broadening of the mercury lines and the increase in the brightness of the continuum. Visibility was restored mainly by adjusting the horizontal traverse of  $P_1$  so as to equate the path lengths of the interfering beams and thus obtain zero order fringes, making the necessary subsequent adjustments to the tilt of  $P_2$ . If the visibility of the fringes was lost before the interferometer was adjusted for zero order fringes, the arc was cooled by directing at it a stream of cold air from an electric air blower until the visibility was restored, and the process continued as before. It was ultimately possible to maintain the visibility of the fringes when the lamp was very hot and at its full operating pressure of 12 atmospheres, when the zero order adjustment and white light fringes had been obtained. Owing to the large number of wavelengths present in the source, the fringes become multi-coloured, and fade away rapidly from the strong



sharp central zero order fringe, making the path length equalization very critical.

The furnace and compensating tube were installed and accurately aligned with the upper and lower beams respectively. The windows on the tubes were arranged perpendicular to the beams and as closely parallel to each other as possible. Like the interferometer plates, their surfaces had been polished flat to within a tenth of a wavelength, and arranged so that their slight wedge angles ( $\sim$  a fringe across their diameter) cancelled each other in each tube. Only a very slight adjustment to the traverse of  $P_1$  and the tilt of  $P_2$  was required in order to recover the zero order adjustment of the system.

For the purpose of adjusting the interferometer, the focal lengths of the lenses  $L_2$  and  $L_3$  - see Fig. (4.1) - were taken as their values in visible light ( $5500 \text{ \AA}$ ). For the actual experiments involving hook photographs, their values at  $3100 \text{ \AA}$  and  $2850 \text{ \AA}$  - for the (0,0) and (1,0) bands respectively - were taken, and their positions altered accordingly, by the necessary 2 cm or so along the optical axis. (The focal lengths of each lens at  $3100 \text{ \AA}$  and  $2850 \text{ \AA}$  were determined as follows. Light from an iron arc was condensed on to a horizontal slit aperture, 2 mm wide, and the lens was used to form an enlarged image of the illuminated aperture on the vertical slit of a medium quartz spectrograph, at a fixed object-image distance  $\ell$ . Spectrograms were taken for varying object-image distances  $d$ . The height of the spectrum (for each value of  $d$ ) varies with wavelength, having a minimum with sharp upper and lower extremes at the wavelength region in focus. The focal length at the required

wavelength was obtained from  $\ell$  and the value of  $d$  corresponding to the spectrogram for which this wavelength was in focus.) Also, the fringe spacing was altered to give about 2 horizontal fringes in the visible field of view, so that 4 or 5 fringes crossed each vertical line in the spectrogram at  $3000 \text{ \AA}$ . A spectro-sil plate  $C_2$ , polished to the same specifications as the windows, was inserted in the lower beam, with its plane perpendicular to the beam, in order to produce the required high order fringes with maximum contrast, and the aperture  $A$  was now focused on  $S$ , by means of  $L_3$ . Two plate thicknesses 3 mm and 5 mm were used.

#### 4.5. Experimental Precautions

Once the interferometer had been adjusted to form visible interference fringes, it was found that these suffered from two different types of instability. The first was a slow drift across the field of view due to thermal disturbances (air currents etc.), and the second was a comparatively high frequency oscillation due to vibrational disturbances.

The vibrational disturbances were safeguarded against by ensuring that the interferometer was completely isolated from any other part of the apparatus or its supporting framework. The optical bench was also screwed to the table through tough foam rubber, but this was not very successful, and since vibrational disturbances were carried by the floor of the laboratory, all rotary pumps on the same floor were switched off before exposures were taken.

The thermal drift of the fringes was more difficult to eliminate. First the interferometer mounts were completely closed up with cardboard,

leaving holes only for the beams of light to enter and leave by. Next the horizontal paths between the interferometer plates and the reaction and compensating tubes were enclosed by hollow cardboard cylinders. The junction with the interferometer was made by means of loose folds of soft tissue paper to eliminate transmission of vibrational disturbances from the rest of the system to the interferometer. The arrangement up to this stage is shown in Plate 3. It was furthermore necessary to screen the furnace from the rest of the system with sections of metal ( $1/16''$  aluminium) sheeting. The compensating tube was also wound round with strips of  $1/64''$  copper foil. Finally, the "closed-up" interferometer mounts and the enclosed path between them and the two tubes up to the water coolers were covered over with rectangular cardboard houses, as may be seen in Plate 1, which gives an overall view of the apparatus.

The fringe pattern was now found to be stable for periods of up to half an hour in the isolated laboratory, but was still sensitive to even the very small atmospheric disturbances produced by people moving about in other parts of the laboratory (even ten or more yards away). This was due to the presence of the hot furnace producing quite large thermal differentials in the atmosphere round the interferometer. It was thus necessary to obtain spectrograms of the fringe pattern overnight. The control of the furnace temperature to  $\pm \frac{1}{2}^{\circ}\text{K}$  was found to be satisfactory from the point of view of fringe stability.

It was found necessary to stop down the cross section of the interferometer beams to about 1 cm in diameter in order to maintain a sufficiently high fringe contrast when the furnace was running, on

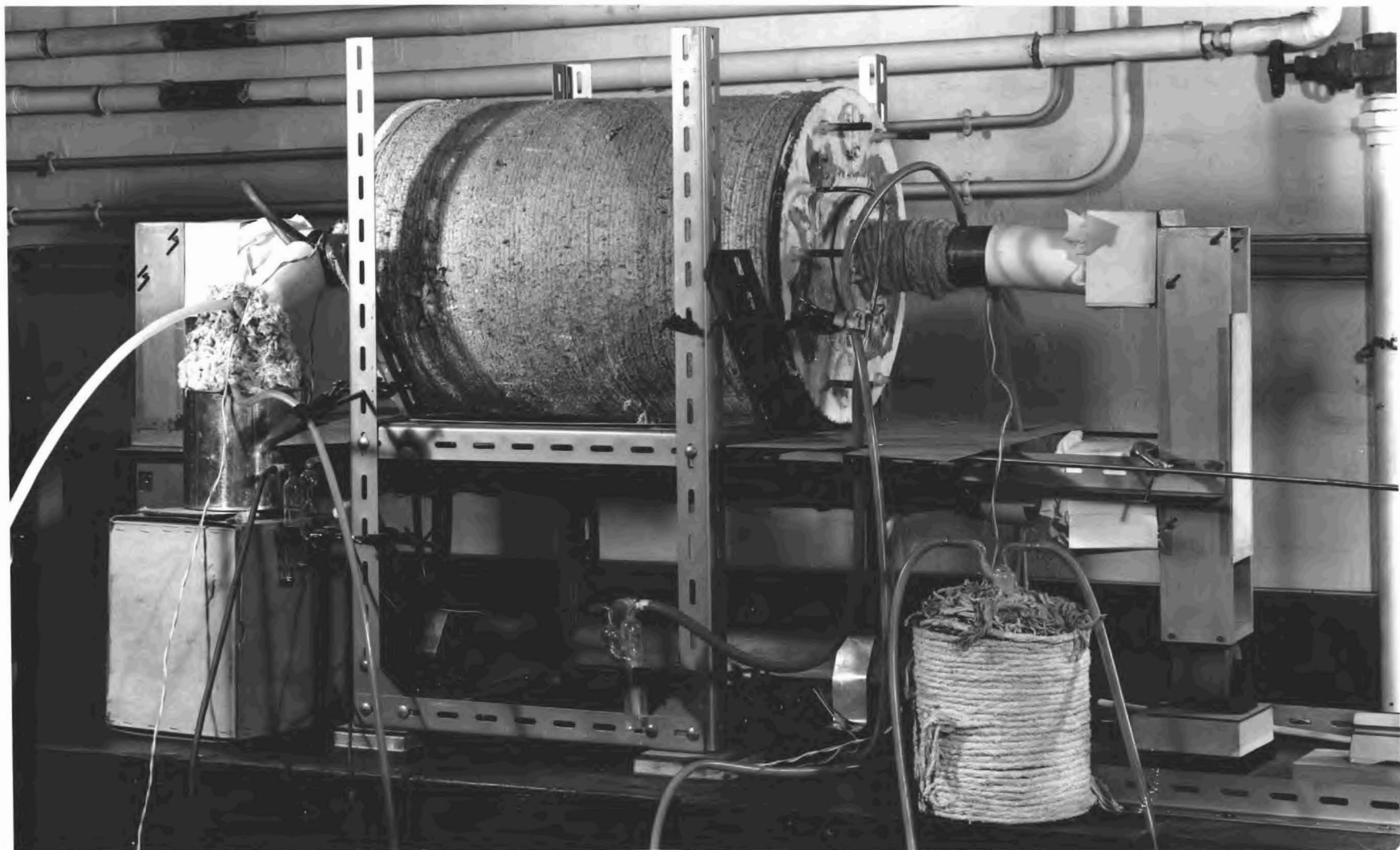


Plate 3: Detail of Thermal Shielding

account of the non-uniformity of the temperature - see section 5.7 - and hence the optical density of the gaseous mixture, over the cross-section of the reaction tube near its ends. This resulted in exposure times of about 3 minutes.

The stability of the basic adjustment of the interferometer was good in view of the fairly simple construction. The interferometer remained in adjustment over long periods, forming white light fringes of high contrast after only a minimum of adjustment to the plates in the mount nearest the spectrograph. The final fine adjustments were made only after the water heating system had reached equilibrium - see 5.4.

When the final adjustments to the interferometer had been made, the high pressure mercury lamp was replaced by the xenon arc.

It was now necessary for the experimenter to have access to the plateholder end of the spectrograph, both to open and close the slit, and also to rack the plateholder down so that about 6 exposures could be made on the same plate. In order to minimise atmospheric disturbances, the experimenter sat at the plateholder end of the spectrograph continuously during exposures, and a cardboard screen was placed between this end and the interferometer. Even after allowing a half hour interval to pass before taking any exposures, only one or two of the 6 exposures on each plate were measurable.

CHAPTER V

EXPERIMENTAL (B) - THE REMAINDER OF THE SYSTEM

5.1. The Background Source

The requirement is a source of continuum both as strong and as free from emission lines as possible, in the regions 3050 - 3175 Å and 2800 - 2900 Å. A previous worker on anomalous dispersion in this laboratory, Chamberlain, 1962,<sup>62</sup> investigated a number of very high pressure gas arcs made available by A.E.I. Ltd.

The gas arcs investigated by Chamberlain were:

- (a) GAE 6 (high pressure xenon arc operating at 18 atmospheres), AC 15 amps;
- (b) XBU (linear xenon arc), AC 25 amps;
- (c) MEX/D (xenon/mercury arc), AC 15 amps.

He found that the GAE 6 was clearly the brightest source of the three, over the whole of the spectral range investigated, 3000 - 7000 Å.

The author found that the more recently available higher powered lamp, the XE/D (high pressure xenon arc), 25 amps, was more intense than the GAE 6 by about a factor of two at 3100 Å. Comparisons were made between the new XE/D, the Osram ME/D (high pressure mercury arc) 4 amps, and the anode crater of a horizontal carbon arc carrying 10 amps. The XE/D was found to be significantly stronger than both those other sources. Moreover, since the XE/D operates at a very high pressure, the three or four emission lines in the relevant regions appeared only as very wide ripples superimposed on the continuum, while in the case of the carbon arc about twenty strong lines are evident. Furthermore,

the carbon arc was found to be inconvenient to use, requiring almost continuous attention during operation.

Chamberlain had also discussed the difficulties involved in using a flash tube in conjunction with the interferometer, on account of the considerable acoustic disturbances produced by the discharge of the condenser bank driving the flash tube. Moreover other workers, experimenting with both flash tubes and the Xe/D in this laboratory, have indicated that there is no significant increase in intensity of the flash tube over the Xe/D in the range relevant to this experiment. Consequently the Xe/D lamp was used as the source of continuum in this experiment.

## 5.2. The Optical System

This is shown in Fig. (5.1). The high pressure xenon arc source at X was imaged on a circular aperture  $\Lambda$  by a short focal length quartz lens  $L_1$  ( $f = 12$  cms, diameter = 5 cms).  $\Lambda$  was situated in the focal plane of a high quality spectroil lens  $L_2$  ( $f = 20$  cms, diameter = 2.5 cms), and the parallel beam of light from  $L_2$  was passed through the interferometer I, used in a Jamin-type arrangement. After passing through the interferometer I, the beam was focussed on the spectrograph slit S by means of a further high quality spectroil lens  $L_3$  ( $f = 40$  cms, diameter = 2.5 cms), the overall magnification of  $\Lambda$  being approximately 2.

All three lenses were plano-convex, and arranged, as shown, to minimise aberrations. Moreover, the surfaces of  $L_2$  and  $L_3$  were polished accurate to  $1/4$  of a wavelength in green light. It may have been possible

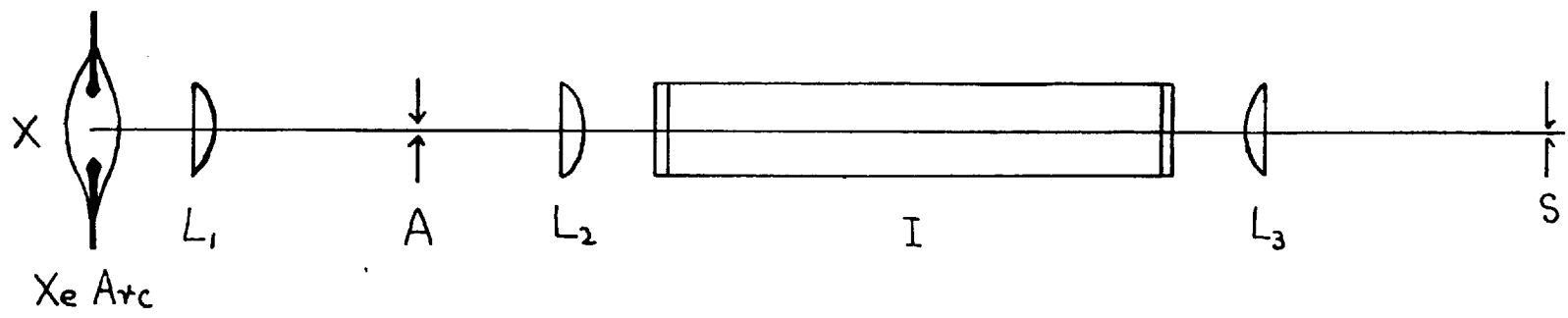


Fig.(5.1): The Optical System



to reduce chromatic aberration by replacing  $L_2$  by a concave mirror, and re-aligning the xenon arc,  $L_1$  and A accordingly, and even more by also replacing  $L_3$  by an achromatic doublet. While having zero chromatic aberration however, a concave mirror has low astigmatism only for small angles of incidence, for which the xenon arc would necessarily be very close to the interferometer. Preliminary investigations showed that the draught round the hot arc produced instabilities in the interference fringes, so a lens had to be used as collimator. Moreover, it would not have been possible to obtain a sufficiently high quality achromat in the time available. The variation of focal length with wavelength for both lenses was found to be sufficiently slow for one setting for each lens to suffice for all the required lines in each of the two bands investigated, (0,0) and (1,0), on account of the small wavelength range ( $\sim 140 \text{ \AA}$ ) over the length of the plate.

The diameter of the stop A was fairly critical. The fringes are most clearly defined for a very small source, so a small aperture is desirable. However, in this case, the height of the field in the spectrograph is small, and can contain only a few fringes in the vortical direction, and consequently only a few hooks for each line. A diameter of 3.5 mm was chosen as optimum.

The lining up of an optical system with so many components is tedious, but it is of the utmost importance. A very small misalignment could necessitate an increase in exposure times by a factor of 2, and in this experiment, on account of long term fringe instability, time is at a premium. In chapter IV, the lining up of the interferometer

on the spectrograph axis is described. The procedure for the alignment of the rest of the optical system is as follows. A pointolite at X was lined up on the axis of the spectrograph. Next the aperture A was adjusted, so that the patch of light passing beyond it fell centrally on the spectrograph grating. Now  $L_1$  was adjusted so that an enlarged image of the source was projected symmetrically onto A. Next  $L_2$  and  $L_3$  were aligned in turn.

### 5.3. The Spectrograph

A stigmatic instrument of high dispersion and moderate resolving power is required, in order that the anomalous dispersion be clearly visible, and the hook separations accurately measured. Preliminary trials on a stigmatised concave grating spectrograph proved unsatisfactory. However, a new plane grating Littrow spectrograph designed and built for this purpose was very satisfactory.

The instrument first tried was a 21 ft concave grating in an Eagle mounting. The grating was a Bausch and Lomb replica, with 1200 lines /mm, and a reciprocal dispersion of  $\frac{1}{2}$  Å/mm in the second order. The instrument was operated at  $f/30$  in the second order at 3100 Å. It was stigmatised by means of a weak spectrosil cylindrical lens ( $\frac{3}{4}$  dioptré) placed inside the spectrograph, about 1 metre from the slit. Whilst this device had proved satisfactory in the first order of the red and near infra-red,

it led to too much loss of definition at  $3100 \text{ \AA}$ , and had to be abandoned. This was due to the difficulty of polishing the surfaces of the cylindrical lens to the required accuracy of  $\frac{1}{4}$  wavelength in the green.

A plane grating, 3 metre,  $f/25$ , spectroil lensed Littrow spectrograph, was therefore designed for use in this experiment. It was designed to make use of a 2160 lines/mm Bausch and Lomb replica plane grating, with a 128 mm ruled width and a 102 mm groove length. The spectrograph was built in the workshop of the Physics Department at Imperial College, and the basic features are shown in Plates 4, 5 and 6.

The blaze wavelength of the grating was  $5000 \text{ \AA}$  in the first order, so that the visible wavelength range is best observed in the 1st order, and the quartz ultra-violet in the 2nd order. The theoretical reciprocal dispersion of the instrument is  $\sim 1 \text{ \AA/mm}$  in the first order, and  $\sim \frac{1}{2} \text{ \AA}$  in the second, so that the wavelength range covered (in the 250 mm long plateholder) is  $\sim 250 \text{ \AA}$  and  $\sim 125 \text{ \AA}$  respectively. Both ranges covered, in the visible as well as the ultra-violet, where the refractive index of quartz varies comparatively quickly with wavelength, are small enough for a simple (as opposed to an achromatic) lens to suffice, together with one value for the radius of curvature of the plateholder ( $\sim \frac{2}{3}$  x the focal length of the lens). The shape of the lens was chosen to be plano-convex, since it is this shape that occurs at the minimum of the plot of coma against lens bending. The lens was also arranged with its curved face nearest the grating, so that the angles made by each ray with both surfaces were as nearly equal as possible, to minimise the aberration for the lens. The lens was made



Plate 4: The Overall Structure of the Spectrograph



Plate 5: The Grating and Lens Carriage




Plate 6: The Slit and Plateholder

of spectro-sil, from a blank 5" in diameter and  $\frac{1}{2}$ " thick, and was ground to give a focal length of 3 metres in the green. Both surfaces were polished accurate to  $\frac{1}{4}$  wavelength in the green.

The measured reciprocal dispersion of the instrument was  $0.53 \text{ \AA}/\text{mm}$  in the second order at  $3100 \text{ \AA}$ , the dispersion being adequate for accurate hook measurements. The resolving power was found to be rather better than 100 000, compared with the theoretical value of 275 000. The resolving power was not investigated more precisely, as a value of 100 000 was judged adequate for this experiment. (A later worker found that the resolving power of the instrument was rather better than 175 000.)

A  $90^\circ$  totally reflecting prism was used, and this was made of spectro-sil, and was 2.5 cm long, the width of both perpendicular faces being 1.25 cm. The slit was a Hilger and Watts single stage slit (F 1497).

#### 5.4. The Gas System

This is shown schematically in Fig. (5.2). Commercial oxygen is bubbled slowly, at a rate of about 2 bubbles/sec, through about 8 cm of distilled water in the bubbler A and the saturated oxygen is then led into the heated reaction tube B at one end, and out free to the atmosphere at the other end, having passed very slowly through the whole length of B. Both ends of the reaction tube are cooled by passing water through the brass water jackets C and C' stuck on with silicone rubber, in order that the ends of the reaction tube may be conveniently closed by spectro-sil windows pressed on to silicone rubber (Edwards High Vacuum,

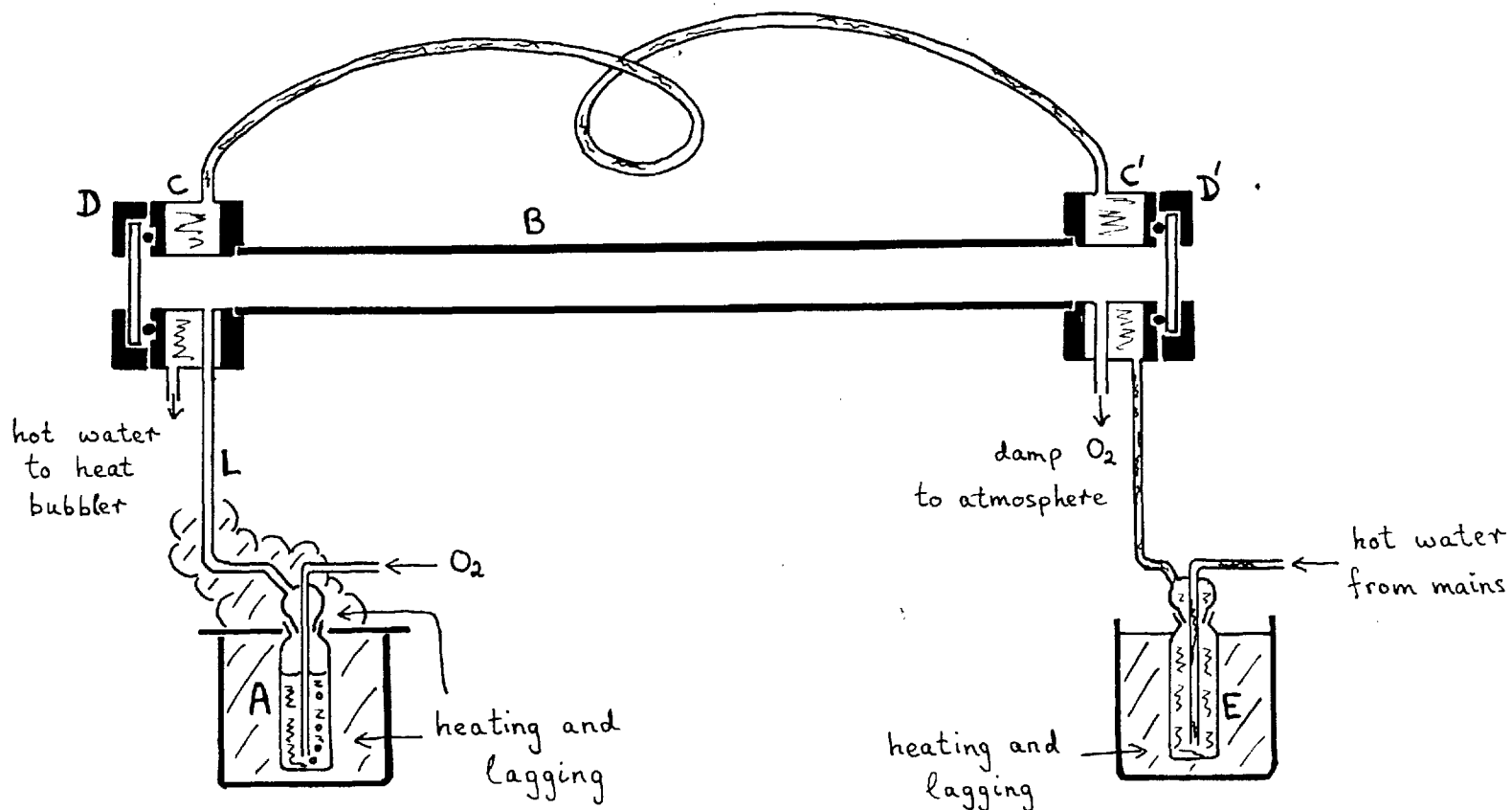


Fig.(5.2): The Gas System



Type VIT 1146) "O" rings by brass rings D and D'. In order to obtain the maximum concentration of OH radicals in the reaction tube, in order that the hook separations be most clearly visible and accurately measured, the ratio of hydrogen to oxygen nuclei present must be 1:1 (Bonhoeffer and Reichardt, 1928<sup>63</sup>). This requires a ratio of 2:1 of water vapour to oxygen molecules in the gaseous mixture before it enters the reaction tube, corresponding to a saturated vapour pressure of water at about 88°C.

In order to fulfil this requirement, it is necessary not only to heat the water in the bubbler, but also to make sure that the gaseous mixture does not come into contact with any surface cooler than the hot water in the bubbler, before it passes out of B. This was fulfilled as follows. Hot water from the mains supply at about 50°C was heated to between 80 and 100°C in the vessel E, before being passed through C' and C. This same hot water was used to heat both the bubbler, and the lead L from the bubbler to the reaction tube, as shown in Fig. (5.3). The hot water was passed through lead piping, wound tightly round L many times in close contact so as to form a sheath round it, and also wound loosely round the bubbler, before it was led away to the drains. The bubbler was stood in a water bath W, and the lead piping was evenly spaced from the bottom to the top of the bubbler, so as to maintain a uniform temperature in the bath. The whole system comprising the water bath, the top of the bubbler, and the heated lead to the reaction tube, was lagged with asbestos wool. A suitably cut cardboard disc was fitted around the neck of the bubbler to take the weight of the asbestos wool

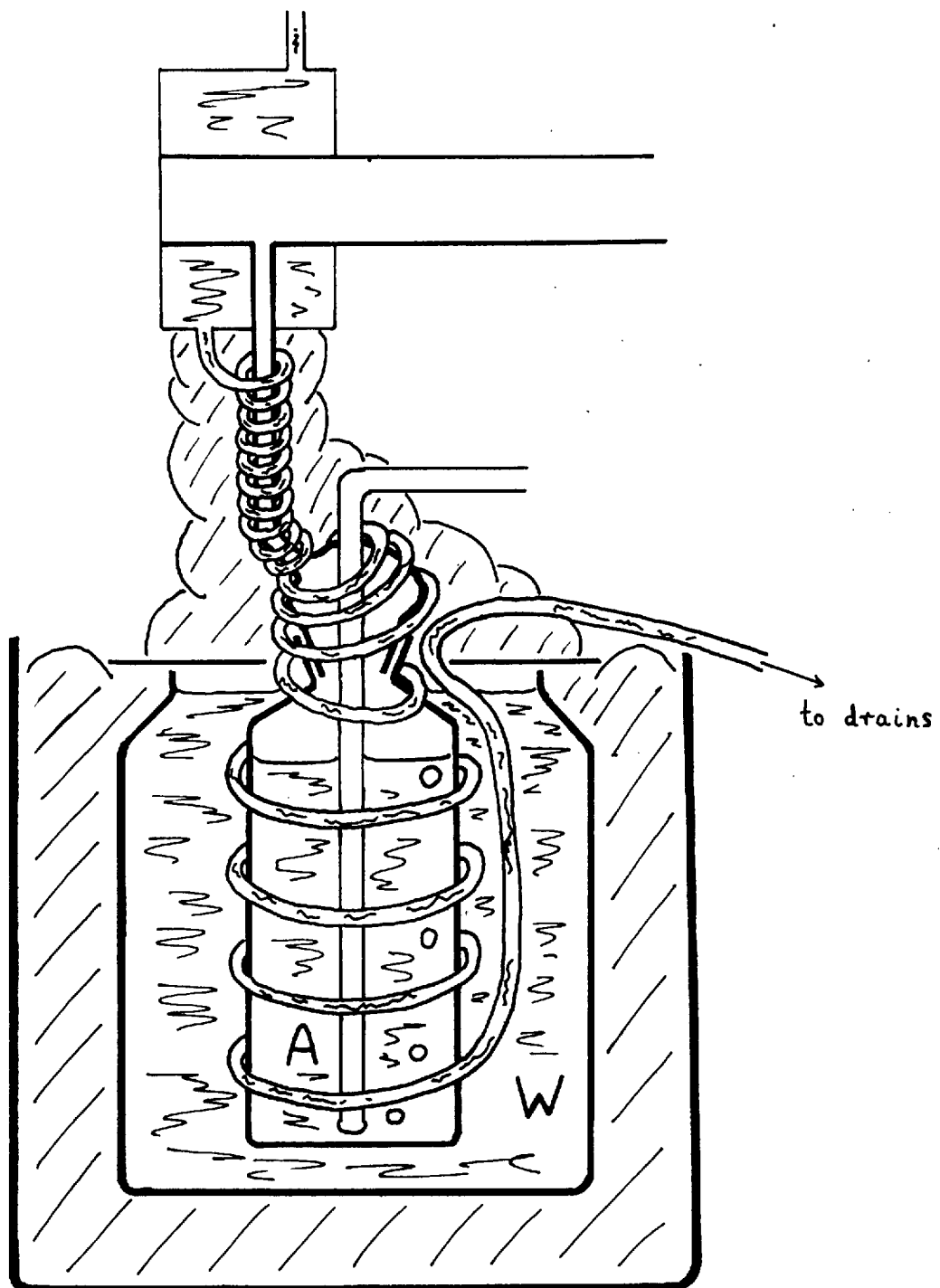


Fig.(5.3): The Bubbler and Associated Apparatus

above the water in the bath, the cardboard itself being supported by the rim of the water bath. A small slot in the cardboard disc enabled a mercury in glass thermometer to be inserted into the water to measure its temperature.

The vessel E was made of pyrex in order to withstand temperature gradients and was heated by three strip heaters, such as are used for heating the mercury in diffusion pumps, running parallel off a variable voltage. This vessel was also lagged with asbestos wool, and the voltage was slowly raised to its desired value over a period of one to two hours. The water heating system reached equilibrium about 2 to 3 hours after the water heater was first turned on. The temperature of the water in the bath W was the same before and after stirring indicating that the temperature of the water was uniform over the volume of the bath. The system was so heated and lagged, that in equilibrium the temperature of the water in the bubbler must of a certainty have been identical with that of the water in the bath. The special windows of the reaction tube were heated by the radiation from the very hot ( $\sim 2000^\circ\text{K}$ ) zone at the centre of the reaction tube, and were too hot to allow condensation of the water vapour on them. The ends of the reaction tube were also hotter than the water coolers, even when these were passing hot water.

It was thus possible to heat the water in the bubbler up to about  $90^\circ\text{C}$ , without producing any loss of water vapour through condensation before the gaseous mixture escaped into the atmosphere.

### 5.5. The Furnace

Preliminary calculations showed that, in order to obtain a sufficiently high density of OH radicals from dissociation of water vapour, it was necessary to heat the water vapour up to temperatures of about 1800°K. A variety of methods of obtaining these temperatures were considered before it was decided to use an alumina tube furnace, wound with molybdenum strip. Commercially available recrystallised alumina tubes can withstand temperatures up to about 2000°K, when the alumina begins to soften, although care must be taken when heating above about 1100°K, when alumina undergoes a change of crystal structure. The melting point of molybdenum is 2890°K, but it begins to oxidise above about 500°K, and needs to operate in a reducing atmosphere above this temperature if it is not to oxidise and burn out, the oxides of molybdenum being volatile.

The furnace design used in this experiment is shown in Fig. (5.4). A is a "purox" impervious recrystallised alumina" tube 75 cm long, internal diameter 5.1 cm, and wall thickness 0.4 cm.

M is the molybdenum strip 3 mm wide, and  $\frac{1}{2}$  mm thick, wound tightly round the tube A. Molybdenum is a very tough, springy metal, and it was obtained in strips rather than as wire so as to make the bending easier. Great care was necessary when winding the molybdenum strip round the tube. The windings were retained at each end by means of two bands S and S' of molybdenum, 3 to 4 cm wide and  $\frac{1}{2}$  mm thick, clamped round them and crewed tight, the loose ends of the narrow molybdenum strip being led out between the screws as shown in the figure.

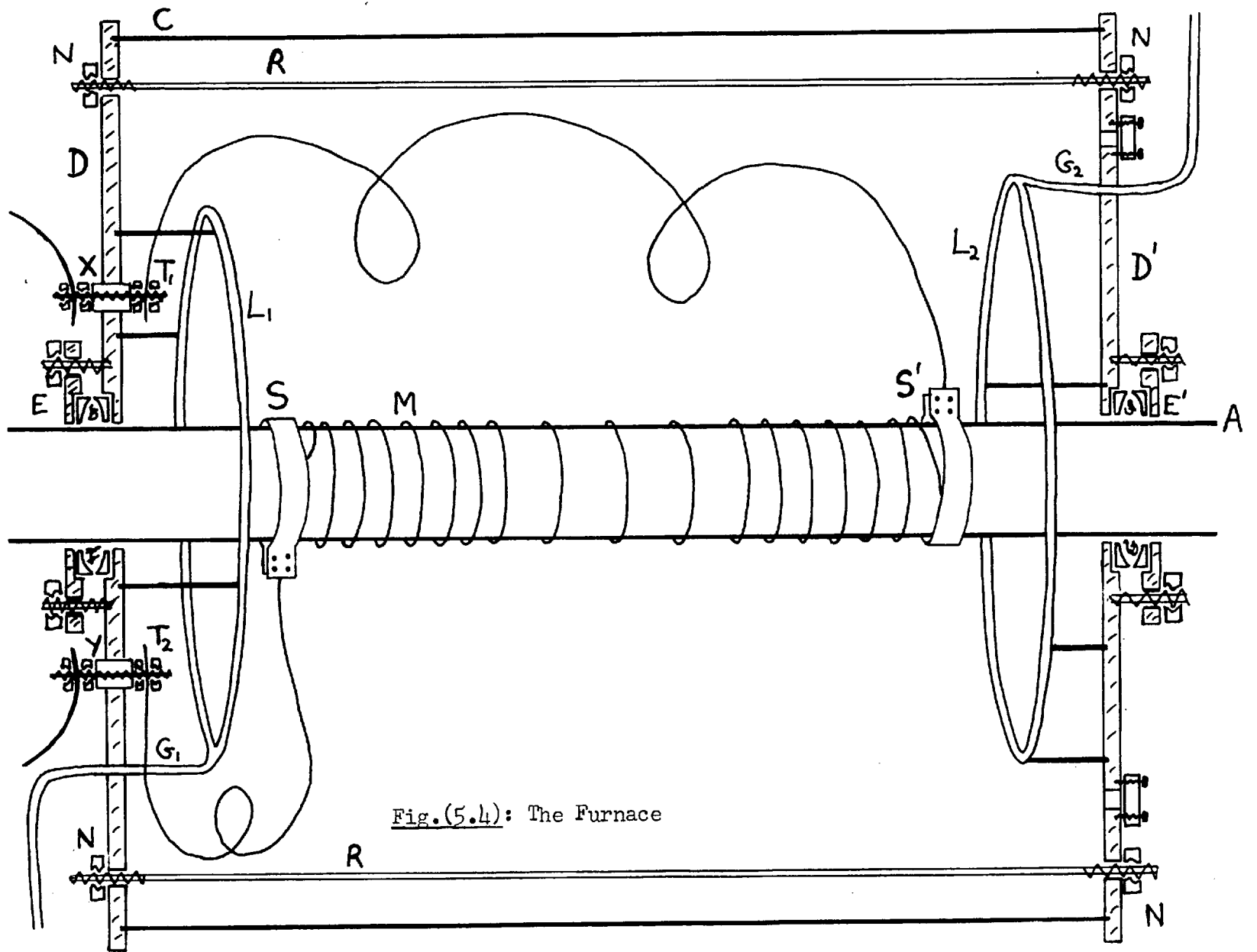


Fig. (5.4): The Furnace

The winding spacing is maintained by spreading a layer of alumina cement about  $\frac{1}{2}$  cm thick over the windings, having previously wetted the tube. The cement was made up by adding water to alumina powder (Morgan's "Pure Alumina 961") and mixing well until the mixture acquired a creamy texture. The cement was left to dry overnight.

The winding spacing over both outer thirds of the wound length were uniform and equal, with a gap of about 1 mm between the turns. The spacing over the central third was also uniform, but greater than for the outer thirds, with about 5 mm between turns, so that the number of turns/cm over the central region was about half that over both outer regions. This was done in order to increase the length of the "hot zone" of the furnace, where the temperature is less than 50°K lower than the maximum temperature. Preliminary investigations with uniform winding spacing over the whole length, showed that the temperature profile for this condition had a sharper peak. Altering the spacing, as described above, gave a more flat-topped, bell shaped curve, with a "hot zone" about  $1\frac{1}{2}$  times as long, as shown in Fig. (5.5).

Nearly the whole length of the furnace tube is encased in a cylindrical metal case, 60 cm long, and 40 cm in diameter, the cylindrical steel sheeting C enclosing the volume between the stool and plates, D and D'. The spacing of the end plates is maintained by means of six rods, R,  $\frac{3}{8}$ " in diameter, with nuts N screwed on to exert pressure on the outsides of the plates.

X and Y are two cylindrical sindanyo plugs insulating the brass screw terminals of the heating section from the metal casing. Two

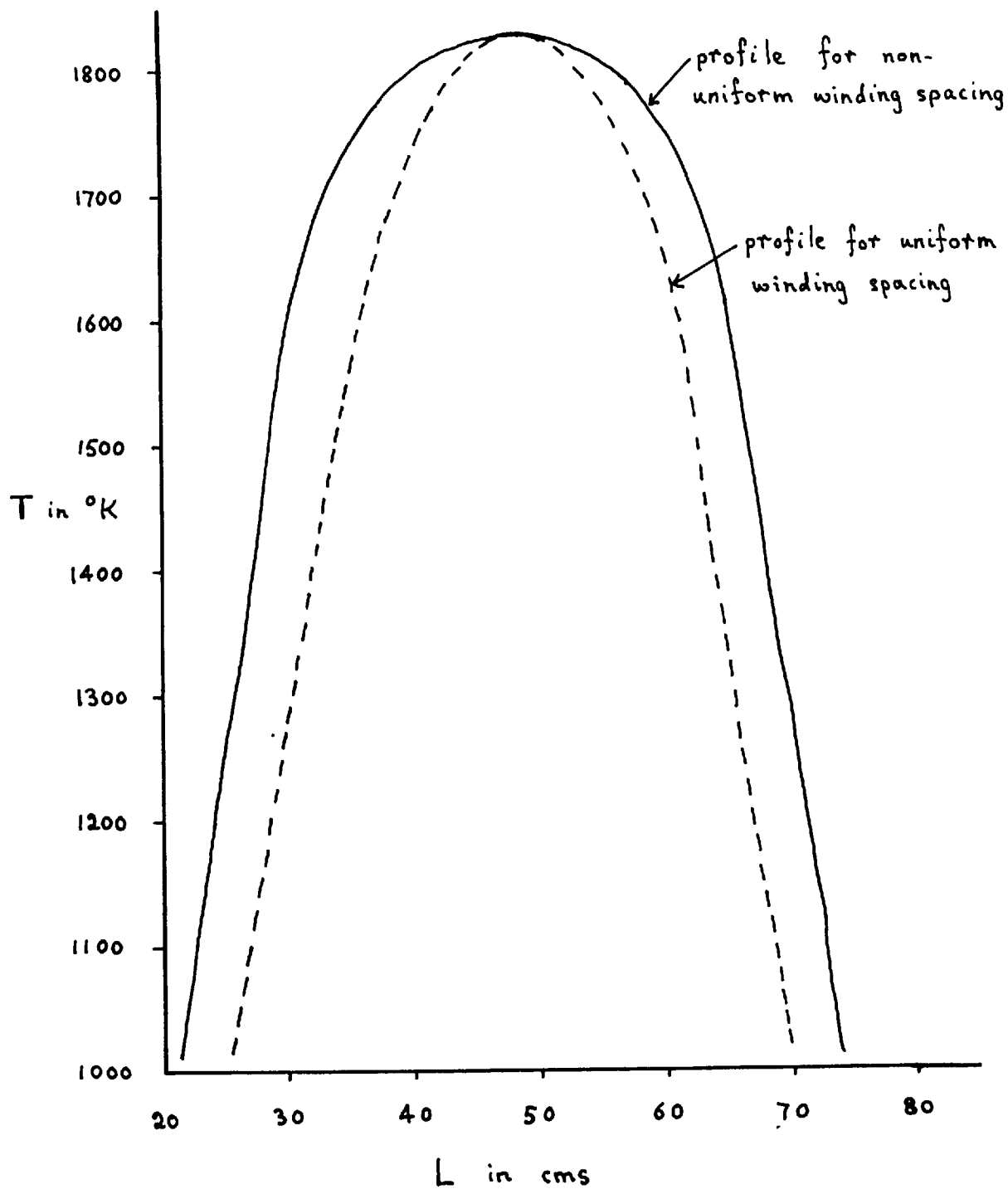


Fig.(5.5): Temperature Distribution along the Length of the Furnace

extra lengths of molybdenum strip are wound round once under the molybdenum bands at each end of the heating element, so that the leads from here to the terminals consist of three strands of molybdenum strip in order to maintain them at a comparatively low temperature. The leads are insulated by running a continuous chain of porcelain beads over them, before securing them between two nuts screwed on to the inner end of each terminal,  $T_1$  and  $T_2$ .

$L_1$  and  $L_2$  are two hollow loops of fine wire gauze wrapped round perforated metal tubing connected to metal tubes,  $G_1$  and  $G_2$ , leading out through the end plates D and D'. They are each supported by three other metal rods screwed into the end plates D and D'. Forming gas, a mixture of hydrogen and nitrogen, is led in through  $G_1$ , diffuses out through  $L_1$ , and passes through the space surrounding the molybdenum strip, maintaining a reducing atmosphere round it, before diffusing into  $L_2$  and passing out through  $G_2$  into the atmosphere.

The small gap between the alumina tube A and each of the end plates is sealed as follows. Two steel discs H, about 1 cm thick, 12 cm in diameter, each with a centre hole to take the tube A, and with a saucer-like curvature on one side, are slid over A, with their curved ends facing each other. One of them partly fits into a shallow hole in the end plate, about  $\frac{1}{4}$  cm deep. The other, outer disc fits into a similar hole in a small end plate E (or E') about 16 cm in diameter and 1 cm thick. The cavity between the inner, curved faces of the discs H, is "overfilled" with "hallite twist" (graphite impregnated asbestos string), well coated with silicone grease. The discs are then pressed



together by pressing the outer end plate E on to them by means of nuts being uniformly tightened on to six threaded rods running through E and screwed into D. The greased hallite twist is then forced round A at the ends, forming a seal. Both ends are treated in this way.

The cavity bounded by the end plates, the cylindrical casing, and the alumina tube, is filled with calcined alumina (furnace grade, - 120 + 300 mesh) as thermal insulation. This is introduced through two holes in one of the end plates symmetrically placed about the alumina tube and about 4 cm in diameter. The powder is packed tight by banging the side C of the furnace with a rubber bung stuck on the end of a metal rod. When the furnace is packed tight with alumina powder, holding about  $1\frac{1}{4}$  cwt of it, the two filling holes are closed by means of two discs screwed down over them.

Now all possible leaks in the furnace casing at the junctions of C and D and D', points of contact between A and D, D', X, Y, N etc., are sealed by painting silicone rubber over them.

The furnace was mounted on a stand constructed from lengths of "Handy Angle". The height of the furnace was adjusted so that the upper beam of the interferometer passed centrally through the reaction tube.

#### 5.6. Temperature Control

The recrystallised alumina reaction tube R (84 cm long, 3.9 cm inside diameter, 4.7 cm outside diameter) was placed inside the furnace tube (75 cm long, 5.1 cm inside diameter) symmetrically with regard to

length. The tubes were a fairly close fit with about 4 mm clear along their uppermost lengths.

The power to heat the furnace was supplied and controlled as shown in Fig. (5.6). R is the reaction tube, inside the furnace tube A, wound with molybdenum strip M. Power from the 240 v AC mains is taken through a (10 amp) "Troidac" variable transformer C, and a 2:1 (3 kw) step down transformer B, and is fed into M. G is an ammeter to measure the current through the furnace. D is a 5 ohm resistor bypassing the mercury switch S, operated by the temperature controller T (Smith's Series 5 Mechanical Proportional Controller). Both T and S are powered from the mains, as shown, and T obtains its information from the controlling thermocouple J.

The controlling thermocouple (5% Pt and Rh / 20% Pt and Rh) is encased in recrystallised alumina sheaths and positioned along the uppermost gap between the alumina tubes, with its junction about  $\frac{1}{3}$  of the way along the total length of the reaction tube. Each arm of the thermocouple was joined to a copper wire leading to T, at a "chocolate box" connector stuck on the top of one of the water coolers with silicone rubber.

The temperature of the thermocouple junction can be read directly off T, and this temperature can be maintained below or equal to a certain constant value by setting the position of a controlling pointer, P, along the temperature scale. If the power fed in is such that the temperature at the junction exceeds the temperature set by the marker, the mercury switch is turned off. The bypass resistor is used to maintain

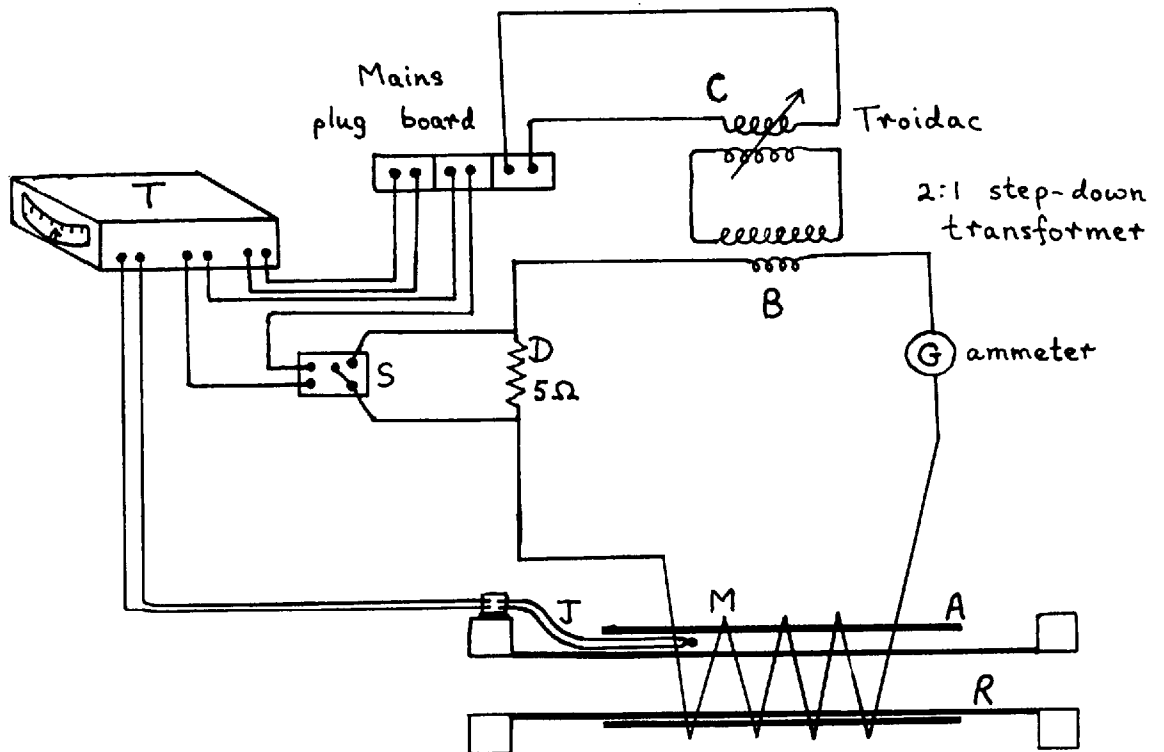


Fig.(5.6): Temperature Control

a current approximately half that with the switch on, so that the furnace temperature does not fall off too rapidly. Its value of 5 ohm is chosen since the resistance of the furnace windings at average operating conditions is about 5 ohm. In practice P oscillates slowly about its mean value, with a period of about 10 sec, and with an amplitude that can be varied up to about  $70^\circ$  at  $1500^\circ\text{K}$ . With this controlling system, the temperature of the thermocouple junction could be maintained constant to  $\pm \frac{1}{2}^\circ$  of the temperature marked out by P at its lowest extreme.

#### 5.7. Temperature Calibration

The temperature measurements inside the reaction tube were made by means of two reference thermocouples (both 5% Rh and Pt / 20% Rh and Pt) which remained permanently inside the tube in fixed positions. The hot junction of one was at the middle point of the tube's length, and that of the other was about  $\frac{1}{3}$  of the way along. Both thermocouples were encased in recrystallised alumina sheaths, and lay on the bottom of the tube. The temperature at any point inside the furnace, corresponding to any pair of fixed temperatures given by the reference thermocouples, was measured by means of a thermocouple that could be slid along the whole length of the tube. This thermocouple, also clothed with recrystallised alumina sheaths, was fixed inside a narrow recrystallised alumina tube, closed at one end and just wide enough to take it, with the hot junction in contact with the closed end of the narrow tube. During the calibration experiment, one of the spectro-sil windows was

replaced by a brass disc fitted with an Edwards High Vacuum seal adapted to allow this alumina tube to slide in and out of the reaction tube. The tube was long enough to reach about 6 or 7 cm past the middle point of the reaction tube.

The two arms of the calibrating thermocouple are connected to two copper leads at a "chocolate box" connection just outside the open end of the sliding alumina tube. These go to one of three pairs of terminals in a slide wire bridge. In reading off the temperature from the tables supplied by the manufacturers, due allowance was made for the e.m.f. at the effective cold junction temperature at the "chocolate box" connection, which was about 10°C above room temperature.

The reference thermocouples led out to opposite ends of the reaction tube. The two arms of each of these thermocouples were soldered on to two stout copper wire terminals, sticking up about  $\frac{1}{2}$  cm above the floor of each water cooler, leading out of each of these through a copper tube, and insulated from each other and from the walls of this tube by silicone rubber which also holds them in place. Copper wire leads were soldered on to the outer ends of these terminals, and led to the remaining two pairs of terminals on the slide wire bridge. The temperature at the effective cold junctions of the reference thermocouples, the inner ends of the terminals through the water coolers, was measured in a subsidiary experiment, positioning the hot junction of a thermocouple about  $\frac{1}{2}$  cm above the floor of one of the water coolers, and leading the two arms directly to the slide wire bridge. The temperature was measured at varying temperatures of the water circulating

through the coolers, and was found to be about 23°C hotter than this water. Due allowance was made for this in reading off the temperatures of the reference thermocouples.

The temperature was measured at 2 cm intervals along the axis of the reaction tube. Preliminary measurements with a uniformly wound furnace tube gave the fairly sharp peaked temperature profile given by the dotted line in Fig. (5.5). In the case of the experimental non-uniformly wound furnace tube described earlier, the bell-shaped profile given by the full line in Fig. (5.5) was obtained.

The temperature profile was measured at varying rates of passing oxygen through the bubbler, from zero to about twice as fast as the experimental conditions of about 2 bubbles/sec. The only noticeable effect was a slight displacement of the profile in the direction of the gas flow. No alteration of the length of the hot zone was observed. At the middle point of the reaction tube, where the profile reached a maximum, the temperature was found to be constant to  $\pm 1^\circ\text{C}$  over a length of about 5 cm. The shift of the temperature profile was less than 2 cm even for the highest bubbling rate. The only factor determining the effective temperature profile was seen to be the temperature given by the thermocouple at the middle part of the reaction tube.

The temperature at off-axis points, both vertical and horizontal, was also investigated. Over the central third of the reaction tube, the temperature at these points was the same as that at the axis. Over the outer thirds of the reaction tube, the temperature on either side of, and above the axis, was found to be higher than that at the axis,

while the temperature below the axis was lower.

The slight effect of the calibrating system on the temperature distribution inside the reaction tube was estimated, and allowed for, by observing the effect on the reference thermocouples as the sliding alumina tube was moved along the axis of the reaction tube. The effect was to raise the temperature of the reference thermocouples by about 5 to 10°K as the end of the sliding tube approached the thermocouple junction.

The temperature profile along the axis of the reaction tube was calibrated for three different maximum temperatures given by  $T_1$ . These were 1770°K, 1820°K and 1920°K. The five maximum temperatures at which photographs were taken and hook separations measured, were 1820°K, 1865°K, 1890°K, 1920°K and 1955°K. The temperature profiles under these conditions for which the maximum temperatures were 1865°K and 1890°K were obtained by interpolation, and that for which the maximum temperature was 1955°K was obtained by extrapolation. The errors in interpolation and extrapolation were estimated to be less than  $\pm 1^\circ\text{K}$  over the significant temperature range.

CHAPTER VIOSCILLATOR STRENGTH RESULTS6.1. Introduction

Interference fringes displaying anomalous dispersion near lines in the (0,0) and (1,0) bands were photographed in the second order spectrum on Zenith plates, using a spectrograph slit width of  $20\mu$ . Zenith plates cut off at  $5200\text{ \AA}$  are thus sufficient in themselves to eliminate the first order spectrum at  $6000\text{ \AA}$ . They are also fairly fast, but still sufficiently fine-grained to allow the hook separations to be measured with reasonable accuracy. A photograph of these fringes showing hooks near lines in the (0,0) band, may be seen in Plate 7. The 18 lines labelled (by their branch designation and  $K^n$  values) are those whose  $f$ -values were obtained and presented in Table 6.1 (the error indicates the experimental scatter only).

Photographs of hooks for the (0,0) band were taken at 5 different temperature settings of the furnace. At each of these furnace settings, photographs were taken with two different thicknesses of plate in the compensating beam for each of two bubbler temperatures. Thus 20 good exposures were obtained for the (0,0) band.

The hook separations and the gradients of the fringes were measured on a Zeiss comparator. The hook separation for each line on a given plate was taken as the mean of measurements made on the three or four hooks present in the vertical field of view. Lines whose hook separations were less than 0.2 mm were judged to have errors greater than the 10%



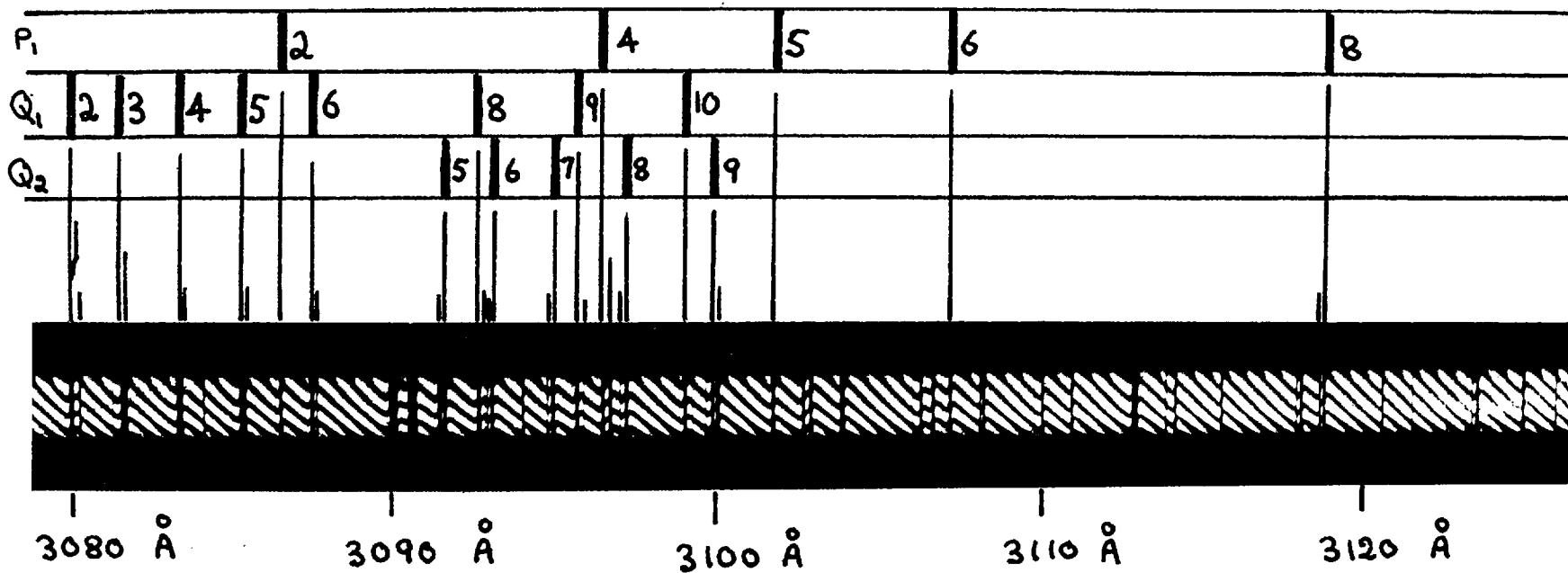


Plate 7: Part of the (0,0) Band showing Hooks near Lines whose f-values are presented in Table 6.1.

Table 6.1. Absolute f-values in the (0,0) Band.

| <u>K<sup>00</sup></u> | <u>f<sub>J<sup>0</sup>J<sup>00</sup></sub> x 10<sup>14</sup></u> |                      |                      |
|-----------------------|--|----------------------|----------------------|
|                       | <u>P<sub>1</sub></u>   | <u>Q<sub>1</sub></u> | <u>Q<sub>2</sub></u> |
| 2                     | 8.3 ± 0.2  | 10.2 ± 0.5           | -                    |
| 3                     | -  | 11.0 ± 0.5           | -                    |
| 4                     | 7.7 ± 0.3  | 12.1 ± 0.4           | -                    |
| 5                     | 7.4 ± 0.2  | 12.4 ± 0.4           | 12.9 ± 0.5           |
| 6                     | 7.6 ± 0.3  | 12.8 ± 0.4           | 12.9 ± 0.5           |
| 7                     | -  | -                    | 13.1 ± 0.3           |
| 8                     | 7.4 ± 0.3  | 13.4 ± 0.4           | 12.1 ± 0.4           |
| 9                     | -  | 12.9 ± 0.3           | 13.3 ± 0.5           |
| 10                    | -  | 12.8 ± 0.5           | -                    |

limit acceptable for the (0,0) band. The reason for the comparatively large errors in the measurements of these small hook separations is that the hooks are measured in a region of rapidly changing intensity when they are very close to the line. Since the  $f$ -value is proportional to the square of the hook separation, and since 20 plates were measured, the random error in these  $f$ -value determinations is less than  $20/\sqrt{20}$  % (about  $4\frac{1}{2}$ %).

About 50 sets of hooks could be measured on each photograph of the (0,0) band, but only 18 lines (for which  $K^m \leq 10$ ) had hook separations  $> 0.2$  mm on all 20 plates, and the remainder were used only in applying the correction procedure described in section 3.4. At  $K = 10$ , the vibration-rotation interaction effect predicted by Learner, 1962,<sup>18</sup> is about 6 to 7%, and should therefore be detectable.

The hooks for the (1,0) band were weaker and adequately measurable on only 8 plates, taken at the two highest temperature settings. About 25 sets of hooks were measured, of which 12 fulfilled the criterion of being  $> 0.2$  mm. The errors in the  $f$ -values of lines in the (1,0) band, given in Table 6.2, are thus considerably larger than those for the (0,0) band.

The spread of results for the (0,0) band was examined in some detail. The experimental scatter of the  $f$ -values of each of the 18 lines obtained from all 20 plates corresponds to a standard deviation of about 17 to 18%. This compares reasonably with the estimated error of less than about 10% for the measurements of the hook separations a ( $f \propto a^2$ ). However, through the random scatter of the  $f$ -values of

Table 6.2. Absolute f-values in the (1,0) Band.

| <u><math>f_{J^0, J^0} \times 10^4</math></u> |                         |                         |                         |
|--|-------------------------|-------------------------|-------------------------|
| <u><math>K^0</math></u>                      | <u><math>P_1</math></u> | <u><math>Q_1</math></u> | <u><math>R_1</math></u> |
| 4  | $4.3 \pm 0.3$           | $4.9 \pm 0.6$           | -                       |
| 5  | -                       | $5.5 \pm 0.8$           | -                       |
| 6  | $3.9 \pm 0.3$           | -                       | -                       |
| 7  | -                       | -                       | -                       |
| 8  | -                       | -                       | $4.8 \pm 0.4$           |
| 9  | -                       | -                       | $5.7 \pm 0.5$           |
| <u><math>K^0</math></u>                      | <u><math>P_2</math></u> | <u><math>Q_2</math></u> | <u><math>R_2</math></u> |
| 5  | $5.0 \pm 0.7$           | $7.4 \pm 0.6$           | $5.2 \pm 0.4$           |
| 6  | $4.4 \pm 0.5$           | -                       | -                       |
| 7  | -                       | $5.7 \pm 0.8$           | -                       |
| 8  | -                       | -                       | $5.0 \pm 0.3$           |

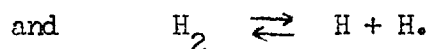
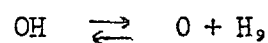
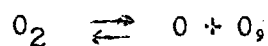
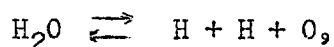
different lines on a given plate, it could be seen that from some plates the  $f$ -values came out consistently high, while from others they came out consistently low, and from two or three plates the scatter was so large that there was no consistency in the magnitude of the  $f$ -values of different lines. The systematic deviation from plate to plate was investigated with regard to furnace setting and bubbler temperature, and there was no correlation with either. It could possibly be due to random errors in the measurement of the maximum temperature of the furnace, from exposure to exposure, or to a systematic subjective error in the measurements of the plates. Measurements on the same lines on different days provide some evidence that the hook separations can be systematically over- or under-estimated from day to day, and hence from plate to plate.

## 6.2. Population Density of the Absorbing Levels

Measurements of the hook separations and fringe gradients give values of the product  $(nf\ell)_{J^{\prime},J^{\prime\prime}} = (n\ell)_{J^{\prime\prime}}f_{J^{\prime},J^{\prime\prime}}$  for each line, as may be seen from equation (3.29), where  $(n\ell)_{J^{\prime\prime}}$  is the population density per unit cross section of the beam, for the lower level of the transition whose  $f$ -value is  $f_{J^{\prime},J^{\prime\prime}}$ . In order to obtain the absolute  $f$ -values of the transition it is necessary to evaluate the quantity  $(n\ell)_{J^{\prime},J^{\prime\prime}}$ . This was done by calculating  $n_{J^{\prime\prime}}$ , the population density per unit volume, for points at 2 cm intervals along the axis of the reaction tube, and integrating over the length of the tube.

$n_{j,m}$  depends on the particular rotational level involved; the ratio of the densities of hydrogen and oxygen nuclei which is determined by the initial water vapour pressure; the total pressure of the mixture of gases in the reaction tube; the equilibrium constants for each particular local temperature; and the temperature explicitly. The calculation was programmed for the IBM 7090 computer.

There are four reversible molecule-atom dissociation reactions involved, namely



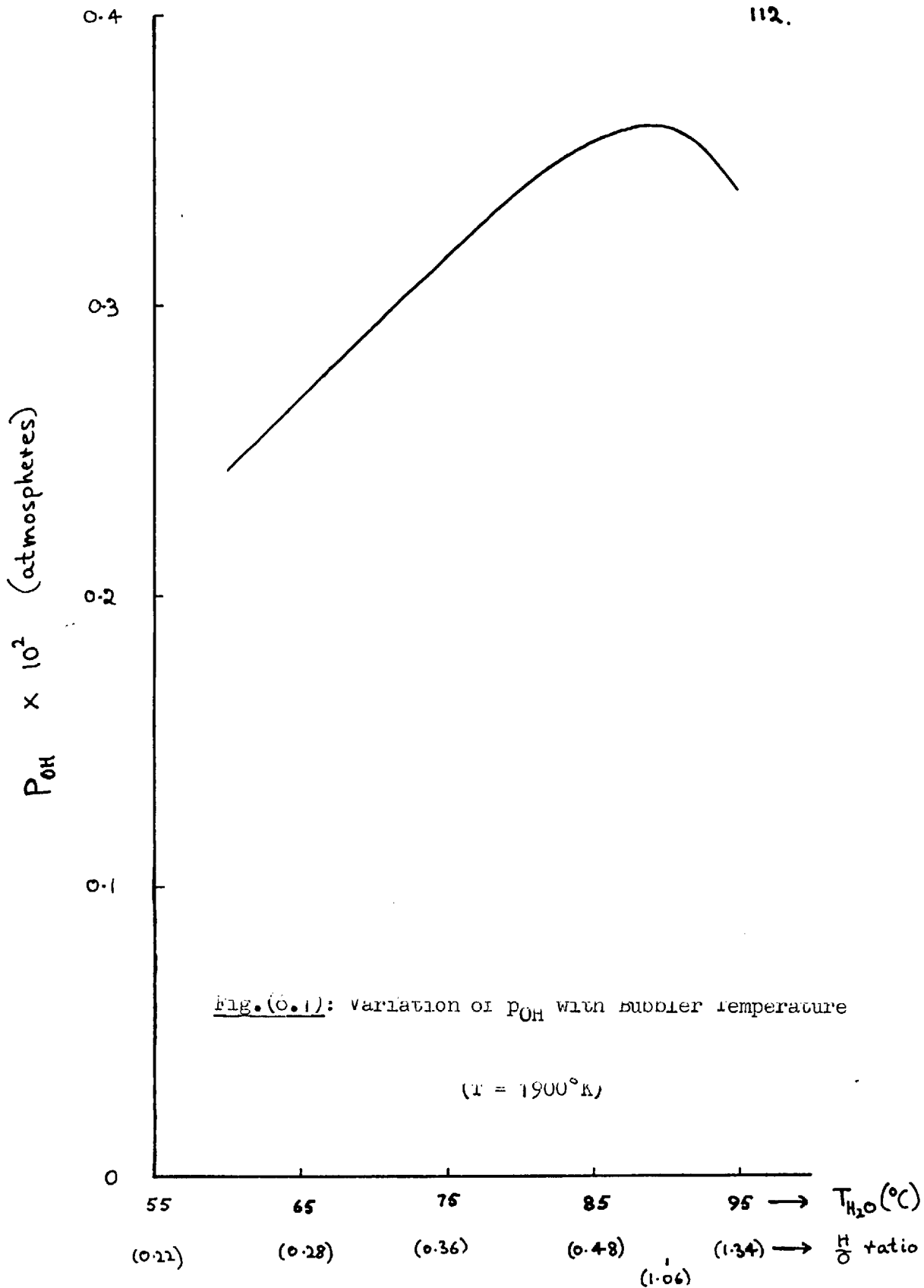
The equilibrium constants for these reactions were computed from the data of the NASA Tables of McBride et al, 1963.<sup>64</sup> The values given by these tables for each reaction at 1000°K, 1500°K, 1800°K and 2000°K were taken and substituted in the expression

$$\log K_i = A_i \log T - B_i T + C_i T^2 + E_i - D_i / (4.5758 T),$$

where  $A_i$ ,  $B_i$ ,  $C_i$  and  $E_i$  are constants for each reaction,  $D_i$  being the dissociation energy of the molecule concerned. Since  $D_i$  is known, the four equations obtained (one for each T) for each reaction are sufficient to evaluate the constants  $A_i$ ,  $B_i$ ,  $C_i$  and  $E_i$ . Now these constants are substituted in the expression for  $\log K_i$  to give the values of the equilibrium constant at all other temperatures  $1000 < T < 2000^\circ\text{K}$ .

The only significant uncertainty in these equilibrium constants was that produced in  $K_{OH}$  by the uncertainty in the dissociation energy of OH. The value given for  $D_{OH}$  in the tables was  $D_{OH} = 101.36 \pm 0.3$  Kcal/mol, from Barroy.<sup>65</sup> The partial pressure of OH,  $p_{OH}$  was found by an iterative process for each local temperature and converted to a local population density, for each initial water vapour pressure. Fig. (6.1) shows the variation of  $p_{OH}$  with bubbler temperature and hydrogen/oxygen ratio for a local temperature of 1900°K. It will be seen that the OH density does indeed peak for a hydrogen/oxygen nuclear ratio of about 1.0, as given by Bonhoeffer and Reichardt, 1928.<sup>63</sup> Fig. (6.2) shows the variation of  $p_{OH}$  with T, for a bubbler temperature of 85°C.

The population density  $n_{J_{00}}$  of the relevant rotational level of the  $V'' = 0$  vibrational state of the  $X^2\Pi$  state was then computed from the vibrational and rotational partition functions,  $Q_{vib}$  and  $Q_{rot}$  respectively, and the Boltzmann factor, using the data of Dieke and Crosswhite, 1948.<sup>21</sup> Finally  $n_{J_{00}}$  was integrated over the central 50 cm of the tube's length, for which  $T > 1000^\circ\text{K}$ . In practice, only the central 30 cm, for which  $T > 1600^\circ\text{K}$ , contributes appreciably to the integral. Over the relevant temperature range 1600 to 1950°K,  $Q_{vib}$  varies from 1.04 to 1.07, and  $Q_{rot}$  is almost exactly 1% below the approximate value given by  $4kT/B$ , where the factor 4 takes into account both spin- and  $\Lambda$ -doubling. Thus we have





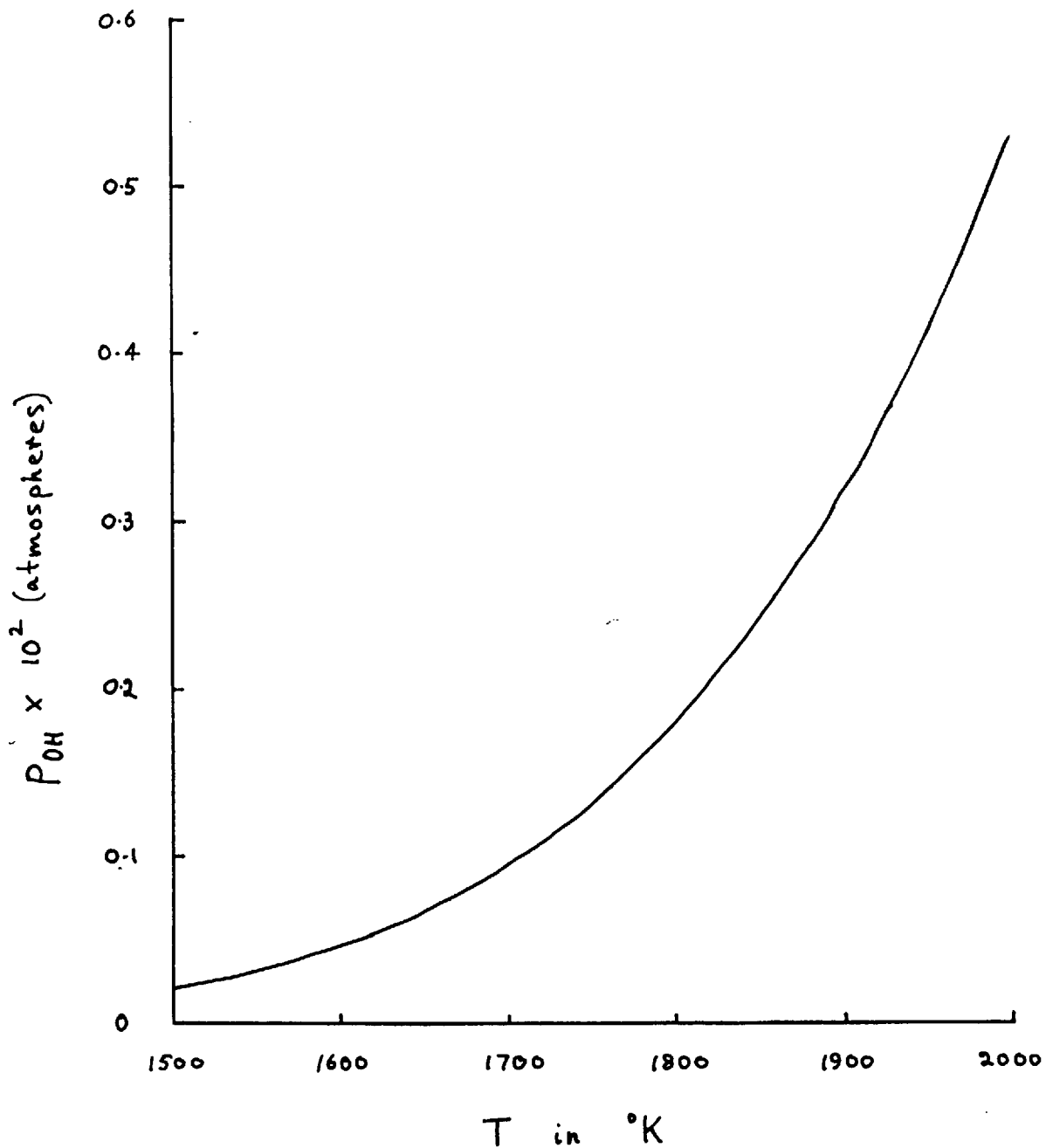


Fig.(6.2): Variation of  $P_{OH}$  with  $T$  ( $T_{H_2O} = 85^{\circ}C$ )

$$(n\ell)_{J''} = \int n_{J''} d\ell \quad \left. \vphantom{(n\ell)_{J''}} \right\} \dots(6.1),$$

with

$$n_{J''} = P_{OH} \frac{273}{T} N_L \frac{(2J'' + 1) e^{-E_{J''}/kT}}{Q_{vib} 3.96kT/B}$$

where  $N_L$  is Loschmidt's number.

It must be noted that the uncertainty in the dissociation energy of OH only leads to an uncertainty in the absolute f-values of the lines. The relative f-values of lines in the (1,0) and (0,0) bands arising from the same lower level are independent of this uncertainty and also of the temperature calibration. The relative f-values of lines within each band and arising from different lower levels depend only on the temperature calibration, which determines the Boltzmann factors.

### 6.3. Vibration-Rotation Interaction in the (0,0) Band

As shown in (2.30), the vibration-rotation interaction effect may be represented by a correction factor  $T_{J''J''}$ , given by

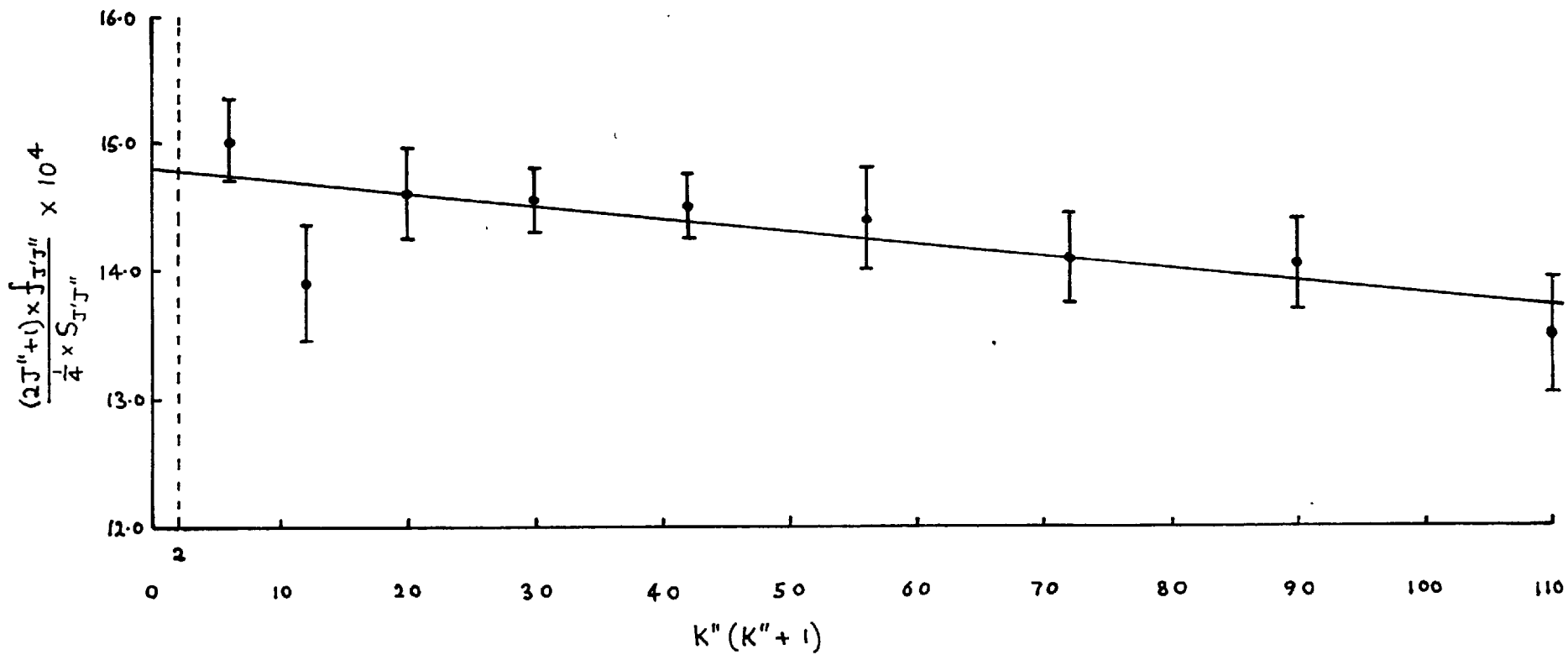
$$f_{J''J''} = f_{v''v''} \frac{\frac{1}{4} S_{J''}^{J''\Lambda''}}{2J'' + 1} T_{J''J''}.$$

As a first approximation, it may be reasonably assumed that  $T_{J''J''}$  is proportional to the rotational energy. The interaction is then best shown by plotting  $(2J'' + 1)f_{J''J''} / \left( \frac{1}{4} S_{J''}^{J''\Lambda''} \right)$  against  $J''(J'' + 1)$  or  $K''(K'' + 1)$  (the latter is more convenient in this case), to give a straight line.

In order to show any variation of  $f$  with  $K$  more clearly, the  $f$ -values were "plate-normalised" as follows, and the normalised  $f$ -values plotted. The "plate strength" was defined as the sum  $S = \sum f_{J^0, J^0}$  over all 18 lines accurately measured, and the mean value  $S_m$ , for all 20 plates, was obtained. Now the  $f$ -values of the 18 lines on each plate were multiplied by  $S_m/S$ . This procedure eliminated the subjective systematic errors referred to in the previous section and any errors in the absolute population density, and reduced the length of the error lines by about 30%, while leaving the mean absolute value of  $f_{00}$  unchanged.

Fig. (6.3) shows a plot of  $(2J^0 + 1)f_{J^0, J^0} / \left( \frac{1}{4} S_{J^0, J^0} \Lambda^0 \right)$  against  $K^0(K^0+1)$ , using the normalised  $f$ -values, and covering values of  $K^0$  from 2 to 10. The differences between the  $f$ -values of different branch types for a given  $K^0$  were smaller than the experimental error, so the three branches  $P_1$ ,  $Q_1$  and  $Q_2$ , for which accurate  $f$ -values were obtained, were plotted together. Each point on the plot is thus the mean of 20, 40 or 60 measurements, depending on whether  $f$ -values from 1, 2 or 3 branches were obtained for the particular value of  $K^0$ . The straight line fitted to the points by the least squares method has a slope of  $-(4.3 \pm 1.4) \times 10^{-4}$ . This corresponds to a decrease in effective vibrational transition probability (i.e. in  $T_{J^0, J^0}$ ) of  $(7.1 \pm 2.3)\%$  between  $K^0 = 1$  and  $K^0 = 10$ , which is in good agreement with Learner's predictions, 1962.<sup>18</sup> It will be seen in the next chapter, however, that this agreement is largely coincidental.

Fig.(6.3): Variation of Effective Band Strength with Increasing Rotation



#### 6.4. Absolute Oscillator Strength of the (0,0) Band

The absolute oscillator strength of the (0,0) band for the rotationless molecule is determined by taking the intercept of the straight line in Fig. (6.3) at  $K'' = 1$ , i.e.  $K''(K'' + 1) = 2$ . The value so obtained is  $f_{00} = (14.8 \pm 0.2) \times 10^{-4}$ , where the error of a little more than 1% is a measure of the experimental scatter only. The same intercept and error were obtained from the straight line given by the original (un-normalised)  $f$ -values. The subjective contribution observed in the scatter of the plate strengths  $S$  may reasonably be assumed to be a random phenomenon, and is therefore taken as included in this error margin.

In order to evaluate possible systematic errors it is necessary to obtain an expression for  $p_{OH}$ , in terms of the equilibrium constants and the initial partial pressure  $P$  of water vapour introduced to the furnace, for use together with equation (6.1). The equilibrium constants are defined as follows:

$$K_{H_2O} = p_H^2 p_O / p_{H_2O}, \quad K_{OH} = p_H p_O / p_{OH},$$

and  $K_{O_2} = p_O^2 / p_{O_2}$ , where  $p_H$ ,  $p_O$ ,  $p_{H_2O}$  and  $p_{O_2}$  are the partial pressures of atomic hydrogen, atomic oxygen, water vapour and molecular oxygen respectively. Thus we have

$$p_{OH} = \frac{p_H p_O}{K_{OH}} \quad \dots(6.2),$$

which may be written as

$$p_{\text{OH}} = \frac{(p_{\text{H}} p_{\text{O}}^{\frac{1}{2}})}{p_{\text{H}_2\text{O}}^{\frac{1}{2}}} p_{\text{H}_2\text{O}}^{\frac{1}{2}} \frac{(p_{\text{O}_2}^{\frac{1}{2}})}{p_{\text{O}_2}^{\frac{1}{4}}} p_{\text{O}_2}^{1/4} \frac{1}{K_{\text{OH}}} \dots(6.3).$$

At the relatively low temperatures of this experiment, there is very little dissociation of  $\text{H}_2\text{O}$  and  $\text{O}_2$ , with  $p_{\text{OH}}$ ,  $p_{\text{O}}$ ,  $p_{\text{H}}$  and  $p_{\text{H}_2} < 5 \times 10^{-3}$  atmospheres. Thus we write  $p_{\text{H}_2\text{O}} = P$ , and since the total gas pressure is 1 atmosphere, we have  $p_{\text{O}_2} = (1 - P)$ . Equation (6.3) may thus be written in the approximate form

$$p_{\text{OH}} = \frac{K_{\text{H}_2\text{O}}^{\frac{1}{2}} K_{\text{O}_2}^{1/4}}{K_{\text{OH}}} P^{\frac{1}{2}} (1 - P)^{1/4} \dots(6.4).$$

This expression is found to be accurate to better than  $\frac{1}{2}\%$  for the conditions of this experiment. Fig. (6.1) shows the dependence of  $p_{\text{OH}}$  on  $P$  (at constant temperature,  $T = 1900^\circ\text{K}$ ), and Fig. (6.2) shows the dependence of  $p_{\text{OH}}$  on  $T$  (at constant  $P$ ) through the equilibrium constants.

The uncertainty of  $0.3\%$  in the dissociation energy of  $\text{OH}$  leads to a corresponding uncertainty of  $8\%$  in  $K_{\text{OH}}$ , and hence in  $p_{\text{OH}}$ , as remarked in section 6.1. Another source of potential systematic error is the uncertainty of  $\pm 5\%$  in the calibration of the thermocouples used to measure the furnace temperature. Consideration of equations (6.1) and (6.4) shows that this results in a  $3\%$  uncertainty in  $n_{\text{JK}}$ , almost entirely due to the dependence of  $p_{\text{OH}}$  on  $T$  shown in Fig. (6.2). Combining all the errors together, we have the final result

$$f_{\text{oo}} = (14.8 \pm 1.3) \times 10^{-4}.$$

### 6.5. Absolute Oscillator Strength of the (1,0) Band

The (1,0) band is significantly weaker than the (0,0) band, and only the strongest lines in each branch, for which  $K'' \sim 5$ , were measurable with reasonable accuracy. Moreover, since only 8 adequate exposures were obtained for the (1,0) band, the random errors in the  $f$ -values are relatively large,  $\sim 20\%$ . The vibration-rotation interaction effect for this band is theoretically rather smaller than for the (0,0) band, the effect at  $K \sim 5$  being only about 1%, which is negligible compared to the experimental scatter. Vibration-rotation interaction has therefore been neglected in the calculation of  $f_{10}$ , <sup>which</sup> ~~and~~ is obtained from each  $f_{J',J''}$  in Table (6.2) by applying equation (2.30) with  $T_{J',J''} = 1$ . The mean for all lines is  $f_{10} = (8.9 \pm 1.5) \times 10^{-4}$ , the error being a measure of the experimental scatter only. Combining this with the potential systematic errors described in the previous section, we have the final result  $f_{10} = (8.9 \pm 1.7) \times 10^{-4}$ . This is the first absolute measurement of the  $f$ -value of the (1,0) band, as far as the author is aware.

The two values of  $f_{10}$  and  $f_{00}$  obtained in this experiment give  $f_{10}/f_{00} = 0.60 \pm 0.1$ . This is independent of population density calculations as well as the temperature calibration, as shown in section 6.1. This value of  $f_{10}/f_{00}$  is incompatible with Learner's 1962<sup>18</sup> calculations ( $f_{10}/f_{00} = 0.23 \pm 0.03$ ), and it is this disagreement that leads to the recalculations of the vibration-rotation interaction effect in the next chapter.

CHAPTER VII

DISCUSSION OF RESULTS

7.1. Comparison of  $f_{00}$  with Previous Measurements

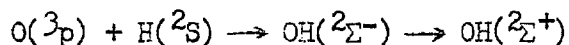
Table 1.1 summarises the published values of  $f_{00}$  to date. In 1963 Golden et al<sup>8</sup> were able to conclude that only Dyne's, 1958,<sup>11</sup> results were inconsistent with a value of  $8 \times 10^{-4} \pm 15\%$ , but the spread of values obtained since then, including the one presented here, has become surprisingly large, the incompatibility of the most recent determinations<sup>8, 14, 15, 16</sup> being particularly strange.

The work of Oldenberg and Rieks<sup>6,7</sup> and Dyne<sup>11</sup> suffers from the effects of incomplete resolution. Both report unexpectedly high values for the observed widths of the absorption lines, with the stronger lines yielding anomalously low results. Kostkowski and Bass, 1956,<sup>17</sup> have discussed the effects of incomplete resolution quantitatively, and have shown that it yields erroneously low results for the  $f$ -values. The error margin on Carrington's 1959<sup>12</sup> result overlaps that obtained for the present work, leaving just the most recent four determinations to be accounted for.

Lifetime methods of determining  $f$ -values are potentially the most reliable, since no calculations of population densities are required. Bennet and Dalby, 1964,<sup>15</sup> determined the lifetime of the  $A^2\Sigma^+ - X^2\Pi$  transition of OH, the transition being isolated by means of a filter having maximum transmission at 3150 Å and a half-width of 200 Å. While



they report that the dominant feature in the spectrum of the source was the (0,0) band (band head 3064 Å), the (1,1) and (2,2) bands are not resolved from the (0,0) band, and the peak transmission of the filter occurs at the region of maximum intensity of the (1,1) band (band head 3122 Å). This lack of resolution results in two possible sources of error. First, the transition probabilities of the (1,1) and (2,2) bands are about 75% and 50% that of the (0,0) band, as given by Dieke and Crosswhite, 1949,<sup>22</sup> and they thus have longer lifetimes than the (0,0) band. The apparent lifetime measured in an experimental system which does not isolate the (0,0) band from these other bands is therefore erroneously long, leading to an incorrectly low value for the f-value of the (0,0) band. Bennett and Dalby estimated that, under the conditions of excitation and observation in their experiment, the error to be expected on this account was small compared to the errors from other sources. This is difficult to check. Secondly, it is possible that the  $v' \geq 1$  levels of the  $A^2\Sigma^+$  state may be populated by the "pre-association" process



described by Gaydon and Wolfhard, 1951.<sup>66</sup> This process is the more probable at the low pressures with which Bennet and Dalby conducted their experiments, since the rate of removal of the free atoms depends on the frequency of collisions and the effective collision life may be comparable with the radiative life, thus lengthening the apparent lifetime of radiation from the (1,1) and (2,2) bands, further decreasing the apparent transition probability of the (0,0) band. In addition,

the (0,0) band itself may be affected by a process described by Douglas, 1966,<sup>67</sup> who has recently discussed in some detail anomalously long radiative lifetimes arising from the mixing of the levels of two electronic states. In this case, the mixing would be between levels of the  $2\Sigma^+$  and  $2\Sigma^-$  states.

The calculation of the population density in the line absorption experiment of Golden et al, 1963,<sup>8</sup> is independent of the dissociation energy of OH, but the f-value determinations are, according to the authors, subject to other possible systematic errors, any of which would lead to a result that was too low rather than too high. Only those aspects concerning the population density of OH will be examined here. The OH in their experiment was produced by the very fast atom-molecule reaction  $H + NO_2 \rightarrow OH + NO$ . This is followed, however, by the two decay reactions  $2OH \rightarrow H_2O + O$  and  $O + OH \rightarrow O_2 + H$ . The effective rate of decay of OH for a stoichiometric mixture of H and  $NO_2$  is about 13 times smaller than the rate of production, and may be reduced by introducing an excess of H over  $NO_2$  in the initial mixture. With a 20-fold excess of H over  $NO_2$ , the authors claimed that the creative process was about 250 times faster than the decay process, and that their experiment was made under conditions where the creative process could be considered as having gone to completion, while the decay processes had not yet made appreciable inroads on the OH concentration. However, a close examination of their results shows a decrease of about 11% in the f-value as the  $NO_2/H$  ratio was increased by a factor of 2.5, from  $1/28$  to  $1/11$ . This detectable variation in the

f-value indicates that the decay process has in fact made significant inroads in the OH concentration. That the OH decay was not detectable as a function of time was probably due to the decay process beginning before the creation process had reached completion, giving a growth and decay curve with a flat topped maximum in a plot of OH population against time. It is also possible that the theoretical population density of OH was further fallen short of, on account of incomplete mixing of H and NO<sub>2</sub>. The fact that the OH population was lower than the calculated value could possibly account for the whole of the discrepancy between their f-value and the one presented in this thesis.

Watson's 1964<sup>14</sup> extra-ordinarily high result has been discussed by Watson and Ferguson, 1965,<sup>68</sup> with special regard for vibration-rotation interaction, but no reason for the discrepancy is suggested.

The value obtained by Bird and Schott, 1965,<sup>16</sup> is nearest to that obtained here. Although the experimental scatter in their results was only about 2%, the authors did not have such high confidence in their results, being faced with the recent determinations of Golden et al, and Bennett and Dalby. In fact, the difference between their result and that of the author is only about 15%, just above the sum of the probable errors of the two determinations.

The present work has also been carefully examined for systematic errors additional to those discussed in section 6.4. The most likely source is incomplete saturation of the oxygen after passing through the water in the bubbler. This would result in an erroneously low f-value if it were significant. In the range of bubbler bath

temperature covered in this experiment, 75°C to 91°C,  $p_{OH}$  is fairly insensitive to changes in  $P$ , as may be seen from Fig. (6.1). Indeed, such a range involves increasing  $P$  by a factor of nearly 2, while  $p_{OH}$  increases by only 20%.

In any case, a systematic variation of much more than about 5% between the  $f$ -values obtained for bubbler temperatures  $\sim 80^\circ\text{C}$  and  $\sim 90^\circ\text{C}$  would have been detectable with the accuracy of the experiment, and no such systematic behaviour was noticeable.

## 7.2. Comparison of $f_{10}$ with Previous Results

No absolute values of  $f_{10}$  exist for comparison, but the author is aware of two experimental values that may be obtained for the ratio  $f_{10}/f_{00}$ . Dieke and Crosswhite, 1949,<sup>22</sup> obtained the value 0.48 for  $p_{10}/p_{00}$ , where the  $p$ 's refer to the band strengths. It will be recalled, from chapter II, that the relations between the oscillator strength for the band  $f_{\nu^i\nu^j}$ , the vibrational transition probability or band strength  $p_{\nu^i\nu^j}$ , and Einstein transition probability  $A_{\nu^i\nu^j}$ , is given by  $f_{\nu^i\nu^j} \propto \nu p_{\nu^i\nu^j}$  and  $A_{\nu^i\nu^j} \propto \nu^3 p_{\nu^i\nu^j}$ . To convert the ratio for  $p_{10}/p_{00}$  to one for  $f_{10}/f_{00}$ , one must multiply each  $p_{\nu^i\nu^j}$  by the average frequency  $\nu_{\nu^i\nu^j}$  of the transition, or divide it by the average wavelength  $\lambda_{\nu^i\nu^j}$ . Taking  $\lambda_{10} = 2830 \text{ \AA}$  and  $\lambda_{00} = 3100 \text{ \AA}$ , we obtain the ratio  $f_{10}/f_{00} = 0.53$  with a probable error of  $\pm 5\%$ , which is in good agreement with the value of  $0.60 \pm 0.1$  presented here. Measurements on the intensities of weak (and optically thin)

lines given in the atlas compiled by Broida and Bass, 1953,<sup>23</sup> using the correction of Lalos, Corrucini and Broida, 1958,<sup>69</sup> and an estimated temperature of 3100°K, lead to a value of  $A_{10}/A_{00} = 0.44 \pm 0.05$ . On dividing by the  $v^2$  factors, one has  $f_{10}/f_{00} = 0.37 \pm 0.05$ . This value is liable to error on account of the uncertainty in the temperature determination.

Taken together, the three experimental results give an average value of  $f_{10}/f_{00} = 0.50 \pm 0.07$  (or  $p_{10}/p_{00} = 0.45$ ). The results of this experiment may therefore be taken as providing confirmation of Dieke and Crosswhite's value of  $p_{10}/p_{00} = 0.48$ , rather than the "smoothed" values of 0.27 and 0.23 presented by Skuler, 1950,<sup>2</sup> and Nicholls, 1956,<sup>25</sup> respectively.

### 7.3. The Electronic Transition Moment for Vibrational Interaction

The confirmation that this experiment gives to Dieke and Crosswhite's 1949<sup>22</sup> experimental ratio of  $p_{10}/p_{00}$  casts doubt on the validity of the exponent in Learner's 1962<sup>18</sup> determination of the electronic transition moment. The exponent had been obtained by fitting theoretical values of  $p_{v'v''}/p_{00}$  to the experimental ratios that had been smoothed by Nicholls, 1956.<sup>25</sup> Nicholl's value for  $p_{10}/p_{00}$  is incompatible with the results of this experiment, consequently a new value for the electronic transition moment has now been obtained by fitting theoretical values to the experimental ratios  $p_{v'v''}/p_{00}$  obtained by Dieke and Crosswhite, 1949.<sup>22</sup> Calculations of the effective relative vibrational transition probabilities

$P_{v'v''}/P_{00}$  for lines in the  $2\Sigma^+ - 2\Pi$  band system were made using Learner's<sup>18,52</sup> method of numerical integration of Morse-Pekeris wave functions. Learner's programme designed for running on a Ferranti Mercury computer, then with the University of London Computer Unit, was modified by the writer to run on the IBM 7090 computer at the Imperial College Computer Unit. The accuracy of the wave functions was checked with regard to orthonormality and the sum rule  $\sum_{v'} q_{v'v''} = \sum_{v''} q_{v'v''} = 1$  for the Franck-Condon factors. The results of these checks are shown in Tables 7.1 and 7.2. The spectroscopic constants used in the computations were taken from the data of Herman and Hornbeck, 1953.<sup>70</sup> The exponential form  $R_e(r) = e^{-ar}$  justified by Learner<sup>18,52</sup> was again chosen for this purpose, and the value of the exponent was determined using a least squares criterion.

In Fig. (7.1) the standard deviation between experimental and theoretical relative band strengths  $P_{v'v''}/P_{00}$  is plotted against the value of the exponent,  $a$ . The theoretical band strengths were calculated for Q lines at  $J = 10\frac{1}{2}$ , for which the transitions are most intense at the reported temperature of observation ( $3000^\circ\text{K}$ ), and were weighted according to the intensities at  $3000^\circ\text{K}$ . The unsmoothed experimental data are seen to be fitted extremely well by an electronic transition moment of  $e^{-5.97r}$ . The error in  $a$  may be assessed as  $\pm 0.15$ . The standard deviation for this value corresponds to less than 3% of the intensity of the (0,0) band, and is of the order of what may reasonably be expected in photoelectric intensity measurements of this kind. Both the deviation at the minimum of the curve and the sharpness of

Table 7.1. Orthonormality of Wave Functions.OH  $X^2\Pi$  State,  $J = 3/2$ 

| $v^i, v^j$ | $\int \Psi_{v^i} \Psi_{v^j} d\tau$ |
|------------|------------------------------------|
| 0,0        | 0.999 992                          |
| 1,1        | 0.999 941                          |
| 2,2        | 0.999 709                          |
| 3,3        | 0.998 796                          |
| 4,4        | 0.992 945                          |

For all  $v^i \neq v^j$ ,  $\int \Psi_{v^i} \Psi_{v^j} d\tau < 1 \times 10^{-6}$

Table 7.2. OH Franck-Condon Factors:  $A^2\Sigma^+ - X^2\Pi$  ( $J = 10\frac{1}{2}$ )

| $v^i \backslash v^j \rightarrow$ | 0      | 1      | 2      | 3      | 4      |
|----------------------------------|--------|--------|--------|--------|--------|
| $\downarrow$ 0                   | 0.8979 | 0.0978 | 0.0043 | 0.0001 | 0.0000 |
| 1                                | 0.0936 | 0.6884 | 0.2015 | 0.0160 | 0.0004 |
| 2                                | 0.0078 | 0.1823 | 0.4706 | 0.2982 | 0.0380 |
| 3                                | 0.0006 | 0.0274 | 0.2491 | 0.2664 | 0.3622 |
| 4                                | 0.0001 | 0.0036 | 0.0597 | 0.2815 | 0.0951 |

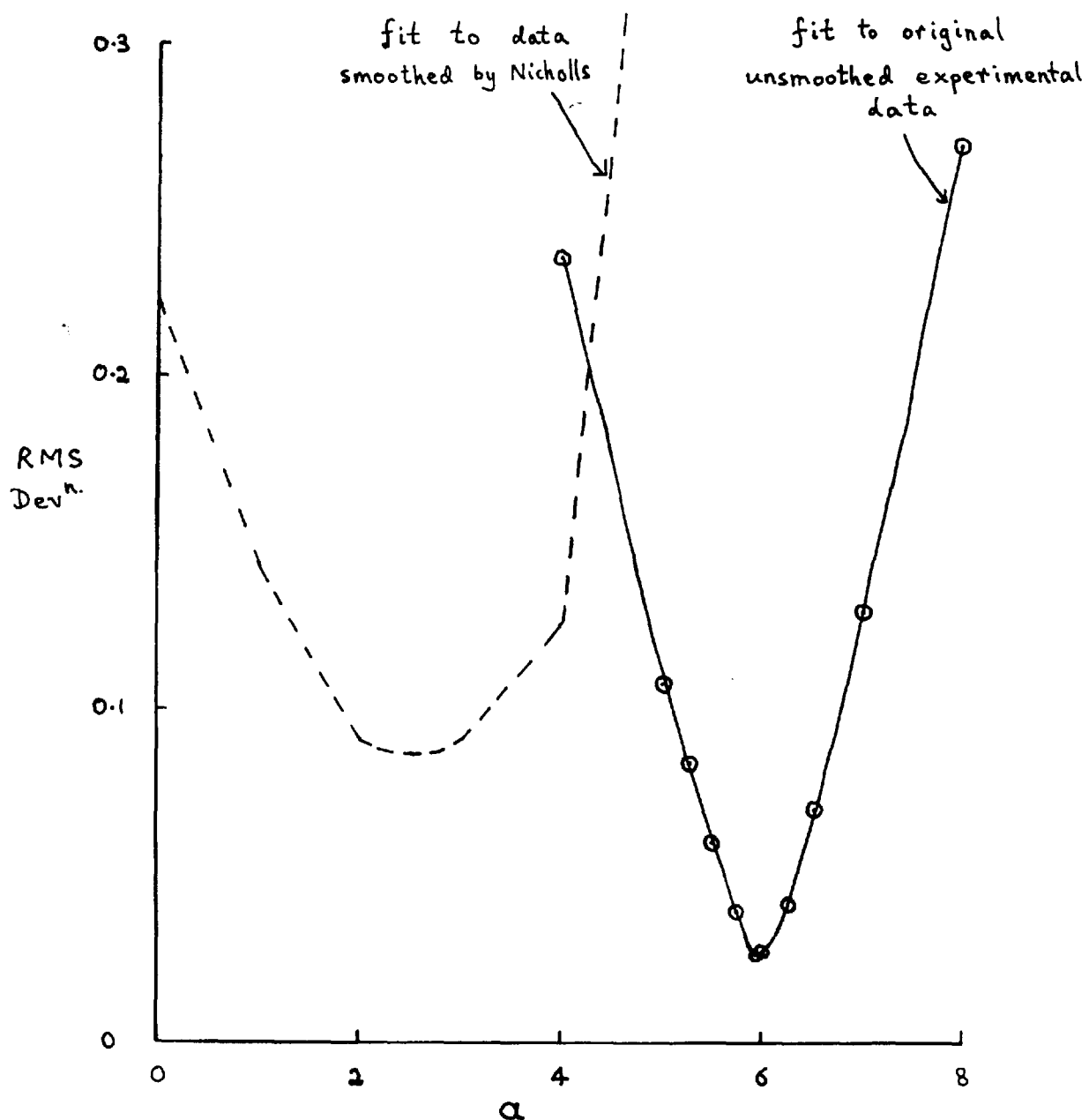


Fig.(7.1): Variation of RMS Deviation between Calculated and Experimental Transition Probabilities with  $a$  in  $R_e(r) = e^{-ar}$



the minimum itself are much improved compared to the fit to the smoothed data (given by the dotted line), and provide further confirmation that the smoothing must be rejected.

Fig. (7.2) shows the dependence of each  $p_{\nu, \nu''}/p_{00}$  on the value of the exponent  $a$ . A value for a one parameter transition moment may be derived from the ratios of the  $p_{\nu, \nu''}$ 's of any two bands. The ratio  $f_{10}/f_{00} = 0.6 \pm 0.1$  from this experiment gives a value  $p_{10}/p_{00} = 0.55 \pm 0.1$  leading to a value of  $a = 6.9 \pm 1.1$ . In emission the ratio of the intensities of the (2,0) and (2,1) bands is independent of temperature. From measurements of lines in these bands given by Bass and Broida, 1953,<sup>23</sup> and using the corrections of Lalos, Curruccini and Broida, 1958,<sup>69</sup> the value  $a = 5.1 \pm 0.8$  is obtained. If the theoretical band strengths are weighted equally rather than weighted according to intensity, then the value  $a = 5.83 \pm 0.3$  is obtained. A weighted mean of all four values of  $a$  derived above gives

$$R_{\nu}(r) = e^{-(5.97 \pm 0.12)r}.$$

Fig. (7.2) also shows that, given an exponential transition moment, the band strengths of most of the bands in the system relative to that of the (0,0) band pass through a minimum, as the exponent is varied from 0 to 8. It is therefore possible to fit these bands, the (0,1) and (0,0) sequences with  $\Delta\nu = -1$  and 0 respectively, with either of two values of the exponent, and it is the (1,0) sequence, whose band strengths relative to the (0,0) band increase continuously with the exponent, that fixes which of the two is correct. The smoothing process carried out by Nicholls, 1956,<sup>25</sup> and mentioned in section 2.5

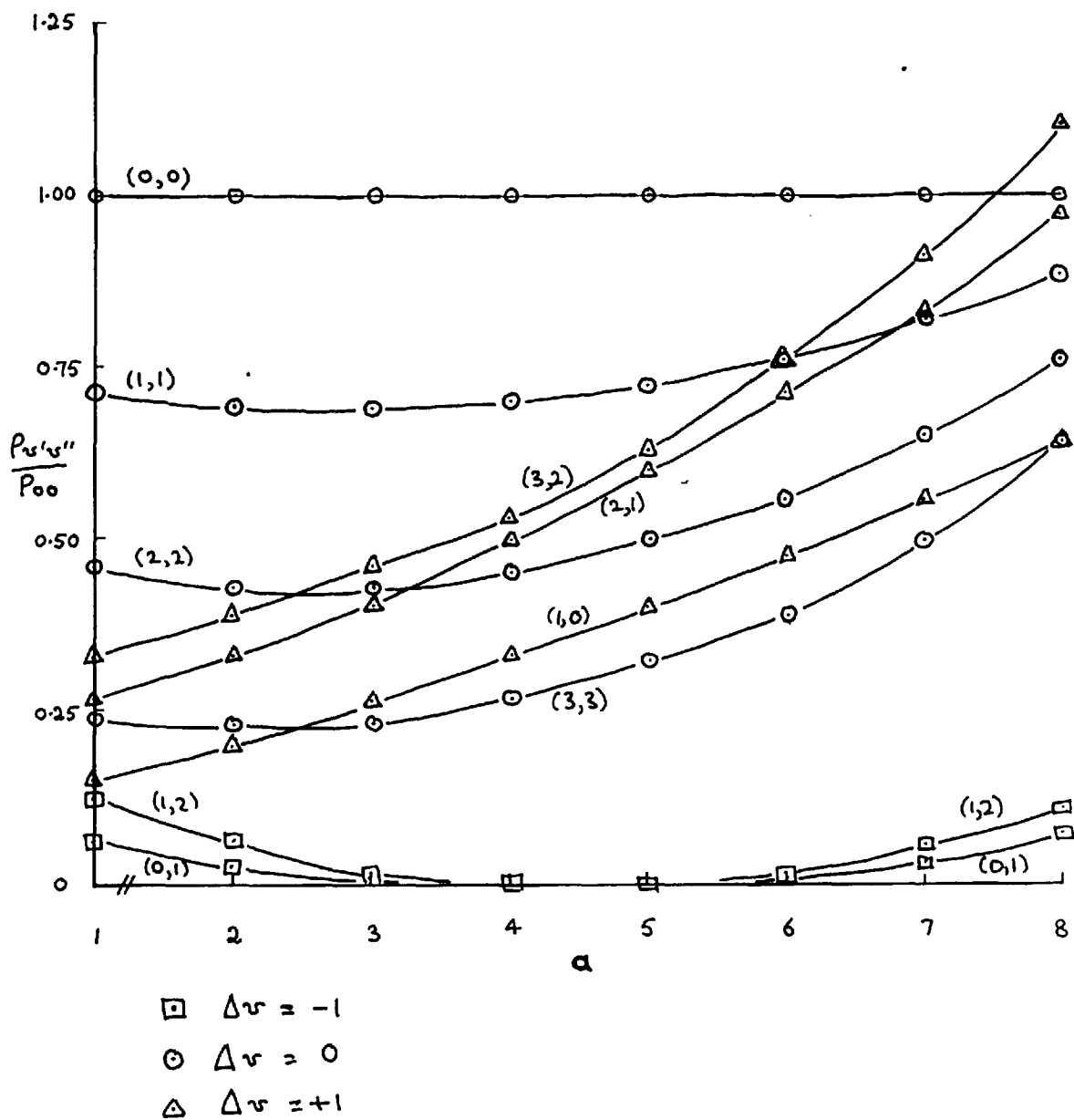


Fig.(7.2): Variation of Relative Band Strengths with  $a$  in  $R_e(r) = e^{-ar}$

was based on the r-centroid approximation. This approach assumes that the electronic transition moment is a slowly varying function of  $r$ , and hence picks out the lower, and incorrect, of the two possible values of the exponent that satisfy the ratio  $p_{v^0v^m}/p_{00}$  for most of the bands in the system.

The form of the ~~electronic~~ transition moment derived here is again (see section 2.5) obtained from the variation of band strengths within the system, and consequently takes into account the breakdown of the Born-Oppenheimer approximation with regard to electronic and vibrational motion. It is therefore suitable to refer to it as the vibrational element in the electronic transition moment, and denote it by  $R_{ov}(r) = e^{-5.97r}$ .

#### 7.4. The Electronic Transition Moment and Rotational Coupling

In section 2.5 it was mentioned that Learner<sup>18,52</sup> used his value of  $R_e(r) = e^{-2.5r}$  for the electronic transition moment to calculate the variation of transition probability with rotational quantum number. Conversely, the variation of f-value with J or K may be used to derive a value for the exponent  $a$  in  $R_e(r) = e^{-ar}$ . A decrease of  $7.1 \pm 2\%$  in the f-value of the (0,0) band between  $K^u = 1$  and  $K^u = 10$  was obtained experimentally and presented in section 6.3. This decrease is close to that calculated by Learner<sup>18,52</sup> and corresponds to a value of  $a = 2.67 \pm 0.9$ . The value of  $5.97 \pm 0.12$  for the exponent corresponds to a decrease of  $14 \pm 0.3\%$  over the same range of  $K^u$ , and is clearly incompatible with the experimental

result.

The electronic transition moment may be examined from the point of view of its effect on rotational temperature determinations. The fact that the effective  $f$ -value of the (0,0) band decreases with increasing  $J$  means that the rotational temperature measurements, whether by a log plot or by the iso-intensity method, would lead to an erroneously low value. Learner<sup>18,52</sup> has calculated and plotted the corrections  $\Delta T$  to be added to the rotational temperatures so determined, up to  $T = 3000^\circ\text{K}$ , for  $R_e(r) = e^{-2.5r}$ . Consider the temperatures derived for the outer cone of a stoichiometric ~~oxy-acetylene~~ flame treated by Broida and Shuler, 1957.<sup>71</sup> The rotational temperature obtained was  $T_{\text{rot}} = 2980^\circ\text{K}$ , while the calculated adiabatic temperature was  $T_{\text{adiabatic}} = 3320^\circ\text{K}$ , and the reversal temperature measured by iron spectrum line reversal was  $T_{\text{Fe}} = 3200^\circ\text{K}$ . The corrected rotational temperatures obtained using  $R_e(r) = e^{-2.67r}$  and  $e^{-5.97r}$  are  $3260^\circ\text{K}$  and  $3560^\circ\text{K}$  respectively. The value of  $e^{-2.67r}$  leads to a temperature very close to  $T_{\text{adiabatic}}$  and  $T_{\text{Fe}}$ , while the value  $e^{-5.97r}$  leads to a temperature that differs by  $\sim 300^\circ\text{K}$ . The temperature measurements of Zirman and Bogdan, 1964,<sup>31</sup> are also consistent with an electronic transition moment of  $e^{-2.7r}$  but not  $e^{-5.97r}$ .

The disagreement between the two transition moments obtained from the vibration-rotation interaction results and the distribution of the band strengths of the vibrational bands in the system may be accounted for if one postulates that the transition moment may be split into two elements. The value  $R_{\text{ev}}(r) = e^{-5.97r}$  obtained in the

previous section accounts for the breakdown of the Born-Oppenheimer approximation with regard to the electronic and vibrational motions. It has also been shown, in section 2.3, that there is an interaction between the electronic and rotational motions of the OH radical. This interaction may be split into two parts, one concerned with the angular part of the eigenfunction, the other with the radial part. The interaction in the angular part manifests itself in the familiar spin decoupling phenomenon, where the coupling between electron spin and orbital motion decreases with increasing  $J$ . The effect on the energy levels is the change of multiplet splitting with increasing rotation, as the coupling scheme changes from being near case (a) to near case (b), and the effect on intensity calculations requires one to replace the Hönl-London formulae, 1925,<sup>42</sup> by those of Hill and Van Vleck, 1928.<sup>49</sup> The radial part of the interaction corresponds to the centrifugal distortion of the rotating molecule, and it is the further effect on the intensities of this distortion that needs to be considered. It seems reasonable, as a first step in the understanding of this interaction, to assume that the interaction between the electronic and rotational motions may be accounted for in the expression for the total electronic transition moment  $R_{\text{ov}J}(r)$ , by a rotational element that is dependent on rotational energy, writing  $R_{\text{ov}J}(r) = R_{\text{ov}}(r) \times R_{\text{O}J}\{J(J+1)\}$ . For the OH(0,0) band, the experimental data are consistent with values  $R_{\text{ov}}(r) = e^{-5.97r}$  and  $R_{\text{ov}J}(r) = e^{-2.67r}$ , giving  $R_{\text{O}J}\{J(J+1)\} = e^{+3.30r}$ . It is postulated that the rotational element  $R_{\text{O}J}\{J(J+1)\}$  is an exponential function of rotational energy as well as internuclear distance for

the simple reasons that the data do not justify the fitting of a function with more than one parameter and that the exponential form is the most convenient single parameter function. Thus we have  $R_{eJ}\{J(J+1)\} = e^{bJ(J+1)}$  and  $R_{\text{ev}J}(r) = e^{-5.97r} e^{bJ(J+1)}$ , where  $bJ(J+1)$  is equivalent to  $(3.30 \pm 1.0)r$ .

The relation between the radial and rotational forms of the exponent in the rotational element of the electronic transition moment may be obtained by considering the centrifugal distortion of the rotating molecule. Fig. (7.3) shows the radial part of the  $v = 0$  eigenfunctions for various rotational states of the OH ground state  $X^2\Pi$ . It shows that the dominant effect of increasing rotation is an outward shift of an otherwise mainly unaltered function. The position of the centre of gravity of the radial part of the eigenfunction is related to the effective B value  $B_{\text{eff}}$ . The rotational energy of the molecule may be represented to a good approximation by

$$\left. \begin{aligned} E_J &= B_v J(J+1) - D_v J^2(J+1)^2 \\ \text{where } B_v &= \frac{h^2}{8\pi^2 \mu r_0^2} \end{aligned} \right\} \dots(7.1),$$

as given by Herzberg.<sup>30</sup> This may be rewritten as

$$E_J = B_{\text{eff}} J(J+1), \quad \text{where } B_{\text{eff}} = \frac{h^2}{8\pi^2 \mu r_{\text{eff}}^2} \quad \dots(7.2),$$

where  $r_{\text{eff}}$  is the effective internuclear separation for the rotating molecule. Thus we have  $B_{\text{eff}} = dE_J/d\{J(J+1)\}$ , so that by combining (7.1) and (7.2), we have

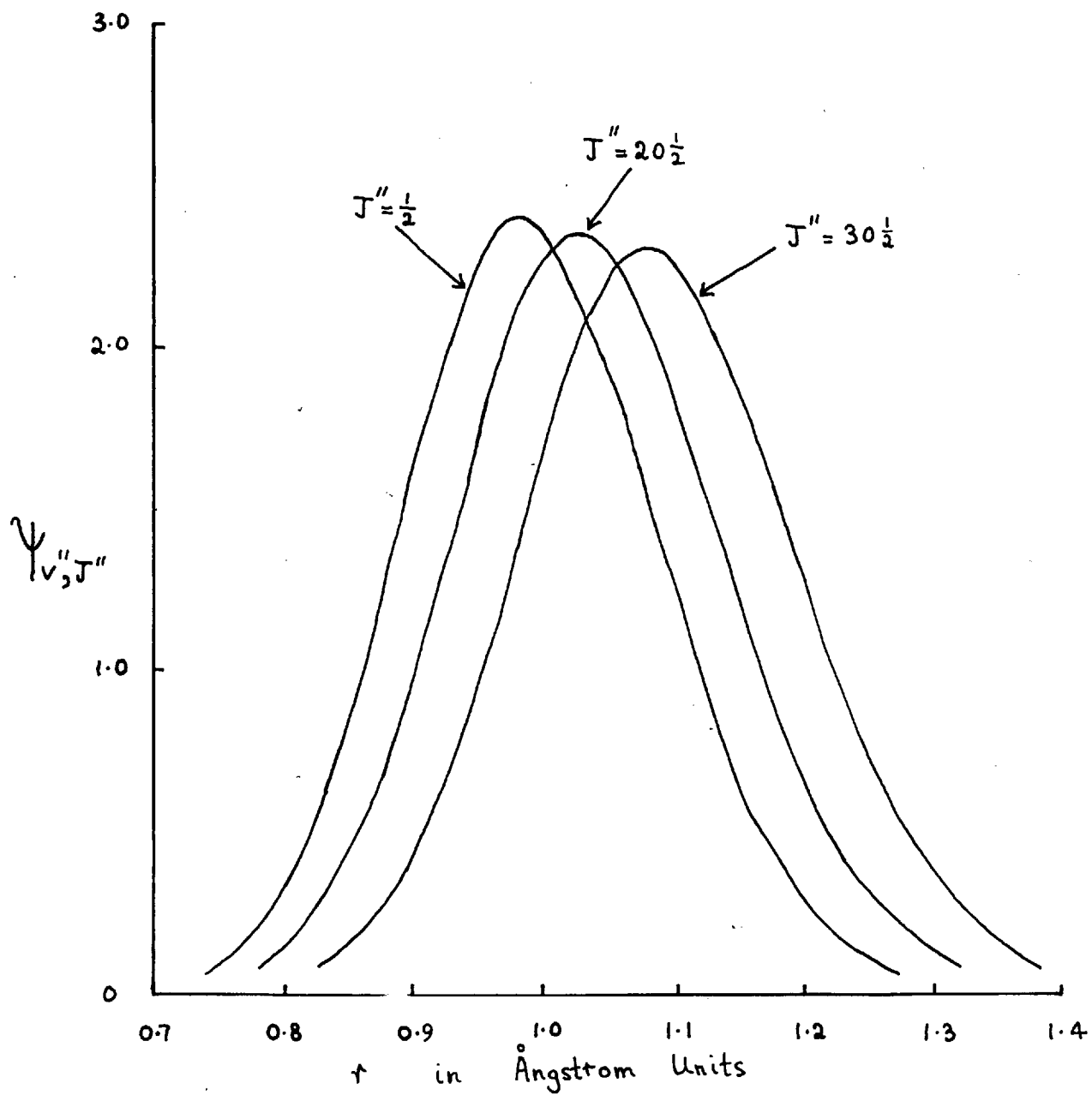


Fig.(7.3): Wave Functions of the  $X^2\Pi$  State, for  $v = 0$

$$B_{\text{eff}} = B_v - 2D_v J(J+1) \quad \dots(7.3).$$

Thus we obtain

$$r_{\text{eff}} = \left( \frac{\hbar^2}{8\pi^2 \mu} \right)^{\frac{1}{2}} \left\{ B_v - 2D_v J(J+1) \right\}^{-\frac{1}{2}}.$$

Then, provided that  $2D_v J(J+1)/B_v \ll 1$ , which is valid for  $J$  less than about 15, we have

$$\begin{aligned} r_{\text{eff}} &= \left( \frac{\hbar^2}{8\pi^2 \mu B_v} \right)^{\frac{1}{2}} \left\{ 1 - \frac{2D_v J(J+1)}{B_v} \right\}^{-\frac{1}{2}} \\ &= r_e \left\{ 1 + D_v J(J+1)/B_v \right\}. \end{aligned}$$

Thus

$$r_{\text{eff}} - r_e = r_e D_v J(J+1)/B_v \quad \dots(7.4).$$

$e^{(r_{\text{eff}} - r_e)}$  = const.  $e^{r_{\text{eff}}}$ , and being here concerned with relative transition probabilities it can be seen that  $e^{3.30r}$  is equivalent to  $e^{bJ(J+1)}$  if

$$b = 3.30 r_e D_v / B_v \quad \dots(7.5).$$

As a first approximation if we use the mean values of  $r$ ,  $B$  and  $D$  for the constants at  $v = 0$  for the two electronic states, we obtain

$$r_0 D_0 / B_0 = 1.095 \times 10^{-4} \quad \text{and} \quad b = 3.62 \times 10^{-4}.$$

In practice the best fit to the experimental data, using an electronic transition moment of the form  $e^{-5.97r} e^{bJ(J+1)}$ , has  $b = (3.60 \pm 1.0) \times 10^{-4}$ .

Learner's<sup>18,52</sup> calculation of  $J$  dependent vibrational transition probabilities  $p_{v',v''}$  were made for  $R_e(r) = e^{-(2.5 \pm 0.5)r}$  and these,



together with the temperature corrections presented, are nearly correct for the (0,0) band, for which the effective value of  $R_{\Theta}(r)$  obtained in this experiment was  $R_{\Theta}(r) = e^{-(2.67 \pm 0.9)r}$ .

Table (7.3) gives relative J dependent vibrational transition probabilities

$$P_{v'v''}(J) = \left| \int \psi_{v'J\Lambda'}(r) e^{-5.97r+3.60 \times 10^{-4}J(J+1)} \psi_{v''J\Lambda''}(r) dr \right|^2$$

for all bands with  $v'$  and  $v'' < 5$ , using Morse-Pekeris wave functions, normalised so that the value for  $P_1(1\frac{1}{2})$  for the (0,0) band is set equal to 1.000.

It is not possible, with the present shortage of adequate data, to determine if the electronic transition moment should include a third term to account for electronic-vibrational-rotational interaction, in addition to the two terms  $R_{ev}(r)$  and  $R_{eJ}\{J(J+1)\}$  accounting for electronic-vibrational and electronic-rotational interaction respectively. That this results in a small change in eigenvalue does not necessarily mean that there will be a correspondingly small change in the transition probability, as discussed in section 2.5. There is thus a need for further accurate measurements of the variation of relative effective vibrational transition probabilities with rotational and vibrational quantum numbers, over the whole band system.

It should be noted that the calculations are not able to distinguish between the two spin states of the molecule for each J value. Accounting for the different spin states in the expressions for the wave functions may indeed lead to different values for the

Table 7.3 Relative J-Dependent Transition Probabilities in OH ( $p_{v'v''}/p_{00}$ )

| v' | v'' | J'' | 0     |       |       | 1     |       |       | 2     |       |                    | 3                  |                    |                    | 4                  |                    |                    |
|----|-----|-----|-------|-------|-------|-------|-------|-------|-------|-------|--------------------|--------------------|--------------------|--------------------|--------------------|--------------------|--------------------|
|    |     |     | P     | Q     | R     | P     | Q     | R     | P     | Q     | R                  | P                  | Q                  | R                  | P                  | Q                  | R                  |
| 0  |     | 1½  | 1.000 | 0.996 | 0.990 | 0.017 | 0.016 | 0.015 | 0.002 | 0.002 | 0.002              | 3x10 <sup>-4</sup> | 3x10 <sup>-4</sup> | 2x10 <sup>-4</sup> | 4x10 <sup>-5</sup> | 4x10 <sup>-5</sup> | 3x10 <sup>-5</sup> |
|    |     | 10½ | 0.941 | 0.917 | 0.890 | 0.018 | 0.013 | 0.009 | 0.002 | 0.002 | 0.002              | 3x10 <sup>-4</sup> | 3x10 <sup>-4</sup> | 2x10 <sup>-4</sup> | 6x10 <sup>-5</sup> | 4x10 <sup>-5</sup> | 3x10 <sup>-5</sup> |
|    |     | 15½ | 0.864 | 0.830 | 0.794 | 0.016 | 0.010 | 0.006 | 0.002 | 0.002 | 0.001              | 4x10 <sup>-4</sup> | 3x10 <sup>-4</sup> | 2x10 <sup>-4</sup> | 7x10 <sup>-5</sup> | 5x10 <sup>-5</sup> | 3x10 <sup>-5</sup> |
|    |     | 20½ | 0.761 | 0.720 | 0.678 | 0.013 | 0.007 | 0.003 | 0.002 | 0.002 | 0.001              | 4x10 <sup>-4</sup> | 2x10 <sup>-4</sup> | 1x10 <sup>-4</sup> | 9x10 <sup>-5</sup> | 5x10 <sup>-5</sup> | 3x10 <sup>-5</sup> |
|    |     | 25½ | 0.640 | 0.595 | 0.550 | 0.010 | 0.004 | 0.001 | 0.002 | 0.001 | 7x10 <sup>-4</sup> | 4x10 <sup>-4</sup> | 2x10 <sup>-4</sup> | 1x10 <sup>-4</sup> | 1x10 <sup>-4</sup> | 7x10 <sup>-5</sup> | 3x10 <sup>-5</sup> |
| 1  |     | 1½  | 0.449 | 0.450 | 0.453 | 0.780 | 0.775 | 0.765 | 0.025 | 0.024 | 0.022              | 0.005              | 0.005              | 0.004              | 8x10 <sup>-4</sup> | 7x10 <sup>-4</sup> | 7x10 <sup>-4</sup> |
|    |     | 10½ | 0.430 | 0.439 | 0.447 | 0.725 | 0.688 | 0.647 | 0.026 | 0.019 | 0.013              | 0.005              | 0.004              | 0.003              | 0.001              | 7x10 <sup>-4</sup> | 5x10 <sup>-4</sup> |
|    |     | 15½ | 0.413 | 0.423 | 0.433 | 0.645 | 0.593 | 0.539 | 0.022 | 0.014 | 0.007              | 0.005              | 0.004              | 0.003              | 0.001              | 7x10 <sup>-4</sup> | 4x10 <sup>-4</sup> |
|    |     | 20½ | 0.390 | 0.400 | 0.407 | 0.537 | 0.476 | 0.415 | 0.017 | 0.008 | 0.003              | 0.005              | 0.003              | 0.002              | 0.001              | 6x10 <sup>-4</sup> | 4x10 <sup>-4</sup> |
|    |     | 25½ | 0.360 | 0.366 | 0.368 | 0.411 | 0.347 | 0.285 | 0.011 | 0.003 | 3x10 <sup>-4</sup> | 0.004              | 0.002              | 0.001              | 0.001              | 6x10 <sup>-4</sup> | 3x10 <sup>-4</sup> |
| 2  |     | 1½  | 0.144 | 0.146 | 0.148 | 0.685 | 0.685 | 0.686 | 0.586 | 0.579 | 0.567              | 0.028              | 0.026              | 0.024              | 0.007              | 0.007              | 0.006              |
|    |     | 10½ | 0.144 | 0.154 | 0.165 | 0.646 | 0.646 | 0.644 | 0.533 | 0.488 | 0.440              | 0.028              | 0.019              | 0.012              | 0.008              | 0.006              | 0.004              |
|    |     | 15½ | 0.149 | 0.163 | 0.178 | 0.602 | 0.598 | 0.588 | 0.452 | 0.392 | 0.332              | 0.023              | 0.013              | 0.006              | 0.007              | 0.005              | 0.003              |
|    |     | 20½ | 0.158 | 0.175 | 0.192 | 0.538 | 0.524 | 0.502 | 0.344 | 0.278 | 0.215              | 0.015              | 0.006              | 0.001              | 0.006              | 0.004              | 0.002              |
|    |     | 25½ | 0.168 | 0.185 | 0.201 | 0.450 | 0.421 | 0.383 | 0.223 | 0.161 | 0.108              | 0.008              | 0.002              | 2x10 <sup>-6</sup> | 0.004              | 0.002              | 0.001              |
| 3  |     | 1½  | 0.043 | 0.043 | 0.045 | 0.339 | 0.342 | 0.346 | 0.751 | 0.749 | 0.745              | 0.422              | 0.414              | 0.402              | 0.027              | 0.025              | 0.023              |
|    |     | 10½ | 0.046 | 0.051 | 0.058 | 0.335 | 0.352 | 0.369 | 0.692 | 0.674 | 0.651              | 0.371              | 0.325              | 0.277              | 0.026              | 0.017              | 0.010              |
|    |     | 15½ | 0.053 | 0.061 | 0.071 | 0.338 | 0.358 | 0.378 | 0.614 | 0.582 | 0.542              | 0.293              | 0.234              | 0.179              | 0.020              | 0.010              | 0.004              |
|    |     | 20½ | 0.065 | 0.077 | 0.091 | 0.339 | 0.356 | 0.368 | 0.500 | 0.449 | 0.390              | 0.192              | 0.134              | 0.085              | 0.012              | 0.004              | 6x10 <sup>-4</sup> |
|    |     | 25½ | 0.084 | 0.100 | 0.116 | 0.323 | 0.326 | 0.317 | 0.346 | 0.280 | 0.212              | 0.091              | 0.049              | 0.020              | 0.005              | 8x10 <sup>-4</sup> | 2x10 <sup>-5</sup> |
| 4  |     | 1½  | 0.013 | 0.013 | 0.014 | 0.139 | 0.141 | 0.144 | 0.508 | 0.511 | 0.515              | 0.698              | 0.693              | 0.684              | 0.289              | 0.281              | 0.270              |
|    |     | 10½ | 0.015 | 0.018 | 0.021 | 0.148 | 0.163 | 0.180 | 0.492 | 0.504 | 0.514              | 0.619              | 0.582              | 0.537              | 0.242              | 0.199              | 0.157              |
|    |     | 15½ | 0.020 | 0.025 | 0.031 | 0.167 | 0.189 | 0.213 | 0.473 | 0.480 | 0.479              | 0.509              | 0.450              | 0.385              | 0.170              | 0.120              | 0.078              |
|    |     | 20½ | 0.030 | 0.039 | 0.049 | 0.196 | 0.221 | 0.244 | 0.427 | 0.413 | 0.385              | 0.351              | 0.276              | 0.202              | 0.086              | 0.046              | 0.019              |
|    |     | 25½ | 0.050 | 0.063 | 0.078 | 0.221 | 0.236 | 0.239 | 0.319 | 0.271 | 0.211              | 0.165              | 0.098              | 0.047              | 0.021              | 0.005              | 8x10 <sup>-5</sup> |

transition probabilities, but in this experiment the values obtained for the  $Q_1$ ,  $Q_2$  and  $P_1$  branches were all equal to within the experimental error.

### 7.5. Thermometric Molecules

The effect of the  $J$  dependence of the effective vibrational transition probability is to increase the uncertainty of rotational temperature determinations. A molecule suitable for accurate measurements of the rotational temperature requires two very similar electronic states, so that the change of overlap integral with  $J$  is a minimum; a high dissociation energy and hence high binding force and low centrifugal distortion; and a slowly varying total electronic transition moment. It is reasonable to suppose that  $R_e(r)$  should change more slowly for transitions that are not forbidden in the separated atoms. It has also been suggested that  $R_e(r)$  varies more slowly for parallel ( $\Delta\Lambda = 0$ ) than for perpendicular ( $\Delta\Lambda \neq 0$ ) transitions.

Very few of the common thermometric molecules satisfy all the conditions listed above. The  $C_2$  Swan system satisfies many of the conditions, but requires higher resolution than the hydride on account of the higher mass, and hence lower  $B$  value, leading to a narrower separation of the spectrum lines. The OH radical does not fulfil any of the conditions, and the temperature corrections referred to here and presented by Learner<sup>18,52</sup> may well represent an upper limit to the uncertainty to be expected in thermometry with the group of molecules CN,  $C_2$ , CH, OH, MgH, and NH. The other molecules quoted partly satisfy the requirements while OH does not, but the whole field does call for a thorough investigation.

REFERENCES

1. Herzberg, G., 1965. *J.Opt.Soc.Am.* 55, 229.
2. Shuler, K.E., 1950. *J.Chem.Phys.* 18, 1221.
3. Carrington, T., 1959. *J.Chem.Phys.* 31, 1243.
4. Pearse, R.W.B. and Gaydon, A.G., 1963. *The Identification of Molecular Spectra*, 3rd. Edn., Chapman & Hall, London.
5. Weinreb, S., Barrett, A.H., Meeks, M.L. and Henry, J.C., 1963. *Nature* 200, 829.
6. Oldenberg, O. and Rieke, F.F., 1938. *J.Chem.Phys.* 6, 439.
7. Dwyer, R.J. and Oldenberg, O., 1944. *J.Chem.Phys.* 12, 351.
8. Golden, D.M., Del Greco, F.P. and Kaufman, F., 1963. *J.Chem.Phys.* 39, 3034.
9. Oldenberg, O. and Rieke, F.F., 1938. *J.Chem.Phys.* 6, 169.
10. Oldenberg, O. and Rieke, F.F., 1938. *J.Chem.Phys.* 6, 779.
11. Dyne, P.J., 1958. *J.Chem.Phys.* 28, 999.
12. Carrington, T., 1959. *J.Chem.Phys.* 31, 1243.
13. Lapp, M., 1960. *J.Q.S.R.T.* 1, 30.
14. Watson, R., 1964. *J.Q.S.R.T.* 4, 1.
15. Bennet, R.G. and Dalby, F.W., 1964. *J.Chem.Phys.* 40, 1414.
16. Bird, P.F. and Schott, G.L., 1965. *J.Q.S.R.T.* 5, 783.
17. Kostkowski, H.J. and Bass, A.M., 1956. *J.Opt.Soc.Am.* 46, 1060.
18. Learner, R.C.M., 1962. *Proc.Roy.Soc.* A.269, 311.
19. Mulliken, R.S. 1940. *J.Chem.Phys.* 8, 382.
20. Hurley, A.C., 1959. *Proc.Roy.Soc.* A.249, 402.
21. Dieke, G.H. and Crosswhite, H.M., 1948. *Bumblebee Series Report No. 87*, reprinted in 1962, *J.Q.S.R.T.* 2, 97.

22. Dieke, G.H. and Crosswhite, H.M., 1949. Quarterly Report, Oct.-Dec. 1949, Contract N Ord 8036 JHB-3 Problem A, Johns Hopkins University (unpublished).
23. Bass, A.M. and Broida, H.P., 1953. N.B.S. Circular 541.
24. Morse, P.M., 1929. Phys.Rev. 34, 57.
25. Nicholls, R.W., 1956. Proc.Phys.Soc. A.69, 741.
26. Nicholls, R.W. and Jarman, W.R., 1956. Proc.Phys.Soc. A.69, 253.
27. Bass, A.M. and Broida, H.P., 1953. J.Chem.Phys. 21, 173.
28. Learner, R.C.M. and Gaydon, A.G., 1959. Nature 183, 242.
29. Pekeris, C.L., 1934. Phys. Rev. 45, 98.
30. James, T.C., 1959. J.Chem.Phys. 32, 1770.
31. Zirman, W.G. and Bogdan, S.I., 1964. J.Chem.Phys. 40, 588.
32. Roschdestwensky, D.S., 1912. Ann.Phys. 39, 307.
33. Roschdestwensky, D.S., 1921. Trans.Opt.Inst. Leningrad 2, No. 13.
34. Puccianti, L., 1901. Nuovo Cimento 2, 257.
35. Puccianti, L., 1904. Memm.Spettrosc. 33, 133.
36. Ostrovskii, Y.I. and Penkin, N.P., 1961. Optics and Spectroscopy 11, 1.
37. Ostrovskii, Y.I. and Penkin, N.P., 1961. Optics and Spectroscopy 11, 307.
38. Mitchell, A.C.G. and Zemansky, M.W., 1934. Resonance Radiation and Excited Atoms, Cambridge Univ. Press.
39. Herzberg, G., 1950. Molecular Spectra and Molecular Structure, I; Spectra of Diatomic Molecules, 2nd Edn., Van Nostrand, New York.
40. Mulliken, R.S., 1939. J.Chem.Phys. 7, 14.
41. Condon, E.U., 1928. Phys.Rev. 32, 858.
42. Hönl, H. and London, F., 1925. Z.Physik 33, 803.

43. Dennison, D.M., 1926. Phys.Rev. 28, 318.
44. Rademacher, H. and Reiche, F., 1927. Z.Physik 41, 453.
45. Franck, J., 1925. Trans. Faraday Soc. 21 536.
46. Condon, E.U., 1926. Phys.Rev. 28, 1182.
47. Condon, E.U., 1947. Am.J.Phys. 15, 365.
48. Van Vleck, J.H., 1929. Phys.Rev. 33, 467.
49. Hill, E. and Van Vleck, J.H., 1928. Phys.Rev. 32, 250.
50. Earls, L.T., 1935. Phys.Rev. 48, 423.
51. Dunham, J.L., 1932. Phys.Rev. 41, 721.
52. Learner, R.C.M., 1961. Ph.D. Thesis, London.
53. Herman, R.C. and Rubin, R.J., 1955. Astrophys.J. 121, 533.
54. Nicholls, R.W. and Fraser, P.A., 1958. Scientific Report No. 6,  
Contract AF 19(604) - 1718, Univ. of W. Ontario,  
London, Ontario.
55. Wood, R.W., 1904. Phil.Mag. 8, 293.
56. Ladenburg, R., 1921. Z.Physik 4, 451.
57. Kramers, H.A., 1924. Nature 113, 673.
58. Rosohdestwensky, D.S. and Penkin, N.P., 1941. J.Phys. U.S.S.R.,  
V, No. 5-6, 319.
59. Pery-Thorne, A. and Chamberlain, J.E., 1963. Proc.Phys.Soc.  
A.82, 133.
60. Mach., E., 1892. Z.f.Instrumentenk 12, 89.
61. Zehnder, L., 1891. Z.f.Instrumentenk 11, 275.
62. Chamberlain, J.E., 1962. Ph.D. Thesis, London.
63. Bonhoeffer, K.E. and Reichardt, H., 1928. Z.Physik.Chemie,  
A.139, 75.
64. McBride, B.J., Heimel, S., Ehlers, J.G. and Gordon, S., 1963.  
N.A.S.A., SP-3001.

65. Barrow, R.F., 1956. Ark.Fys. 11, 281.
66. Gaydon, A.G. and Wolfhard, H.G., 1951. Proc.Roy.Soc. A.208, 63.
67. Douglas, A.E., 1966. J.Chem.Phys. 45, 1007.
68. Watson, R. and Ferguson, W.R., 1965. J.Q.S.R.T. 5, 595.
69. Lalos, G.T., Corruccini, R.J. and Broida, H.P., 1958.  
Rev.Sci.Instrum. 29, 505.
70. Herman, R.C. and Hornbeck, G.A., 1953. Astrophys.J. 118, 214.
71. Broida, H.P. and Shuler, K.E., 1957. J.Chem.Phys. 27, 933.